Regulation of Kidney Distal Convoluted Tubule (DCT) Cell Function

---

Dissertation

zur

Erlangung der naturwissenschaftlichen Doktorwürde
(Dr.sc.nat.)

vorgelegt der
Mathematisch-naturwissenschaftlichen Fakultät
der
Universität Zürich

von
Katja Trompf
aus Deutschland

Promotionskomitee:
Prof. Dr. Johannes Loffing
Prof. Dr. Carsten Wagner
Prof. Dr. François Verrey
Prof. Dr. Markus Bleich

Zürich, 2013

Contents

1. Introduction 1

1.1. Anatomy and function of the kidney 1

1.2. Reabsorption of Na^+ by the kidney 2

1.3. Function of the DCT 3

1.4. The Na^+Cl^--cotransporter- NCC 5

1.4.1. Structure of NCC 5

1.4.2. Mechanism of NCC regulation 7

1.4.3. Phosphorylation of NCC 8

1.4.4. Trafficking of NCC 9

1.4.5. Ubiquitylation of NCC 10

1.4.6. Regulation of NCC by the WNK –SPAK/OSR1 pathway 11

1.4.7. Additional pathways controlling NCC 18

1.4.8. Novel candidates for NCC regulation 20

1.5. Thesis projects 24

1.5.1. Investigating the role of I1 in DCT function 24

1.5.2. Investigating the role of PKD1 in DCT function 24

1.5.3. Using transcriptomic analysis to identify mediators of DCT cell growth 24

1.5.4. Establishing *ex vivo* DCT cell culture as a tool to study DCT cell function 24

2. Material and Methods 25

2.1. Mouse work 25

2.1.1. PV-eGFP mice 25

2.1.2. I1 KO mice 26

2.1.3. PKD1 PV cre mice/ PKD1 PVcre eGFP 26

2.1.4. Aldosterone-synthase deficient mice (AS-KO) 26

2.1.5. Genotyping 27

2.1.6. Metabolic cage experiments 28

2.1.7. Measurment of blood plasma parameters 28

2.1.8. Diet experiments 29

2.1.9. Hydrochlorothiazide test (HCTZ) 29

2.1.10. Blood pressure measurements by tail cuff method 29

2.2. Immunohistochemistry 29

2.3. Protein sample preparation and western blot analysis 30

2.4. RNA extraction from kidney 31

2.5. RNA extraction from COPAS sorted DCT 31
2.6. Real-time PCR 31
2.7. Isolation of single tubular fragments using the complex object parametric analyzer biosorter (COPAS) 33
2.8. Transcriptomic analysis after diuretic treatment using Agilent Microarray hybridization and analysis 33
2.9. Cell culture 34
2.9.1. Primary cell culture of COPAS- isolated DCTs 34
2.9.2. Immunocytochemistry 34
2.9.3. RNA isolation and cDNA synthesis of DCT primary cell culture 35
2.9.4. Cultivation and transfection of HEK 293T cells 35
2.9.5. PKD1 plasmids 35
2.9.6. Protein preparation of transfected HEK293T cells 36
3. Results 38
3.1. Project 1: Investigating the role of the Ppp1r1a-transcript (I1) for NCC regulation 38
3.1.1. Localization of I1 in the kidney 38
3.1.2. I1 regulates phosphorylation and activity of NCC in vitro 39
3.1.3. I1 regulates phosphorylation of NCC *in vivo* 41
3.1.4. Lower blood pressure in I1-deficient mice 43
3.1.5. I1-KO mice show no overt Gitelman syndrome phenotype 44
3.1.6. Thiazide response and fractional cortical tubular volume in wildtype and I1-deficient mice 49
3.1.7. I1-deficient mice do not show alterations of the RAA-system 50
3.1.8. I1-deficient mice show no changes in mRNA expression of DCT specific proteins 51
3.1.9. Compensatory up-regulation of pendrin in I1 deficient mice 51
3.1.10. Unaltered SPAK phosphorylation in I1-deficient mice 53
3.2. Project 2: Investigating the role of PKD1 for NCC regulation 54
3.2.1. Localization of PKD1 in the kidney 54
3.2.2. Aldosterone regulates PKD1 in vivo 54
3.2.3. Reduced total PKD1 expression and phosphorylation levels in AS-deficient mice 56
3.2.4. Mice with DCT1-specific deletion of PKD1 57
3.2.5. PKD1 regulates the phosphorylation of NCC in vivo 58
3.2.6. Mice with DCT1-specific deletion of PKD1 show a reduction in blood pressure 60
3.2.7. No evidence for disturbed HCTZ-response in PKD1-KO mice 61
3.2.8. PKD1-KO mice show no overt Gitelman syndrom 62

3.2.9. PKD1-KO mice display significantly elevated aldosterone levels but unaltered renin expression 64
3.2.10. PKD1-KO mice do not show no an altered expression of NCC, WNK kinases and other distal tubule marker mRNAs 65
3.2.11. Compensatory up-regulation of ENaC in PKD1 KO mice 65
3.2.12. Preliminary data: PKD1 increases the abundance of total NCC in transiently transfected HEK293T cells 67
3.3. Project 3: Using transcriptomic analysis to identify mediators of DCT cell growth 68
3.3.1. Identification of potential mediators of DCT cell growth 68
3.3.2. Confirmation of potential mediators of DCT cell growth by qRT-PCR 71
3.4. Project 4: Establishing ex vivo DCT cell culture as a tool to study DCT cell function 72
3.4.1. Outgrowing cells form a polarized epithelium 72
3.4.2. Characterization of DCT primary cell culture 72
4. Discussion 74
4.1. I1 controls phosphorylation of NCC *in vitro* and *in vivo* 74
4.2. I1-mediated phosphorylation of NCC is independent of the SPAK/WNK4 pathway 76
4.3. I1 knockout mice show features of NCC-deficiency 77
4.4. I1 deficiency in the kidney is compensated by up-regulation of pendrin 78
4.5. Further directions 79
4.6. PKD1 is an aldosterone-induced protein 80
4.7. Mice with PKD1 loss in the DCT1 show features of Gitelman-sydrome 82
4.8. Further directions 83
4.9. TRPM6, Chac1, SIK1 and Prox1 are differently regulated in DCT cells in response to diuretic treatment that alters DCT cell growth 83
4.10. Ex vivo DCT cell cultures as a tool to study DCT function 85
4.11. General conclusion 86
5. Bibliography 87
Acknowledgements 98
Curriculum Vitae 99

Summary

The distal convoluted tubule (DCT) plays an important role in the regulation of Na^+ homeostasis and blood pressure. Furthermore, the DCT is responsible for the fine-tuning of renal Ca^{++}, Mg^{++} and K^+ excretion. The DCT has also a remarkable structural plasticity, which contributes to its functional adaptation to altered ion transport requirements. The thiazide-sensitive Na^+Cl^- co-transporter (NCC) is the major apical Na^+ transport pathway in the DCT. NCC activity and DCT salt transport are regulated by the tubular Na^+ load, dietary ion intake, metabolic alkalosis and acidosis as well as by many hormones including aldosterone, angiotensin II, and vasopressin. The functional significance of the DCT and NCC is evidenced by the fact that the DCT is an important target of diuretics and that monogenic diseases with NCC dysfunction (i.e. Gitelman and Gordon syndrome) profoundly alter blood pressure.

The identification of the With No lysine (K) kinases (WNK) as important regulators of NCC phosphorylation and activity was a major step towards the understanding of the molecular mechanisms controlling DCT function. Nevertheless, we still know very little about the regulatory mechanisms that interfere with the WNK-pathway or that otherwise regulate NCC and DCT ion transport. Based on the fact that many of the so far described NCC-regulating proteins (e.g., kidney specific-WNK1, WNK4, STE20/SPS1-related proline/alanine-rich kinase (SPAK), Kelch-like 3 Protein (Klhl3) or parvalbumin (PV)) are enriched in the DCT, we hypothesized that the DCT expresses a specific repertoire of regulatory proteins that control its function. In a recent screen by group, two gene products were found to be highly enriched in the DCT, i.e., the Ppp1r1a gene encoding for the protein phosphatase inhibitor 1 (I1) and the Prkcμ gene encoding for protein kinase D1 (PKD1). The aim of the present thesis was to investigate the role of I1 and PKD1 for the regulation of NCC activity and DCT function using appropriate gene-modified mouse models. Moreover, transcriptomic analyses on isolated DCTs were used to identify novel regulators that contribute to the remarkable structural plasticity of the DCT. Furthermore, a protocol for primary DCT cell culture was established.

First, siRNA-mediated knockdown experiments in HEK293 cells overexpressing NCC were used to study the role of the phosphatase inhibitor I1 for NCC regulation. Knockdown of I1 caused a pronounced reduction of NCC phosphorylation, while the total expression of NCC remained unchanged. Co-expression of I1 with NCC in *Xenopus laevis oocytes* increased thiazide-dependent Na^+ uptake providing further *in vitro* evidence that I1 regulates NCC. To assess the functional role of I1 *in vivo*, I1 knockout mice (I1-KO) were studied. Similar to the findings in HEK293 cells, I1-KO mice exhibited an approximately 50 % reduction in NCC phosphorylation without any changes in total NCC abundance. Compared with wildtype mice, I1-KO mice did not show any differences in urinary ion excretion, plasma ion, and plasma aldosterone concentrations. However, on a low K^+ diet, I1-KO mice had lower plasma K^+ levels than their corresponding wildtype littermates. Moreover, compared with

wildtype mice, I1-KO mice showed a reduced arterial blood pressure on standard and low salt diet, but not on a high salt diet. Thus, I1 regulates NCC phosphorylation in heterologous expression systems and in the DCT *in vivo* and it controls arterial blood pressure in mice.

Next, we studied the role of PKD1 for NCC regulation. Immunohistochemistry confirmed that PKD1 is highly expressed in mouse and rat DCT. In adrenalectomized rats, a single aldosterone injection rapidly (<2h) increased total and phosphorylated PKD1 specifically in the DCT. The induction of PKD1 went along with an enhanced phosphorylation of NCC. Conversely, aldosterone synthase-deficient mice lacking any endogenous aldosterone production, showed decreased PKD1 mRNA and protein abundance, PKD1 phosphorylation and NCC phosphorylation. To further investigate the role of PKD1 in the DCT *in vivo*, we generated mice with a specific deletion of PKD1 in the early DCT (PKD1-KO) by breeding $PKD1^{flox/flox}$ mice with mice expressing cre under the control of the DCT-specific parvalbumin promoter (PV-cre mice). PKD1-KO mice showed a profound reduction in NCC phosphorylation without any effect on total NCC abundance. Urinary ion excretions and plasma ion concentrations were not different between PKD1-KO and control mice. However, urinary aldosterone excretion was increased in PKD1-KO mice suggesting a mild urinary salt wasting phenotype. Consistently, with the elevated aldosterone levels, PKD1-KO mice exhibited an up-regulation of the epithelial sodium channel ENaC in the renal collecting system. Blood pressure of PKD1-KO animals on a low Na^+ diet was decreased in comparison to control animals. Thus, PKD1 is another DCT-enriched gene product that controls both NCC phosphorylation and arterial blood pressure.

Interestingly, altered NCC and hence DCT Na^+-transport activity are often associated with marked structural changes to the DCT epithelium. For example, enhanced salt transport usually goes along with hypertrophy and hyperplasia while lowered transport rates are associated with atrophy or even apoptosis of the DCT cells. To identify underlying molecular mechanisms in mice, we stimulated and inhibited DCT cell growth by pharmacological interventions (i.e. furosemide and thiazide treatment). Subsequently, we used fluorescence-activated renal tubule sorting (complex object and parametric analysis and sorting - COPAS) to isolate green fluorescent DCTs for differential microarray analysis. More than 500 genes were found to be differently regulated within 4 h after furosemide or thiazide treatment. Four potentially relevant genes were selected and their differential regulation was confirmed by quantitative RT-PCR (i.e, the transient receptor potential melastatin 6 channel (TRPM6), the salt inducible kinase 1 (SIK1), the cation transport regulator (Chac1) and the transcription factor, Prox1). Further experiments will have to address the specific roles of these differently regulated genes for DCT growth and function.

As an appropriate DCT cell model is lacking, we also aimed at developing a DCT cell culture system in which the function of target genes can be studied in an *ex vivo* setting. Therefore, we used the COPAS technique to isolate DCTs in large scale from transgenic mice expressing eGFP specifically

in the early DCT (PV-EGFP mice). DCTs were sorted in cell culture dishes and on permeable filter supports to allow an outgrowth of DCT cells under cell culture conditions. After 10 days, outgrowing DCT cells formed a polarized epithelium with a sizeable transepithelial resistance. qRT-PCR and immunocytochemistry confirmed that the outgrown DCT cells maintained many DCT cell characteristics including NCC and WNK1 expression. However, the level of NCC expression was drastically reduced compared with the *in vivo* conditions and it was too low for biochemical studies. Hence, additional work is needed to further optimize the cell culture conditions.

Taken together, our data support the hypothesis that the DCT has a specific repertoire of proteins that regulate its function. Two novel candidate genes (i.e. I1 and PKD1) that control NCC function and blood pressure were identified and studied in appropriate gene-modified mouse models. Moreover, several new candidate genes that potentially contribute to the marked structural plasticity of the DCT have been identified. Furthermore, a protocol for primary DCT cell cultures from wildtype and transgenic mice was established, which may allow to test for the functional significance of target genes in *ex vivo* conditions. Thus, this thesis provides several novel insights into the molecular mechanism of NCC regulation and blood pressure control. Novel data and tools were established, which will facilitate future experiment elucidating DCT function.

Zusammenfassung

Die pars convoluta des distalen Tubulus (DCT) spielt eine wichtige Rolle bei der Regulierung der Natriumhomöostase und des Blutdrucks. Ausserdem ist der DCT für die Feineinstellung der renalen Ca^{++}-, Mg^{++}- und K^{+}-Ausscheidung verantwortlich. Seine außerordentliche strukturelle Plastizität trägt dabei zur funktionellen Anpassung an veränderten Bedingungen bei. Der Thiazid-sensitive $Na^{+}Cl^{-}$-Co-Transporter (NCC) ist der wichtigste apikale Na^{+}-Transporter im DCT. Die Aktivität von NCC und der Salztransport im DCT werden durch die tubuläre Salzfracht, den Salzgehalt der Nahrung, den Säure-Basen-Haushalt, sowie durch eine Reihe von Hormonen wie Aldosteron, Angiotensin II und Vasopressin reguliert. Die funktionelle Bedeutung des DCT und des NCC wird daraus deutlich, dass der DCT ein wichtiger Angriffspunkt für Diuretika ist und dass monogenische Erkrankungen mit NCC-Dysfunktion (d.h. Gitelman- und Gordon-Syndrom) den Blutdruck stark verändern.

Die Identifizierung der With No lysine (K) Kinases (WNK) als wichtige Regulatoren der NCC-Phosphorylierung und damit der NCC-Aktivität war ein entscheidender Schritt zum Verständnis molekularer Mechanismen, die die DCT-Funktion kontrollieren. Dennoch wissen wir noch sehr wenig über die regulatorischen Mechanismen, die mit dem WNK-Signalweg interferieren und/oder den NCC- und DCT-Ionentransport steuern. Ausgehend von der Tatsache, dass viele der bislang beschriebenen NCC regulierenden Proteine (z.B. WNK1 (nierenspezifisch), WNK4, STE20/SPS1-related proline/alanine-rich kinase (SPAK), Kelch-like 3 Protein (Klhl3) oder Parvalbumin (PV)) besonders im DCT angereichert sind, stellten wir die Hypothese auf, dass der DCT ein spezifisches Repertoire an regulatorischen Proteinen besitzt, die seine Funktion steuern. In einer Screening-Untersuchung an isolierten DCTs, die unsere Gruppe kürzlich durchgeführt hat, wurden zwei Gene identifiziert, die im DCT stark exprimiert sind, das Ppp1r1a-Gen, kodierend für den Phosphatase-Inhibitor 1, und das Prkcμ-Gen, kodierend für die Proteinkinase D1. Das Ziel der vorliegenden Arbeit war, die Rolle von I1 und PKD1 in der Regulation der NCC-Aktivität und der DCT-Funktion mit geeigneten genveränderten Mausmodellen zu untersuchen. Darüber hinaus wurden Transkriptom-Analysen an isolierten DCTs verwendet, um neue Regulatoren der strukturellen Plastizität des DCT zu identifizieren. Weiterhin wurde ein Protokoll für primäre DCT-Zellkulturen entwickelt.

Um die Rolle des Phosphatase-Inhibitors 1 (I1), bei der NCC-Regulation zu analysieren, wurden zunächst siRNA-vermittelte Knockdown-Experimente in NCC-überexprimierenden HEK293-Zellen durchgeführt. Der Knockdown von I1 führte zu einer ausgeprägten Reduzierung der NCC-Phosphorylierung, während die totale NCC-Expression unverändert blieb. Die Co-Expression von I1 mit NCC in *Xenopus laevis Oozyten* erhöhte die Thiazid-abhängige Na^{+}-Aufnahme. Dies ist ein weiterer *in vitro*-Nachweis, dass I1 NCC reguliert. Um die funktionelle Rolle von I1 *in vivo* zu beurteilen, wurden I1-Knockout-Mäuse (I1-KO) untersucht. In Analogie zu den Ergebnissen in HEK293-Zellen zeigten I1-KO-Mäuse eine etwa 50%ige Reduktion der NCC-Phosphorylierung ohne

Veränderungen der gesamten NCC-Expression. Im Vergleich zu Wildtyp-Mäusen ergaben sich in I1-KO-Mäusen keine Unterschiede in der renalen Ionenausscheidung und in den Plasmaionen-und Plasmaaldosteron-Konzentrationen. Allerdings wiesen I1-KO Mäuse unter K^+-armer Diät eine niedrigere Plasma K^+-Konzentration als ihre entsprechenden Wildtyp-Geschwister auf. Zudem fand sich bei I1-KO-Mäusen im Vergleich zu Wildtyp-Mäusen ein verminderter arterieller Blutdruck sowohl unter Standard- als auch unter salzarmer Diät, nicht aber unter einer Hochsalzdiät. Zusammengefasst konnten wir zeigen, dass I1 die Phosphorylierung von NCC sowohl in heterologen Expressionssystemen als auch im DCT *in vivo* reguliert, und dass I1 bei Mäusen den arteriellen Blutdruck steuert.

In einem nächsten Schritt untersuchten wir die Rolle von PKD1 in der Regulierung von NCC. Immunohistochemische Analysen bestätigten, dass PKD1 im DCT von Mäusen und Ratten stark exprimiert ist. In adrenalektomierten Ratten erhöhte eine einzelne Injektion von Aldosteron (<2h) rasch sowohl die Gesamtexpression wie auch die Phosphorylierung von PKD1 im DCT. Die Induktion von PKD1 ging mit einer verstärkten Phosphorylierung von NCC einher. Umgekehrt zeigten Aldosteronsynthase-defiziente Mäuse, die keine endogene Aldosteron-Produktion besitzen, eine Verminderung der PKD1-mRNA-Konzentration und -Proteinexpression sowie eine Verminderung der Phosphorylierung von PKD1 und NCC. Zur weiteren Untersuchung der Rolle von PKD1 im DCT *in vivo* generierten wir Mäuse mit einer spezifischen Deletion von PKD1 im frühen DCT (PKD1-KO) durch die Kreuzung von $PKD1^{flox/flox}$-Mäusen mit Mäusen, die cre unter der Kontrolle des DCT-spezifischen Parvalbumin-Promotors exprimieren (PV-cre-Mäuse). PKD1-KO Mäuse zeigten eine geringere NCC-Phosphorylierung ohne dass dabei die Gesamtexpression von NCC verändert war. Bezüglich der renalen Ionenausscheidung sowie der Plasmaionenkonzentration unterschieden sich die PKD1-KO Tiere nicht von ihren Kontroll-Geschwistern. Allerdings war die renale Aldosteron-Ausscheidung in PKD1-KO-Mäusen erhöht, was auf einen milden renalen Salzverlust hinweist. In Übereinstimmung mit den erhöhten Aldosteronwerten wiesen die PKD1-KO Mäuse eine erhöhte Expression des epithelialen Natrium-Kanals, ENaC, im Sammelrohrsystem auf. Unter salzarmer Diät war der Blutdruck der PKD1-KO-Tiere im Vergleich zu den Kontrolltieren verringert. Daraus schlossen wir, dass PKD1 ein weiteres DCT-angereichertes Genprodukt ist, das sowohl die NCC-Phosphorylierung als auch den arteriellen Blutdruck steuert.

Interessanterweise sind Veränderungen in der NCC-Aktivität und damit des DCT-Natriumtransportes häufig mit einer ausgeprägten strukturellen Veränderung des DCT-Epithels assoziiert. So geht ein verstärkter Salztransport im DCT beispielsweise mit eine Hypertrophie und Hyperplasie der DCT-Zellen einher, während bei einem verminderten Salztransport das Segment atrophiert oder sogar eine Apoptose der DCT-Zellen auftreten kann. Um die zugrunde liegenden molekularen Mechanismen für diese Plastizität des DCTs bei Mäusen zu identifizieren, stimulierten

bzw. inhibierten wir das DCT-Zellwachstum durch verschiedene pharmakologische Interventionen (d.h. Furosemid- und Thiazid-Behandlung). Anschließend verwendeten wir die Fluoreszenz-aktivierte Sortierung-mehrzelliger Objekte (complex object and parametric analysis and sorting - COPAS) um grün fluoreszierende DCTs zu isolieren welche dann für die differentielle Microarray-Analyse aufbereitet wurden. Mehr als 500 unterschiedlich regulierte Gene wurden nach vierstündiger Furosemid- oder Thiazid-Behandlung gefunden. Vier potenziell relevante Gene wurden ausgewählt und ihre differentielle Regulation mittels quantitativer RT-PCR bestätigt: transientes Rezeptor-Potential-Melastatin 6-Kanal (TRPM6), Salz-induzierbare Kinase 1 (SIK1), Kationentransport-Regler (Chac1) und Transkriptions-Faktor Prox1. Die spezifischen Rollen dieser unterschiedlich regulierten Gene für DCT-Wachstum und -Funktion muss in weiteren Experimenten untersucht werden.

Mangels eines geeigneten DCT-Zellmodells war es ein weiteres Ziel, ein DCT-Zellkultursystem zu entwickeln, in dem die Funktion von Zielgenen *ex vivo* analysiert werden kann. Wir setzten die COPAS-Technik ein, um in großem Maßstab DCTs aus transgenen Mäusen, die eGFP spezifisch im DCT1 exprimieren (PV-eGFP-Mäuse), zu isolieren. Die isolierten DCTs wurden in Zellkulturschalen und auf semipermeablen Filter sortiert, um ein Wachstum unter Zellkultur-Bedingungen zu ermöglichen. Nach 10 Tagen in Kultur bildeten die DCT-Zellen ein dichtes, polarisiertes Epithel mit einem beträchtlichen transepithelialen Widerstand. qRT-PCR und Immunozytochemie bestätigten, dass die herangewachsenen Zellen viele DCT-Zelleigenschaften einschließlich der Expression von NCC und WNK1 beibehielten. Allerdings war die NCC-Expression im Vergleich zu *in vivo*-Bedingungen so stark reduziert, dass biochemische Analysen nicht mehr möglich waren. Eine weiterführende Optimierung der Zellkultur-Bedingungen ist notwendig um ein zuverlässiges, DCT-spezifisches *in vitro* System zu generieren.

Zusammenfassend unterstützen unsere Daten die Hypothese, dass der DCT über ein spezifisches Repertoire an Proteinen verfügt, die seine Funktion gezielt regulieren. Für zwei dieser Proteine (I1 und PKD1), konnte gezeigt werden, dass sie in die Regulierung der Funktion von NCC und des Blutdruck involviert sind. Weiter wurde die Bedeutung diese Proteine in entsprechenden Gen-veränderten Mausmodellen studiert. Bezüglich der Regulierung der strukturellen Plastizität des DCTs konnten mehrere neue Kandidatengene, identifiziert werden. Weiterhin wurde ein Protokoll zur Gewinnung primärer DCT-Zellkulturen aus Wildtyp- und transgenen Mäusen etabliert, das die Testung der funktionellen Bedeutung von Zielgenen *ex vivo* ermöglicht. Diese Arbeit liefert somit neue Einblicke in die molekularen Mechanismen der NCC-Regulierung und der Kontrolle des Blutdrucks. Darüber hinaus stellt sie neue Daten und Werkzeuge vor, welche für die zukünftige Erforschung der Funktion des DCT relevant sind.

1. Introduction

1.1. Anatomy and function of the kidney

The human kidneys are paired organs located on each side of the spinal cord in the abdominal cavity [5]. Each kidney consists of two different parts, the granular outer region (cortex) and the darker inner region (medulla) that in turn comprises an outer region and an inner region. The kidneys serve several important functions in the human body, such as reabsorption of glucose, vitamins and amino acids, production of hormones (e.g., erythropoietin, renin and calcitriol), and excretion of toxic metabolites (e.g., K^+, organic acids and bases). Moreover, the kidneys maintain whole-body water and electrolyte homeostasis, including the regulation of extracellular ion concentration (e.g., Na^+, K^+, Cl^-), water retention and acid-base balance. The functional unit of the kidney is the nephron. It consists of a cluster of blood vessels, the glomerulus where initial filtration takes place, and a tubule system in which the blood filtrate is converted into urine [5]. The tubule system comprises the proximal tubule (PT), the thin loop of Henle´s loop (TL) and the distal tubule. The distal tubule can be subdivided into the thick ascending limb of Henle´s loop (TAL), the early distal convoluted tubule (DCT1), the late distal convoluted tubule (DCT2), the connecting tubule (CNT) and the collecting duct (CD) [6] (Figure 1).

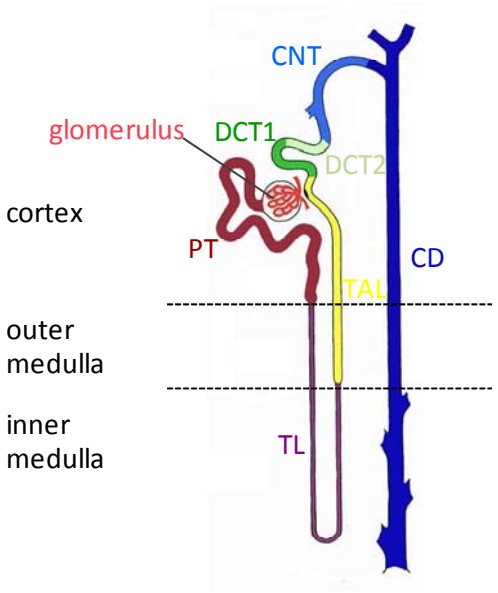

Figure 1: Structure of the nephron. The nephron consists of a glomerulus and a tubule system. The tubular system can be divided into the proximal tubule (PT), the thin loop of Henle´s loop (TL), the thick ascending limb of Henle´s loop (TAL), the early distal convoluted tubule (DCT1), the late distal convoluted tubule (DCT2), the connecting tubule (CNT) and the collecting duct (CD).

1.2. Reabsorption of Na^+ by the kidney

One main function of the kidney is to maintain the body`s water- and electrolyte-homeostasis by regulating the amount of Na^+ in the urine [5]. Approximately 98% of the filtered Na^+ is reabsorbed along the renal tubular system. Na^+ reabsorption depends on the activity of the basolaterally expressed sodium-potassium adenosine triphosphatase (Na^+/K^+ ATPase). Under ATP hydrolysis, the Na^+/K^+ ATPase pumps 3 Na^+ out and 2 K^+ into the cell and hence establishes an electrochemical gradient that helps to reabsorb Na^+ from the lumen into the cell. The majority of Na^+ reabsorption occurs in the proximal tubules and in the thick ascending limbs of Henle's loop which jointly reabsorb about 85% of the filtered sodium. However, the fine-tuning of the renal Na^+ absorption as well as Ca^{++}, Mg^{++} and K^+ excretion takes place in the post-macula-densa segments of the distal tubule [6, 7], including DCT, CNT and CD.

In the **PT**, sodium is reabsorbed by means of a variety of co-transporters that transfer sodium as well as solutes such as glucose, amino acids or phosphate across the apical membrane. In addition, sodium is reabsorbed by the sodium-hydrogen-exchanger (NHE3) [5, 8]. Sympathetic nervous system activation, low Na^+ diet as well as renal injury up-regulate the salt transport rate in the PT, whereas hypertension, inhibition of angiotensin II (AngII) production and high Na^+ diet decrease sodium uptake in the PT [8].

The electroneutral Na^+-K^+-$2Cl^-$ cotransporter (NKCC2) is the main sodium transporter in the **TAL**. The NHE3 is also present, but contributes to a much lesser extent [5]. The activity of NKCC2 depends on the function of the renal outer medulla potassium channel (ROMK) which recycles K^+ across the luminal membrane [9, 10]. Mutations in NKCC2 and mutations in the genes encoding for ROMK, chloride channel Kb, Barttin or calcium-sensing receptor can cause Bartter syndrome [11-16]. Patients suffering from this syndrome show hypokalemia and metabolic alkalosis associated with elevated plasma renin and aldosterone levels [12]. Hormones such as vasopressin, glucagon and isoproterenol via cAMP-generation stimulate salt reabsorption in the TAL, whereas atrial natriuretic peptide and nitric oxide have opposite effects [17]. Salt transport in the TAL can be blocked by loop diuretics such as bumetanide or furosemide [18].

Approximately 8% of the sodium is reabsorbed in the **DCT** by the apical localized thiazide-sensitive NaCl cotransporter (NCC). In the late DCT (DCT 2), NCC expression overlaps with the expression of the amiloride-sensitive epithelial Na^+ channel (ENaC) [19, 20]. Salt transport in the DCT is affected by hormones (e.g. AngII, aldosterone, glucocorticoids, estrogen) and other factors (e.g., alkalosis, acidosis and dietary factors) [6]. The underlying mechanisms are described in greater detail in chapter 1.4.

ENaC establishes sodium uptake in the **CNT** and **CD**. The bulk of sodium uptake occurs in the **CNT** (5%) and decreases along the downstream segment of the tubular system (1% in CD) [20]. All tubule parts that show ENaC expression are jointly referred to as the "aldosterone-sensitive distal nephron" (ASDN) which includes the DCT2, CNT and CD [21]. Sodium reabsorption in the CNT and CD is regulated by non-hormonal factors (e.g., soluble proteases or membrane-bound proteases) [22-24] and hormonal factors (e.g., aldosterone, insulin or vaspression) [25, 26]. Dysregulation of ENaC leads to a salt-losing syndrome with hypotension called pseudohypoaldosteronism type 1 or to Liddle´s syndrome including hypertension in combination with low renin and plasma aldosterone levels in combination with hypokalemia [27, 28].

1.3. Function of the DCT

The DCT is a rather short segment within the nephron. It is located downstream of the macula densa and ends at the transition to the CNT [20]. The DCT is involved in the renal control of blood pressure and in the fine-tuning of renal ion concentration (Figure 2) [6]. Ellison and co-workers have shown that transcellular Na^+ and Cl^- transport for the most part is mediated by the thiazide-sensitive NCC in the DCT1, whereas in the late DCT, Na^+ is also transported by the amiloride-sensitive ENaC [29]. Na^+ leaves the cell via the Na^+/K^+-ATPase, whereas Cl^- passes through Cl^- channels (CLC-K channels) in the DCT basolateral membrane [30, 31]. DCT cells show the highest expression of Na^+/K^+-ATPase activity along the nephron, which is located in the extensively invaginated basolateral cell membrane and driven by ATP generated by numerous mitochondria. Moreover, the DCT contributes to the fine-tuning of renal calcium, magnesium and potassium excretion (Figure2) [6]. Transcellular Ca^{++}-transport via TRPV5 and NCX, respectively, is restricted to the late DCT and CNT [7, 32], whereas Mg^{++} reabsorption is mediated by TRPM6 that co-localizes with the cytoplasmic Ca^{++} and Mg^{++}-binding protein parvalbumin (PV), suggesting that only the early DCT is involved in Mg^{++} transport [7, 33].

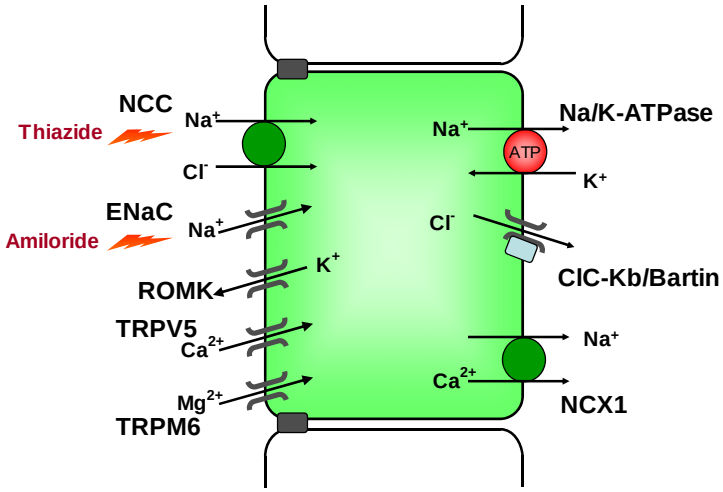

Figure 2: DCT cell model. Localization of ion channels and ion co-transporters in the DCT that contribute to the fine-tuning of Na^+, K^+, Ca^{++} and Mg^{++} transport. Thiazide-sensitive NaCl cotransporter NCC; amiloride-sensitive epithelia Na^+ channel ENaC; K^+ cannel ROMK, Ca^{++} channel TRPV5, Mg^{++} channel TRPM6 are localized in the apical membrane. Cl^- channel ClC-Kb, Na^+ Ca^{++} exchanger NCX1 and Na^+/K^+-ATPase are localized in the basolateral membrane.

The functional significance of the DCT is evidenced by the fact that the DCT serves as an important target for diuretics, by monogenic diseases and respective gene-modified mouse models [6, 34, 35]. Loss-of-function mutations in the gene encoding NCC can lead to the salt-losing Gitelman syndrome an autosomal-recessive disorder with hypokalemic alkalosis, hypocalciuria, hypokalemia, hypomagnesemia and hypotension [36]. Schultheis and coworkers have generated a mouse model with a complete deletion of NCC to investigate altered sodium homeostasis and changes in renal K^+, Ca^{++} and Mg^{++} excretion and their pathophysiological implications [37]. NCC knockout mice show some clinical features of the Gitelman syndrome including hypocalciuria and hypomagnesemia [37]. Furthermore, morphological changes in the DCT [38], higher renin [37] and aldosterone levels [38] and a decrease in mean arterial blood pressure on low Na diet$^+$ [37] could be observed. In addition, Morris and coworkers could show that NCC knockout mice become hypokalemic under low K^+ diet [39]. Reduced glomerular filtration rate and increased ENaC expression may represent compensatory effects of the Na^+ transport defect in the DCT, which might explain the lack of changes in urinary Na^+ or K^+ excretion in NCC knockout mice [38].

In contrast to the Gitelman syndrome, increased NCC activity due to mutations in the NCC-regulating **W**ith-**N**o-**L**ysine (**K**) kinases WNK1 or WNK4 are associated with Gordon syndrome or pseudohypoaldosteronism type II (PHAII). This is a rare autosomal-dominant disorder characterized by severe salt-sensitive hypertension, hyperkalemia, metabolic acidosis and hypercalciuria [40, 41]. To mimic PHAII in mice, Lalioti and coworkers introduced genomic segments harboring either

wildtype *WNK4* ($WNK4^{wt}$) or a PHAII-causing mutant of *WNK4* ($WNK4^{PHAII}$) into the mouse genome [42]. The observed phenotype including increased blood pressure, hypercalciura, hyperkalemia and enhanced NCC activity in $WNK4^{PHAII}$ mice are opposite to those of $WNK4^{wt}$ mice that display hypotension, hypocalciuria, hypokalemia and a decreased NCC expression. Thus, $WNK4^{PHAII}$ mice are a perfect model to investigate the pathophysiological consequences of increased NCC activity, whereas $WNK4^{wt}$ mice can be used to further investigate the implications of reduced NCC activity. Surprisingly, transgenic mice that over-express NCC do not show any symptoms of PHAII [43]. Furthermore, an increase in the expression of NCC could be linked to renal sodium retention in liver cirrhosis [44], obesity [45] and diabetes mellitus [46].

A characteristic feature of the DCT is its marked structural plasticity. Alterations in its ion transport activity by diuretic treatment of arterial blood pressure (e.g., thiazide, furosemide) or genetic variations (e.g., Gitelman syndrome) induce marked structural and functional changes in the DCT. Thus, an increased sodium transport rate as occurring in response to Na^+ transport inhibition by furosemide in the TAL induces cellular hypertrophy [18, 47, 48] and hyperplasia [49]. In contrast, a decrease in sodium transport rate due to the administration of thiazides leads to structural atrophy of the DCT in mice [50] and DCT cell apoptosis in rats [51]. Gene-modified mice likewise illustrate the high structural plasticity of the DCT. For example, ROMK-deficient mice show abnormalities in Na^+Cl^- reabsorption in the TAL and a compensatory increase in DCT cell growth [52, 53]. Furthermore, $WNK4^{PHAII}$ mice display strong hyperplasia of the DCT [42], whereas NCC loss-of-function mutations (Gitelman syndrome) cause atrophy of the DCT [38].

1.4. The Na^+Cl^--cotransporter- NCC

1.4.1. Structure of NCC

NCC belongs to the electroneutral cation-chloride cotransporter family that is characterized by its ability to transport Cl^- together with Na^+ and/or K^+ with a stoichiometry of 1:1 (Cl:cation) [34, 35]. Already in the nineteen-seventies, Renfro and co-workers discovered an electrically silent co-transport in teleost winter flounder (*Pseudopleuronectes americanus*), suggesting the presence of an electroneutral Na^+Cl^--cotransporter [54, 55]. In the following years, this mode of salt transport was observed to be sensitive to thiazide drugs [56]. Further research revealed that the DCT also shows a similar thiazide-sensitive Na^+Cl^--cotransport mechanism. However, a major breakthrough was achieved with the isolation of a cDNA clone encoding the electroneutral, thiazide-sensitive NCC from flounder urinary bladder [57]. Thereafter, the molecular identification of NCC from human [36, 58], rat [59], mouse [60], rabbit [61], and eel kidney [62] was successful. Hence it was possible to generate antibodies against NCC and to demonstrate that NCC is specifically expressed in the DCT

[63, 64]. The gene encoding NCC is located on chromosome 16q13 in humans, on chromosome 19p12 in rats and on chromosome 8 in mice [35]. In humans, NCC is encoded by a 55kb-long *SLCA13* gene containing 26 exons [36]. Interestingly, two sequences of human NCC were described. Simon and coworkers identified an NCC-sequence containing 1021 residues [36], whereas Mastroinanni and colleagues [58] described a 1030-long NCC sequence, with both sequences differing in 17-26 amino acid residues in the domain that are not present in mice and rats [34]. Human NCC displays 90% identity with other mammalian NCC [34].

NCC is a membrane-protein comprising 12 transmembrane-spanning regions that are flanked by a short hydrophilic amino-terminal domain and a predominantly hydrophilic long carboxy-terminal domain located within the cell (Figure 3) [34]. Transmembrane domain 7 is connected to the transmembrane region 8 by a hydrophilic loop, containing two N-glycosylation sites (N404 and N424). Glycosylation of NCC is assumed to be essential for its activity. Mutations in one glycosylation site cause a decrease in NCC activity by 50% and the elimination of both sites leads to a reduction of 95% [65]. Furthermore, lack of glycosylation leads to reduced surface expression [65]. On western blot, NCC is characterized by a glycosylated band (120 to 140 kDa) and a non-glycosylated (95 to 110 kDa) form [60, 66], with both forms present in the kidney [60].

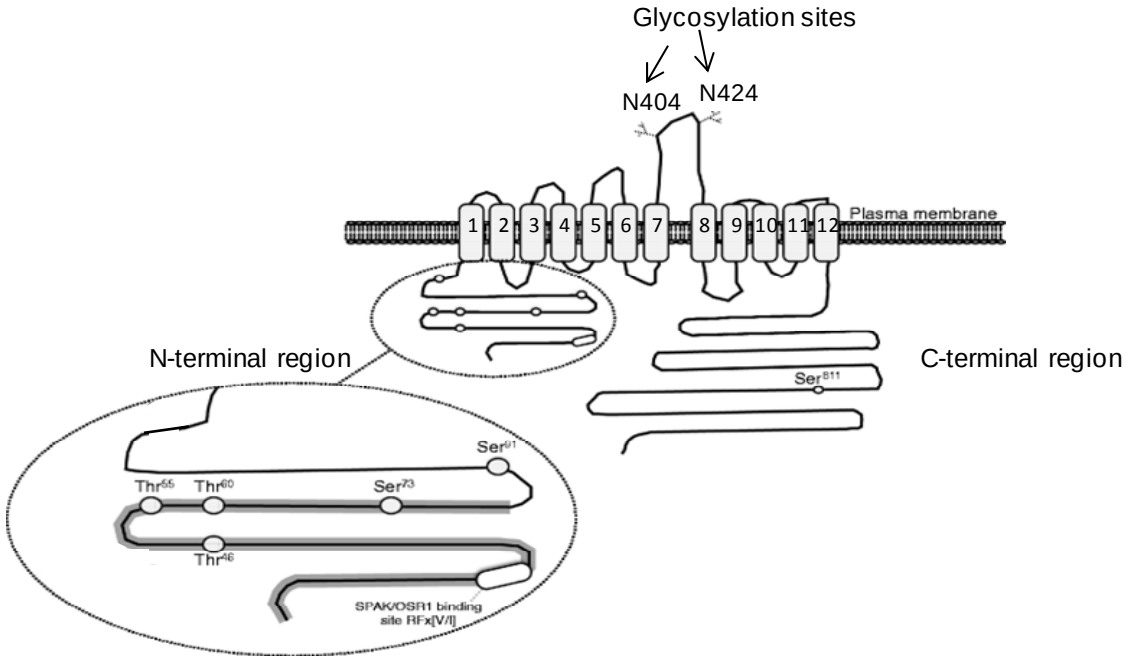

Figure 3: Proposed topology for NCC. NCC is encoded by the gene *SLCA13* in humans and consists of 12 transmembrane regions that are flanked by a short N-terminal domain and a long C-terminal domain. A cellular loop exhibits two N-glycosylation sites and links transmembrane region 7 and transmembrane region 8. The N-terminal region is characterized by the presence of several phosphorylation sites, including Thr 46, Thr 55, Thr 60, Ser 73 and Ser 91. In addition, a highly conserved motif (RFXI) that interacts with SPAK and OSR1 is also found in the N-terminal domain. Adapted from [67].

Initially it was thought that NCC is specifically expressed in the DCT of the kidney. However, Bazzini and coworkers have shown that NCC might also play a role in Ca^{++}-homeostasis of the intestine [68]. Moreover, data generated by Dvorak and coworkers suggest that thiazides increase bone mineral density and stimulate osteoblast differentiation by interacting with NCC [69]. NCC expression has likewise been suggested in brain [70], blood vessels [71], pancreas [72], peripheral blood mononuclear cells [73], gallbladder [74] and heart [75]. However further studies are necessary to confirm the abundance of NCC in these organs.

1.4.2. Mechanism of NCC regulation

NCC activity is regulated by hormonal (e.g. Ang II, aldosterone, AVP, insulin) and non-hormonal factors (e.g. tubular sodium load, metabolic alkalosis or acidosis, different Na^+ diet) [6, 34, 35]. Furthermore, recent studies have identified a network of kinases and phosphatases (e.g., WNK kinases, Ste20-Related Proline/Alanine-Rich Kinase (SPAK)/oxidative stress-responsive kinase 1(OSR1)

and Protein Phosphatase 4 (PP4)) that can regulate NCC as well [67, 76-78]. All these regulatory factors influence NCC activity by several mechanisms including changes in protein expression by ubiquitylation, trafficking to the apical membrane or phosphorylation.

1.4.3. Phosphorylation of NCC

The N-terminal region of NCC in humans comprises several phosphorylation sites including threonine 46, threonine 55, threonine 60, serine 73 and serine 91 (Figure 3) that are equivalent to the phosphorylation site threonine 44, threonine 53, threonine 58, serine 71 and serine 89 in mice and rats [2]. Pacheco-Alvarez and coworkers were the first to show that increases in NCC activity correlate with enhanced phosphorylation of conserved threonine and serine amino acids within the N-terminal region [79]. The group used *Xenopus laevis* oozytes expressing rat NCC, demonstrating that incubation in a hypotonic low Cl^--medium elevates phosphorylation levels at threonine 53 and threonine 58 and is associated with an increase in NCC-transport activity without any changes in membrane protein expression. Conversely, changing these threonine residues to alanine prevents NCC activation in response to intracellular Cl^- depletion. Further experiments using human embryonic kidney 293 cells (HEK 293 cells) expressing human NCC could confirm that low Cl^- hypotonic stress enhances the phosphorylation of threonine 55 and threonine 60, and revealed two new phosphorylation sites at threonine 46 and serine 91 that react in the same way [80]. Furthermore, these studies also confirmed that changing threonine 60 to alanine prevents the phosphorylation of all other phosphorylation sites, supporting the assumption brought forward by Pacheco-Alvarez and coworkers [79] that threonine 60 and threonine 58 are the key elements in the regulation of NCC activity in humans and rodents, respectively. The importance of this phosphorylation site is underlined by the fact that some patients suffering from Gitelman syndrome show a mutation in threonine 60 [81, 82]. Moreover, mice harboring a $WNK4^{D561A/+}$ mutant in the genome and presenting the phenotype of PHAII display elevated NCC phosphorylation levels at serine 71 [83]. All these observations suggest that NCC phosphorylation is necessary for NCC-dependent control of renal Na^+ Cl^- excretion and blood pressure.

Large-scale proteomics of human urine and rat kidney cortex revealed two further phosphorylation sites. Serine 811 is present in humans but could not be detected in rodents [84], Serine 124 was found in rat [85]. Recently, Rosenbaek and coworkers reported that Serine 124 abundance is increased by administration of a vasopressin type-2 receptor specific agonist and by a reduction in dietary Na^+ intake [86].

The cellular site where NCC phosphorylation occurs is not yet clear. Studies in *Xennopus laevis* ooytes have revealed that NCC phosphorylation is associated with the apical plasma

membrane without altering protein abundance at the cell surface [78, 79]. Furthermore, Sorensen and coworkers showed in mice that dietary K^+ causes dephosphorylation of NCC in the apical membrane while the total expression of NCC remain unchanged (Sorensen et al. 2012, in press). However*, in vivo*, following vasopressin treatment NCC phosphorylation already occurs in sub-apical intracellular vesicles with an enhanced luminal abundance of NCC [87]. Corroborating these findings, Rosenbaek and coworkers [86] detected the NCC phosphorylation site Serine 124 in sub-apical intracellular vesicles and also in the apical plasma membrane. Furthermore, $WNK4^{D561A/+}$ mice show an increased NCC phosphorylation level alongside an increase in NCC expression on the cell surface [83]. A RFXI motif is present in the N-terminal domain and is responsible for SPAK/OSR1 interaction and it was also shown that this motif is necessary for maximal phosphorylation and activation of NCC in HEK 293 cells [2].

1.4.4. Trafficking of NCC

Under physiological conditions, NCC is present in intracellular vesicles that undergo exocytosis and endocytosis. However, little is known about the interplay with other proteins that might regulate trafficking of NCC to the membrane and degradation of the protein.

It is suggested that WNK4 plays a key role in the mechanism behind the degradation of NCC via the lysosomal pathway [88, 89]. Subramanya and coworkers demonstrated that WNK4 attenuates NCC delivery from the trans-Golgi apparatus to the cell surface without affecting the net rate of co-transporter internalization. In addition, they could show that WNK4 enhances the interaction with NCC and AP-3, an adaptor protein that modulates the transport from endosomes to lysosomes [89]. WNK4 promotes the degradation of NCC in the lysosome also via a sortilin-mediated pathway [88]. Sortilin is a single-pass transmembrane protein in the DCT that transports peptides from the Golgi apparatus to the lysosomes [88]. However, these data were mainly obtained in transient over-expression experiments and indirect protein-protein interaction studies. Further research is needed to investigate NCC trafficking under more physiological conditions *in vivo*. It is already known that Ang II promotes the trafficking of NCC from sub-apical vesicles to the cell surface in rats [90], but which protein mediates the transport of NCC to the apical membrane is unclear. Lee and coworkers found that acute hypertension induces NCC trafficking from the cell surface to cytoplasmic vesicles [91]. However, the underlying molecular pathway is likewise not yet known.

1.4.5. Ubiquitylation of NCC

Ubiquitin is a highly conserved, 76 amino acid-long polypeptide that binds to its target protein via an isopeptide bond on the ε-amino group of lysine [92]. Ubiquitin can also be conjugated to other ubiquitin peptides via lysine residues [93]. The conjugation with ubiquitin is dependent on an enzymatic mechanism including an E1 (ubiquitin-activating) enzyme, E2 (ubiquitin-conjugating enzyme) and an E3 (ubiquitin-ligase) enzyme [92]. So far, two classes of E3 ligases have been described. The largest family of E3 ligases comprises over 600 members and contains a RING (really interesting new gene) domain that enables the transfer of ubiquitin from E2 to the substrate [92]. The second class is the HECT (homologous to E6-AP C-terminus) family that comprises 28 members and can be divided into Nedd4-2, HERC- and other HECT families [94]. The HECT family directly binds to ubiquitin and transfers it onto the substrate [92].

Many channels and co-transporters in the kidney are controlled by ubiquitylation [92]. The conjugation with ubiquitin often results in the degradation of the protein by proteasomes or lysosomes [95, 96]. A well-studied protein in this context is ENaC. Nedd4-2 directly binds ubiquitin to a proline- and tyrosine-rich (PY) motif within this channel, which leads to endocytosis of the protein [92]. NCC is also known to be modulated by ubiquitylation [97-99]. Arroyo and coworkers have demonstrated that Nedd4-2 decreases NCC expression on the cell surface and also hampers its activity [98]. This effect is abolished by serum-glucocorticoid-regulated kinase (SGK1) which inhibits the interaction of Nedd4-2 with NCC. In contrast to ENaC, this mechanism does not require the PY motif in NCC [98]. These results were strengthened by the observation that mice with a conditional knockout of Need4-2 in the kidney show enhanced NCC expression [98], whereas mice without SGK1 expression in the kidney exhibit a decrease in NCC expression [100].

That NCC might be regulated by ubiquitylation is also indicated by the recent finding that mutations in genes encoding for kelch-like 3 and Cullin 3, which are implicated in complex-binding with a RING ubiquitin-ligase, cause PHAII [101]. Consistent with this assumption, kelch-like 3 is mostly expressed in the DCT and its down-regulation by siRNA in transiently transfected NCC-HEK cells results in enhanced NCC expression on the cell surface [102]. Kelch-like 3, encoded by the *KLHL3* gene, comprises three domains, the N-terminal-localized BTB (bric-a-brac, tramtrack, broad complex) domain, a BACK (BTB and C-terminal kelch region) domain and a kelch domain composed of six kelch repeats [102]. The BTB and BACK domains of Kelch 3 are recognized by Cullin 3-containing RING-ubiquitin ligase complex [103] which promotes the transfer of ubiquitin from E2 ligases onto the substrate [104]. Interestingly, PHAII-patients who exhibit mutations in Kelch 3 or Cullin 3 show a more severe phenotype than patients with WNK1 or WNK4 mutations [101].

1.4.6. Regulation of NCC by the WNK –SPAK/OSR1 pathway

The identification of the WNK-SPAK/OSR1 regulatory pathway was a major advance in the understanding of the molecular mechanisms that control NCC function. After phosphorylation of OSR1 and SPAK by WNK kinases, OSR1 and SPAK phosphorylate NCC on conserved serine/threonine residues in the N-terminal region and hence activate NCC.

WNK kinases are serine/threonine kinases and bear their name because they lack a highly conserved lysine residue crucial for binding ATP in the subdomain II of the catalytic domain where it is located in most other serine/threonine kinases [105]. Many organisms express WNK kinases, e.g., *Arabidopsis thaliana* exhibits nine WNK kinases while four WNK kinases have been described in mammals, two in *Xenopus sp.* and one WNK kinase in *Caenorhabditis elegans* [4, 106]. Interestingly, so far no WNK kinases have been found in yeast or bacteria, suggesting that WNK kinases are rather involved in multi-cellular biological functions [106].

In humans, genes encoding for WNK1-4 are located on chromosome 12p13.33 (WNK1), 9q22.31 (WNK2), Xp11.22 (WNK3) and 17q21.31 (WNK4) [4]. RT-PCR and Northern Blot analysis have revealed that WNK kinases are expressed not only in the kidney but also in brain, heart, lung, bone, testes and the gastrointestinal tract [4, 105]. However, due to the lack of well-validated antibodies for WNK kinases, respective data on protein levels are still missing.

The structure of WNK kinases can be divided into a homologous kinase region located in the N-terminus of the protein, followed by an autoinhibitory region with phenylalanine residues that are separated by a single amino acid, an autophosphorylation region, and coiled-coil domains near the C-terminus (Figure 4). The kinase domains of WNK kinases display 84% homology. WNK1 has two major transcripts, the ubiquitously expressed long isoform (L-WNK1) which contains the whole kinase domain, and the kidney-specific short isoform (KS-WNK1) that lacks kinase activity [4] (Figure 4). The autoinhibitory domain consists of around 70 amino acids, is located outside the catalytic domain and displays 46% identity between the members of the WNK family [107, 108]. Furthermore, it is known that WNK kinases can regulate the activity of other WNK kinases. For example, Yang and coworkers described that WNK1 and WNK3 can phosphorylate WNK4 *in vitro* [109]. In addition, other *in vitro* experiments revealed that the WNK4 autoinhibitory domain suppresses the catalytic domains of WNK1, WNK2 and WNK3 [107, 109, 110]. The coiled-coil domain that is also present in all WNK kinases, is assumed to play an important role in the interaction with other proteins and in the formation of protein complexes [4].

A variety of additional data suggest that WNK kinases do not only regulate NCC but also NKCC2, ENaC and ROMK, which may contribute to the rather complex phenotype of patients with FHHt. However it needs to be kept in mind that most of these data were generated in *in vitro*-systems while the FHHt

phenotype of mouse models usually can be corrected by giving thiazides, only [4, 35, 105, 106, 111]. In summary, WNK kinases have important roles in the regulation of blood pressure [111], cardiovascular system development [112] and function of the sensory nervous system [113]. Furthermore, mutations of WNK kinases are associated with cancer [114], autism [115] and osteoporosis [116].

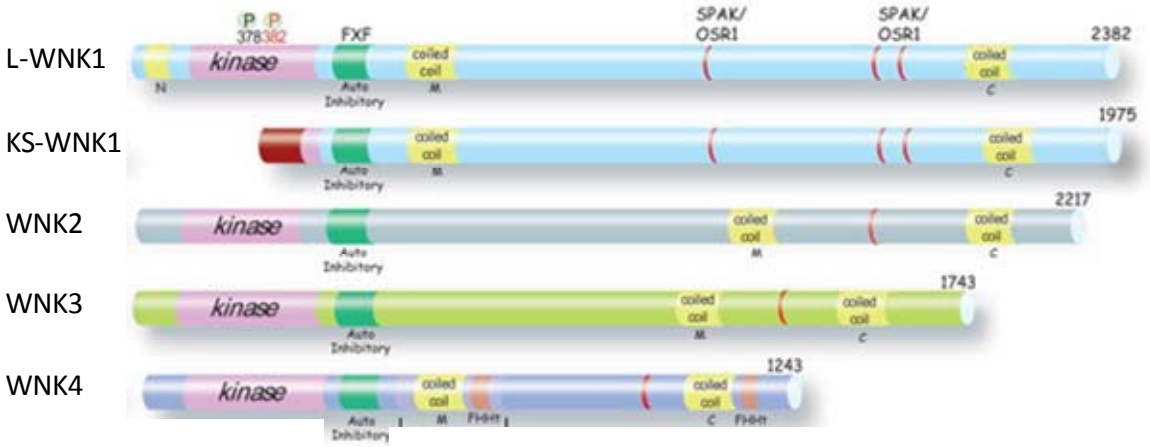

Figure 4: Structure of WNK kinases. WNK kinases are shown in amino-acids-length. All members of the WNK family except KS-WNK consist of a kinase domain (pink). All kinases contain an autoinhibitory domain (green) with essential phenylalanine residues (F) that are separated by a single amino acid (X) as well as coiled domains (yellow) located in the middle (M) and on the C-terminus (C) of the protein. In addition, WNK1 exhibits an N-terminal-located coiled-coil region (N). Phosphorylation sites P378 and P382 that are required for proper function of WNK1 are also shown. A cysteine-rich region located at the N-terminus of KS-WNK1 is shown in dark red. SPAK/OSR1 binding sites are colored red and FHHt mutations are marked orange. Figure adapted from [4].

WNK kinases are not able to directly phosphorylate members of the *SLCA12* family (NCC, NKCC1, NKCC2). So far only SPAK and OSR1 represent physiological substrates of WNK kinases in the kidney. They are members of STE20 family and share 68% of their sequence. The N-terminal located catalytic domains of these proteins display 89% homology and are followed by a conserved 51 amino acids long serine-motif and a C-terminus-located CCT domain that is 80% identical in sequence (Figure 5) [117, 118]. The CCT domain has a multipurpose docking site and interacts with an RFXI/V motif that is present in all members of the SLCA12 family as well as in WNK kinases [118, 119]. SPAK and OSR1 differ only in an additional proline-alanine-rich domain that is present within the first 50 amino acid

residues of SPAK but not in OSR1 [117, 118]. In mammals, SPAK and OSR1 are widely expressed [119]. In the kidney, OSR1 is expressed along the entire nephron [120], whereas SPAK expression is restricted to the TAL and DCT [121]. Interestingly, a recent study by McCormick and coworkers has shown that three SPAK isoforms are expressed in the kidney, i.e., full-length SPAK, SPAK2 and kidney-specific SPAK (KS-SPAK) [122]. Full-length SPAK is mostly abundant in the DCT and to a lesser extent in the TAL, whereas KS-SPAK is predominantly expressed in the TAL and less so in the DCT. The study also indicates that KS-SPAK inhibits full-length SPAK, OSR1 as well as NCC *in vitro*.

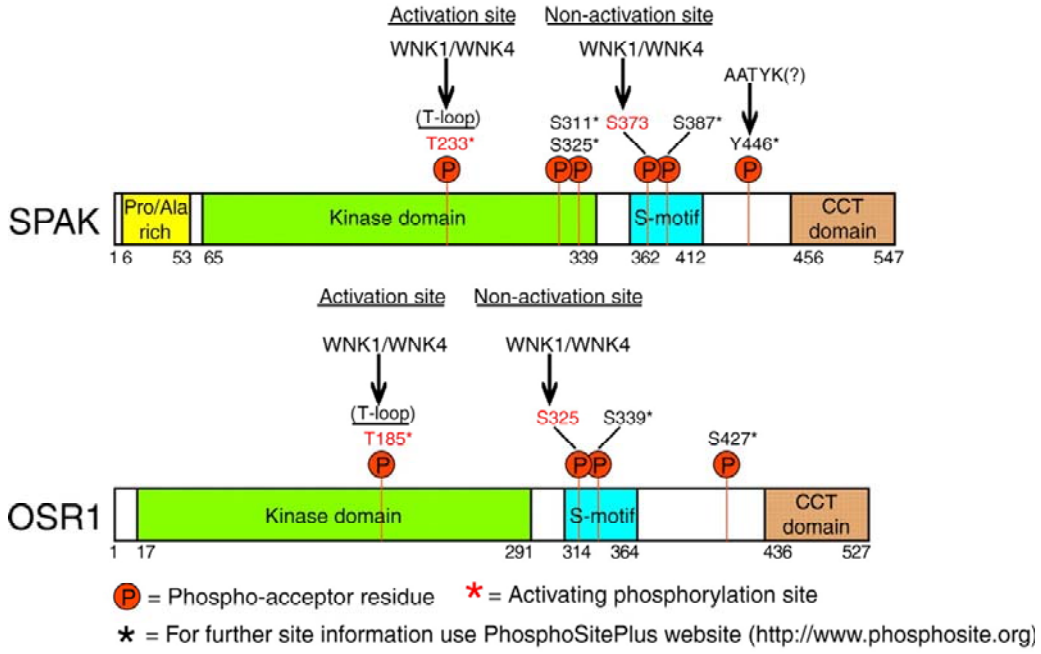

Figure 5: Structure of SPAK and OSR1. Both proteins are shown in amino-acids-length. They consist of a kinase domain, followed by a serine-motif (S-motif) and a CCT region located at the C-terminus. The major difference between SPAK and OSR1 is the proline-alanine-rich domain (P/A rich) that is present at the N-terminus of SPAK. WNK1 and WNK4 can activate both proteins by phosphorylation of threonine 233 in SPAK and threonine 185 in OSR1. In addition, WNK1 and WNK4 are able to phosphorylate SPAK and OSR1 at serine 373 and serine 325, respectively. Further phosphorylation sites are highlighted in black and are reported on the PhosphoSitePlus website. Figure was taken from [2].

WNK1 and WNK4 activate SPAK and OSR1 by phosphorylation of conserved threonine residues in the T-loop of the catalytic region (threonine 233 in human SPAK, threonine 185 in human OSR1, threonine 243 in mouse SPAK) [117]. In addition, WNK1 and WNK4 phosphorylate SPAK and OSR1 also at serine residues in the S-region (serine 373 in human SPAK, serine 325 in human OSR1) but this phosphorylation does not lead to an activation of SPAK or OSR1 [117]. Once activated, SPAK and

OSR1 can activate their target proteins including NKCC1, NKCC2 and NCC. Richardson and coworkers have shown that SPAK and OSR1 are able to directly phosphorylate human NCC at three conserved residues (threonine 46, threonine 55 and threonine 60) [80]. They could further show that NCC also interacts with SPAK and OSR1 via the RFXI motif located at the N-terminus. The importance of NCC-phosphorylation by SPAK was underlined by studying the phenotype of SPAK Thr243Ala knockin ($SPAK^{243A/243A}$) [121] and SPAK knockout mice [119, 123]. Rafiqi and coworker generated knockin mice in which SPAK cannot be activated by WNK1 and WNK4 due to substitution of SPAK threonine 243 with an alanine [121]. These knockin mice show a salt-dependent reduction in blood pressure, hypomagnesemia and hypocalciuria. Furthermore, mild hypokalemia develops when $SPAK^{243A/243A}$ mice received a low Na^+ diet. Expression and phosphorylation levels of NCC and NKCC2 are significantly reduced, which might explain reduced blood pressure in $SPAK^{243A/243A}$ knockin mice [121]. Yang and coworkers generated SPAK knockout mice via the deletion of exon 9 and exon 10 of the SPAK gene [123]. These mice exhibit also some features of the Gitelman-sydrome including hypotension, hypokalemia, hypomagnesemia and hypocalciuria. NCC phosphorylation and expression are likewise decreased. However, SPAK knockout mice show an increase in total NKCC2 expression as well as elevated NKCC2-phosphorylation levels and increased levels of OSR1. This phenotype of SPAK knockout mice could be partially confirmed by a study of McCormick and coworkers [122] who examined SPAK knockout mice with a disruption of the SPAK gene after exon 6 originally generated by Delpire and colleagues [119]. These SPAK knockout mice show no change in arterial blood pressure on a normal diet. However, under Na^+ depletion, the mice become hypotensive. Furthermore, they show a tendency to hypokalemia and hypomagnesemia and have significantly lower urinary calcium levels. Moreover, this SPAK deletion causes a reduction in NCC expression and phosphorylation, while NKCC2 abundance and phosphorylation is increased. In addition, phosphorylation of OSR1 is likewise increased. The observation that SPAK deletion stimulates NKCC2 but inhibits NCC might be explained by the fact that there are no isoforms of SPAK in both knockout models. McCormick and coworkers therefore suggested that KS-SPAK (predominantly expressed in the TAL) acts more strongly as an inhibitor of NKCC2 rather than an activator of NKCC2, whereas the full-length SPAK (predominantly expressed in the DCT) serves as an activator of NCC. When SPAK is entirely deleted along the nephron, the inhibitory effect of KS-SPAK is also absent and expression of NKCC2 increases whereas in the DCT, the stimulatory effect of full-length SPAK on NCC is disrupted, leading to a decrease in NCC expression. The function of OSR1 *in vivo* has not been clarified yet because mice with an inactive OSR1 or mice with OSR1 knockout die *in utero* [119, 121, 123].

1.4.6.1. Role of WNK1 in the regulation of NCC

As outlined above, two splice variants of WNK1 are expressed in the kidney, i.e., the full-length WNK1 (L-WNK) and the DCT- and CNT-specific KS-WNK1 isoform. So far there is no evidence that WNK1 directly interacts with NCC. Instead, WNK1 appears to be a key element in the regulation of other WNK kinases, thereby indirectly affecting NCC activity [110, 124, 125]. Yang and coworkers could show that L-WNK1 suppresses WNK4 and hence activates NCC [126]. This process is modulated by KS-WNK1 as it prevents the L-WNK1-induced inhibition of WNK4, thereby allowing WNK4 to inhibit, respectively, down-regulate NCC [127] (Figure 6). This mechanism might explain the development of PHAII, where a deletion of intron 1 in WNK1, results in increased expression of L-WNK1 and elevated NCC activity , which enhances salt reabsorption in the DCT and thus increases arterial blood pressure [35, 128].

Experiments with transgenic mice demonstrate how L-WNK1 and KS-WNK1 affect NCC activity and blood pressure. A complete deletion of WNK1 causes embryonic lethality, suggesting an important role of WNK1 during development [129]. Zambrowicz and coworkers analyzed WNK1 heterozygous mice and showed that these mice are hypotensive due to a decrease in WNK1 expression [129]. Liu and colleagues investigated the role of KS-WNK1 *in vivo*. They generated KS-WNK1 over-expressing and KS-WNK1 deficient mice [125]. Mice over-expressing KS-WNK1 are hypotensive with reduced expression and phosphorylation of NCC. In addition, these mice exhibit elevated aldosterone and Ang II levels. In contrast, KS-WNK1 knockout mice show enhanced levels of NCC expression and phosphorylation. However, blood pressure does not differ between wildtype and KS-WNK1 knockout animals on standard diet, but KS-WNK1 knockout animals that are fed a high Na^+ diet become hypertensive [125]. Another KS-WNK1 knockout model was generated by Hadchouel and coworkers [130]. On standard diet, these KS-WNK1 knockout mice show increased expression and phosphorylation of NCC without increased blood pressure [130]. Moreover, they display a decrease in expression and activation of ENaC that could be due to decreased plasma aldosterone levels [130]. The authors explain the lack of change in blood pressure in these mice with the possible emergence of compensatory mechanisms so that the increase in NCC expression might not be sufficient to cause hypertension.

1.4.6.2. Role of WNK3 in the regulation of NCC

WNK3 can be found in all tubules segments of the nephron as well as in several epithelial and non-epithelial cells outside the kidney [76]. In the kidney, WNK3 is a powerful activator of NCC and in turn, NCC activity is inhibited in kinase-dead WNK3 mutants [76, 128]. WNK3-induced NCC activation is associated with increased abundance of NCC at the cell surface [128, 131] as well as phosphorylation of its threonine residue T58 [132]. Glover and colleagues assume that this mechanism relies on a SPAK-independent pathway because co-expression studies with WNK3, NCC and a dominant negative SPAK kinase-dead mutant (D212A) revealed that the activation of NCC by WNK3 is not affected [131]. However, Pacheco-Alvarez and coworkers mutated all SPAK binding sites (241 RFxV, 872 RFxV and 1336 RFxV) in WNK3 and showed that the elimination of sites F873 and F1337 does not prevent the WNK3-activation of NCC but that the deletion of F242 results in a complete inhibition of NCC, suggesting that WNK3-SPAK interaction is required [132]. Furthermore, it is proposed that WNK3 and WNK4 are associated in protein complexes and compete with each other to regulate NCC activity [109]. Interestingly, FHHt-mutant WNK4 (Q562E) completely lacks the ability to suppress WNK3 activation of NCC [109].

1.4.6.3. Role of WNK4 in the regulation of NCC

WNK4 is mainly expressed in the aldosterone-sensitive nephron [41]. Over-expression of wildtype-WNK4 together with NCC in *Xenopus laevis oocytes* as well as in mammalian cells demonstrated that WNK4 inhibits the activity of NCC by reducing NCC expression in the plasma membrane [126, 133-135]. Further studies revealed that WNK4 promotes the degradation of NCC into lysosomes by a sortilin-dependent pathway [88, 89, 134]. Chimeric studies of WNK3 and WNK4 showed that the N-terminus of WNK4 is an important mediator of the inhibitory effect on NCC [136]. In contrast, PHAII-WNK4 mutation (Q562) causes a decrease in the inhibitory effect of WNK4 on NCC activity and trafficking [126, 133]. San-Cristobal and coworkers demonstrated in *Xenopus laevis oozytes* that Ang II converts WNK4 into a stimulator of NCC by activation of the SPAK/OSR1 pathway [137]. This result was confirmed by Castaneda-Bueno and colleagues who demonstrated the same mechanism *in vivo* [138]. Furthermore, recent studies aiming at unraveling the effect of WNK4 on NCC function revealed that aldosterone as well as insulin can also convert WNK4 into an activator of NCC [139, 140]. In summary, WNK4 is able to activate or inhibit NCC depending on its state of activation. Under standard conditions WNK4 is assumed to reduce NCC activity whereas, in the presence of stimuli (e.g., Ang, aldosterone, insulin) or when WNK4 is mutated, leading to PHAII, the inhibitory effect of WNK4 on NCC can be converted to an activation of NCC (Figure 6).

Experiments in transgenic mice bearing either two additional copies of wildtype-WNK4 ($WNK4^{wt}$) or of PHAII mutant WNK4 (Q562E; $WNK4^{PHAII}$) support the assumption that wildtype WNK4 is a negative regulator of NCC whereas the PHAII WNK4 mutant has stimulatory effects on NCC [42]. $WNK4^{wt}$ mice show reduced blood pressure, a modest decrease in Mg^{++} level and hypocalciuria. In addition, $WNK4^{wt}$ mice on low K^+ diet become hypokalemic. Furthermore, morphological studies revealed that additional copies of WNK4 decrease the expression of NCC in the kidney cortex. In contrast, mice harboring the PHAII WNK4 mutant exhibit arterial hypertension, hypercalciura, hyperkalemia and increased abundance of NCC with hyperplasia of the DCT. These defects could be corrected by administration of thiazide or by crossing $WNK4^{PHAII}$ mice with NCC null mice, suggesting that the $WNK4^{PHAII}$-phenotype depends on the activation of NCC. Yang and coworkers could confirm these findings by using another transgenic mouse model that has one normal allele of WNK4 and one WNK4 PHAII mutant allele (D561, $WNK4^{D561A/+}$)[83]. This model mimics PHAII with regard to hyperkalemia, metabolic acidosis and hypertension. Furthermore, $WNK4^{D561A/+}$ mice show increased phosphorylation of NCC, SPAK and OSR1. This PHAII phenotype could be likewise corrected by thiazide administration. Chiga and coworkers used the same mice to investigate dietary effects on the phosphorylation levels of SPAK, OSR1 and NCC [141]. They could show that a low Na^+ diet enhances the phosphorylation of the SPAK/OSR1-NCC cascade, whereas a high Na^+ diet leads to a decrease in the phosphorylation levels of SPAK, OSR1 and NCC. Furthermore, the elevated phosphorylation levels were reversed by spironolactone treatment and the administration of aldosterone caused an increase in the phosphorylation of the SPAK/OSR1-NCC cascade. These regulatory mechanisms were completely lost in $WNK4^{D561A/+}$ mice due to a constitutively active NCC.

Mu and coworkers demonstrated that salt loading promotes the down-regulation of WNK4 by beta-adrenergic pathways leading to an increase in NCC expression and the development of salt-sensitive hypertension [142]. Interestingly, glucocorticoid receptors appear to play an important role in the regulation of WNK4. In addition, it is suggested that calcineurin inhibitors (e.g., cyclosporine and tacrolimus) that are used to prevent rejection of transplanted organs are in involved in the WNK4-SPAK/OSR1-NCC pathway. Hoorn and coworkers discovered that tacrolimus leads to an increase in the phosphorylation of NCC, WNK3, WNK4 and hence salt-sensitive hypotension [143]. Treatment with thiazide diuretics reversed the tacrolimus-induced hypertension. Additionally, Melnikov and colleagues showed that cyclosporine treatment leads to hypertension and increases WNK4 protein expression in the rat kidney. Furthermore, they also observed elevated WNK4 protein expression followed by increased levels of NCC phosphorylation in vitro [144].

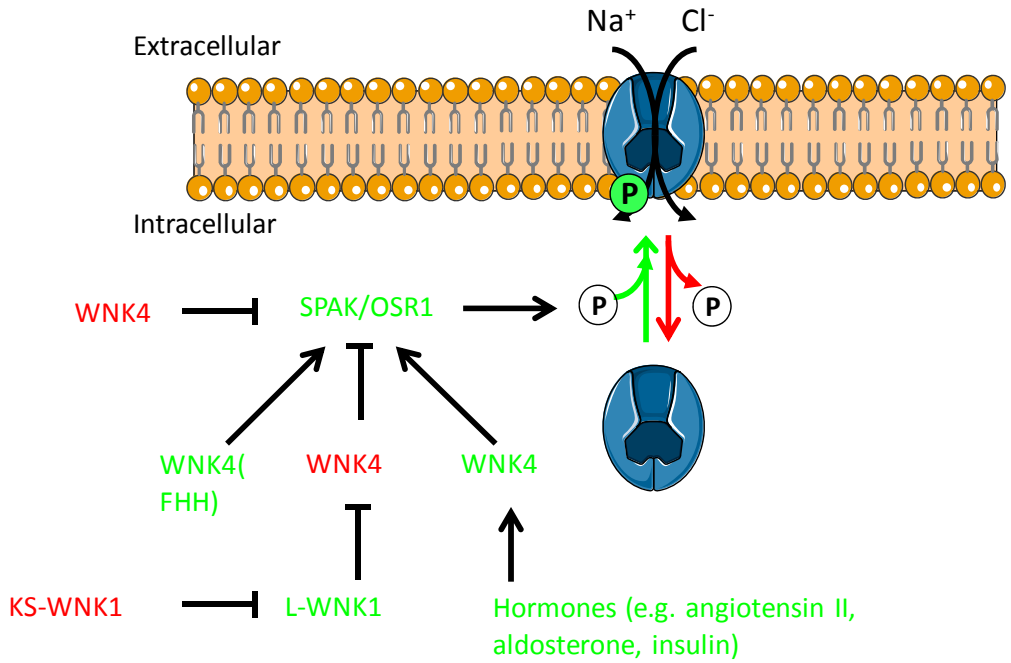

Figure 6: Control of NCC by WNK-SPAK/OSR1 pathway. WNK1 and WNK4 are serine/threonine kinases that interact with SPAK and OSR1 to regulate phosphorylation and hence activity of NCC. Under standard conditions WNK4 is thought to reduce NCC activity. However, WNK4 mutations or hormones such as angiotensin II or aldosterone can convert WNK4 to an activator of NCC. Furthermore, WNK4 can be regulated by WNK1. WNK1 has two splice variants. The long isoform (L-WNK1) suppresses WNK4 and hence activates NCC. The kidney-specific short isoform of WNK1 (KS-WNK1) suppresses L-WNK and hence inactivates NCC. NCC activating and inhibiting kinases are printed in green and red, respectively.

1.4.7. Additional pathways controlling NCC

1.4.7.1. Serum- and glucocorticoid-inducible kinase 1 (SGK1)

The aldosterone-induced protein serum- and glucocorticoid-inducible kinase 1 (SGK1) is involved in the regulation of renal Na^+ and K^+ homeostasis [38, 145, 146]. Experiments in heterologous expression systems as well as in transgenic mice indicate an import role for SGK1 not only in the regulation of ENaC [147] but also in the control of NCC [148-150]. It is known that dietary Na^+ restriction leads to an increase in NCC expression and elevated NCC phosphorylation at threonine 53, threonine 58 and serine 71 [6, 34]. Interestingly, this positive effect on NCC expression and phosphorylation is attenuated in mice lacking the SGK1-gene, suggesting that SGK1 to a certain extent affects the phosphorylation of NCC [149]. Moreover, Rozansky and coworkers have described an inhibitory effect of SGK1 on WNK4 *in vitro*. SGK1 binds and phosphorylates WNK4 at two sites, i.e.

serine 1169 and serine 1196, leading to the activation of NCC [150]. Mutation of these two phosphorylation sites into aspartate reverses the inhibitory effect of WNK4 on NCC activity [150].

1.4.7.2. γ-adducin

Adducins are heteromeric cytoskeletal membrane proteins implicated in spectrin-actin binding [151]. Previous studies in humans and hypertensive rat models suggested a role of adducins in renal salt homeostasis and blood pressure regulation [152-154]. Dimke and coworkers identified γ-adducin as a novel binding partner of NCC by mass spectrometry in pull-down experiments on mouse kidney lysates using the N-terminal domain of NCC as bait [155]. The authors also showed that γ-adducin co-localizes with NCC and by over-expression-studies in *Xenopus laevis* oocytes demonstrated that γ-adducin stimulates NCC activity in a dose-dependent manner. Mutations of the phosphorylation sites threonine 55, threonine 60 and serine 73 of NCC into aspartates completely abolish the positive effect of γ-adducin, suggesting that γ-adducin only binds NCC when the co-transporter is dephosphorylated [155].

1.4.7.3. Protein phosphatase 4

Protein phosphatase 4 (PP4) is a ubiquitously expressed serine/threonine phosphatase of the phospho-protein family (PPP) and serves a variety of functions in the cell [156]. Interestingly, other members of the PPP family (PP1 and PP2) are known to regulate the phosphorylation of K^+-coupled-chloride-co-transporters in the kidney. Recently, Glover and coworkers have shown in *Xenopus laevis* oocytes that PP4 strongly inhibits NCC activity whereas PP2A has no effect on the co-transporter [78]. This inhibitory effect of PP4 is dependent on the presence of the conserved phosphorylation site threonine 58 of NCC. Furthermore, the authors could show that PP4 is expressed in the distal nephron, suggesting that PP4 is involved in the regulation of NCC phosphorylation and activity.

1.4.7.4. Arginine vasopression

Arginine vasopression (AVP), also known as antidiuretic hormone (ADH), is released from the posterior pituitary when plasma osmolality rises or when blood pressure drops. Hence, AVP is able to increase arterial pressure as well as urine osmolarity. It binds to G-coupled receptors (V1 and V2) so that cellular cAMP levels are increased.

It is well established that AVP is involved in the regulation of NKCC2, ENaC and aquaporin 2 [157]. However, for some time it was not clear if AVP also acts on the DCT. Mutig and colleagues were the first who described the presence of the V2-receptor in human-, mouse- and rat-DCT [158]. Later work

of the same group indicated that short-term treatment with AVP (30 min) causes an increase of NCC expression on the cell surface as well as increased phosphorylation levels of NCC at threonine 53 and serine 71 [87]. Interestingly, the increase in the phosphorylation of serine 71 was not observed in DCT2 cells, suggesting that AVP affects NCC activity only in the DCT1. In contrast, Pedersen and coworker found that the early and late DCT respond to AVP by increasing intracellular Ca^{++} [159]. Furthermore, they also showed that AVP increases the phosphorylation of NCC independent of the activation of the renin-angiotensin-aldosterone system (RAA-system), and that SPAK/OSR1 is involved in the AVP-induced activation of NCC [87]. Nevertheless, Morel and coworkers reported that isolated mouse and rat DCTs have no or very little vasopressin sensitivity when exposed *in vitro* to the V2-agonist DDAVP [160]. Thus, additional research is needed to confirm that the effects described by Mutig et al. and Pedersen et al. in rodents *in vivo* are mediated by direct effects on the DCT rather than mediated by effects of vasopressin on other sites which then indirectly impact on the DCT.

1.4.8. Novel candidates for NCC regulation

1.4.8.1. Protein phosphatase 1 inhibitor

Protein phosphatase 1 (PP1) is one of the major eukaryotic serine/threonine phosphatases and belongs to the PPP family, which comprises also subfamilies PP2A, PP2B/calcineurin, PP4, PP6, PP5 and PP7 [156]. All members share the same core- structure and display similar catalytic mechanisms [161]. PP1 is a 35-38 kDa ubiquitously expressed protein that is encoded by three PP1 genes, yielding three isoforms of PP1, i.e., PP1α, PP1γ and PP1β/δ [161]. PP1 contributes to a variety of cell functions including cell metabolism, cell growth and cell differentiation [161]. In the kidney, PP1 is involved in the regulation of the medullary Na^+-K^+-ATPase [162]. Furthermore, Lin and coworkers have recently shown that PP1 is associated with WNK4 and plays a role in the WNK4-mediated inhibition of ROMK channels [163].

The activity of PP1 is controlled by regulatory and inhibitory proteins that interact with its catalytic subunit PP1c. So far, about fifty regulatory and inhibitory subunits of PP1c have been described [156, 161]. Most of the subunits interact with a short conserved RVxF-binding motif located in a small hydrophobic groove on the surface of PP1c [156]. Up to now, around ten PP1 inhibitory subunits are known, two of which are expressed in the kidney, i.e., inhibitor 1 (I1) and the dopamine and cAMP-regulated phosphoprotein Mr32000 (DARPP32) [156].

In 1976, Huang and coworkers were able to isolate I1 from rabbit skeletal muscle, describing it as the first endogenous inhibitor of PP1 [164]. I1 is encoded by the Ppp1r1a gene and forms a small, 171 amino acid-long, cytosolic protein [1]. It is expressed in many organs including the brain, skeletal

muscle, and heart, where it is assumed to contribute to neuronal plasticity [165], muscle glycogen metabolism [166], and cardiac contractility and excitability [1, 167]. The N-terminus of I1 contains a highly conserved consensus motif (KIQF) that is required for binding PP1 [168] (Figure 7). Furthermore, two phosphorylation sites (threonine 35 and threonine 67) are present in the central region. Protein kinase A is able to phosphorylate I1 at threonine 35, leading to the activation of I1 and the subsequent inhibition of PP1. In contrast, phosphorylation of I1 at threonine 65 by protein kinase C attenuates the inhibitory effect of I1 on PP1 [1]. El-Armouche and colleagues showed in cardiac myocytes that PP2A and PP2B terminate the action of I1 by dephosphorylation of threonine 35 [169] (Figure7).

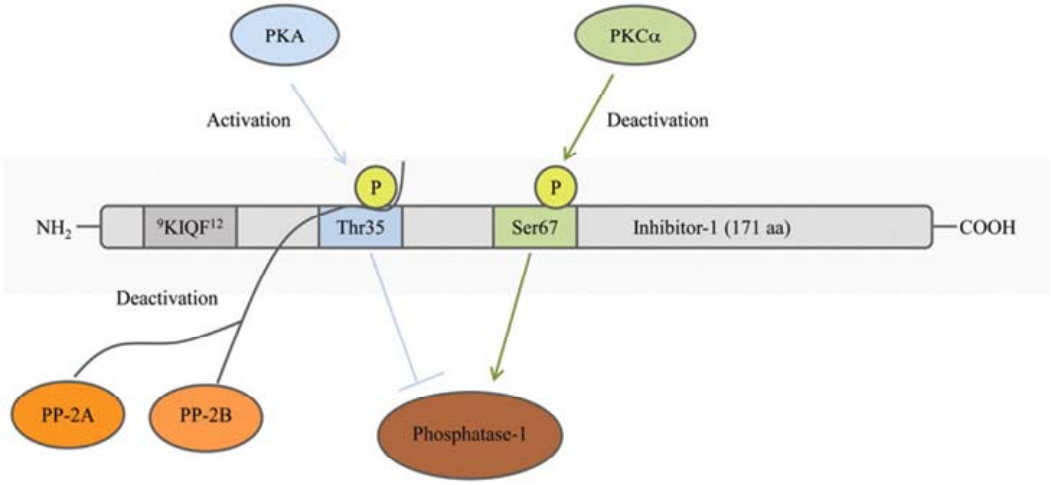

Figure 7: Structure of inhibitor 1. I1 is composed of 171 amino acids and an N-terminal-located consensus motif (KIQF). Protein kinase A (PKA)-dependent phosphorylation of threonine 35 (Thr35) activates the inhibitory function of I1 and hence leads to the inhibition of PP1, while protein kinase C (PKC)-dependent phosphorylation of serine 67 (Ser67) is thought to deactivate I1 and attenuate the inhibitory effect of I1 on PP1. PP2A and Ca^{++}-dependent phosphatase-2B (PP2B) deactivate I1 by dephosphorylation of threonine 35 (Thr35). Figure taken from [1].

Interestingly, I1 appears to be involved in beta-adrenergic signaling in skeletal and heart muscle [1, 167]. In fact, infusion of adrenalin rapidly increases I1 phosphorylation in skeletal muscle [170]. Overexpression of I1 in cardiac myocytes leads to an amplification of beta-adrenergic signaling due to enhanced inhibition of PP1 [171]. Studies in mice with targeted inactivation of I1 confirmed the significance of I1 for cardiac physiology. Isolated hearts from I1-deficient mice show a significantly

blunted response to beta-adrenergic stimuli [172]. Consistently, the I1-deficient mice are partly protected from isoprenaline-induced cardiac remodeling and arrhythmia [173]. Interestingly, baseline contractility of the heart is not or only very mildly affected and I1-deficient mice are healthy and have a normal life expectancy [172, 173]. They display a reduced long-term potentiation in the dentate granule cells of the hippocampus, but do not show any spatial learning deficits [165]. Moreover, although I1 is strongly expressed in arterial smooth muscle cells, I1-deficient mice show normal contractility of the aorta, indicating a redundant function of I1 in certain organs [174].

1.4.8.2. Protein kinase D1 (PKD1)

PKD1 is a serine/threonine kinase of the Ca^{++}/calmodulin and DAG-dependent kinase family expressed in many tissues and cell types [3, 175, 176]. In 1994, cDNA clones encoding PKD1 from human and mouse species were first identified by two different groups [177, 178]. The PKD1 gene (*Prkcm*) is localized on human chromosome 14q11, mouse chromosome 6 and rat chromosome 8m [3]. Based on the observation that the kinase domain and the regulatory region of PKD1 share some homologies with those of other members of the protein kinase C family (PKC), PKD1 was initially described as PKCμ an atypical member of the PKC family [177]. However, PKD1 has an unique transmembrane and pleckstrin homology region and a unique N-terminal sequence with a potential signal peptide. In addition, PKD1 lacks the C2 domain of the Ca^{++}-dependent PKCs [177]. Because of these structural features, PKD1 has been assigned to a new protein kinase subfamily namely protein kinase D (PKD). The PKD family consists of two other kinases, PKD2 and PKD3 [3]. All members of the PKD family share a similar modular structure which comprises an alanine and proline rich domain (AP), a cysteine-rich region (C1, divided into two subdomains; C1a and C1b), a pleckstrin homology (PH), an acidic-rich region and the kinase domain [3, 179] (Figure 8). These domains mediate specific protein-protein interactions and are likely decisive for the cell-type specific functions of PKD1 [179].

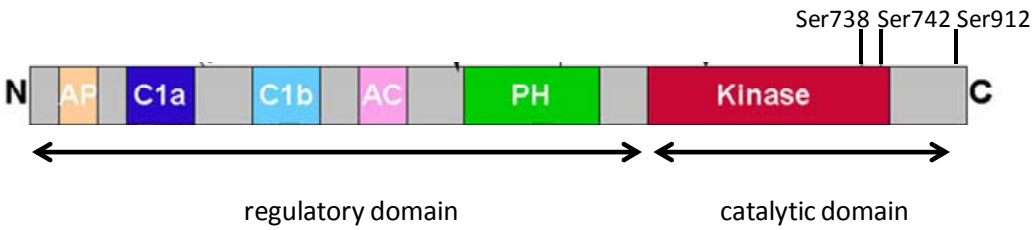

Figure 8: Structure of PKD1. PKD1 is composed of a regulatory region which consists of an alanine and proline rich domain (AP), a cysteine-rich region (C1, divided into two subdomains; C1a and C1b), acidic-rich region (AC) and a pleckstrin hololology (PH) and a catalytic domain. The phosphorylation sites serine 738 (Ser738), serine 742 (Ser742) and serine 912 (Ser912) are also shown. Figure was adapted from [3].

PKD1 is involved in a variety of cell functions including cell proliferation, differentiation, apoptosis and protein trafficking [3, 175]. Furthermore, depending on the cellular context PKD1 was shown to be regulated by hormones (e.g. aldosterone [180, 181] AngII [182, 183]), growth factors (e.g. Insulin-like growth factor [184, 185]) and oxidative stress [184]. Interestingly, PKD1 is thought to be involved in the regulation of Na^+/H^+ exchanger activity [186] and participates in the aldosterone-dependent activation of ENaC in kidney cells [181]. Upstream regulators are kinases (e.g PKC) [175] as well as proteases (e.g. caspase-3) [187] which activate PKD1 by phosphorylation and proteolytic cleavage, respectively. Iglesias and colleagues showed that the phosphorylation at serine 744 and serine 748 (serine 738 and serine 742 in humans, Figure 8) of PKD1 is required to activate the protein [188]. They substituted serine 744 and serine 748 of PKD1 with either an alanine (S744A/S34748A) or with glutamic acid (S744E/S748E). Substitution to alanine completely prevented PKD1 activation, whereas substitution to glutamic acid resulted in an activation of the protein. Furthermore, Matthews and coworkers characterized serine 916 as an auto-phosphorylation-site of PKD1 that correlates with the PKD1 catalytic activity [189]. When PKD1 gets activated it phosphorylates serine and threonine residues in the PKD1 consensus motif LXHXXS*/T* [190]. This consensus motif is present in many proteins, but only a few downstream targets have been identified [179, 191].

It is known that a complete loss of PKD1 leads to embryonic lethality [182]. Therefore, to investigate PKD1 loss *in vivo* conditional knockout approaches are necessary. Fielitz and coworkers used the Cre-loxP recombination system (see material and methods) to generate mice with a cardiac-specific deletion of PKD1 [182]. These mice were protected from Ang II-induced pathological cardiac remodeling [182], while cardiac-specific expression of a constitutively active PKD1 mutant in transgenic mice leads to cardiac hypertrophy [192]. So far, nothing is known about the specific effects of PKD1 on the kidney in general and on the DCT in particular.

1.5. Thesis projects

The overall objective of this thesis is to obtain insights into the molecular mechanisms that control DCT function and NCC activity, respectively. Based on the fact that many of the so far described NCC regulating proteins (e.g., KS-WNK1, WNK4, SPAK, Klhl3, PV) are enriched in the DCT, we hypothesize that the DCT may express a specific repertoire of regulatory proteins that control its function. To this end, the following **four specific aims** are addressed:

1.5.1. Investigating the role of I1 in DCT function

In a recent screen for DCT-specific genes, the phosphatase inhibitor 1 (I1) was identified to be highly expressed in the DCT. We investigated if I1 is involved in the regulation of DCT function and NCC activity.

1.5.2. Investigating the role of PKD1 in DCT function

PKD1 was also found to be a highly abundant transcript in the DCT. We tested if PKD1 is important for DCT and NCC function.

1.5.3. Using transcriptomic analysis to identify mediators of DCT cell growth

Our search for DCT-enriched genes revealed novel regulators of DCT and NCC function. To identify other genes that might be important for DCT growth and function, we performed a microarray analysis on isolated DCT from mice in which DCT cells growth was either stimulated or inhibited.

1.5.4. Establishing *ex vivo* DCT cell culture as a tool to study DCT cell function

Studies on DCT function require not only *in vivo* experiments but also *ex vivo* systems in which experiments can be performed under more controlled conditions than in the living animal. Until recently, two DCT cell lines had been available. However, none of these cell lines is suitable for studies on DCT epithelial function. Therefore, we established primary DCT cell culture derived from a transgenic mouse model (PV-eGFP) expressing EGFP specifically in the DCT, by using complex object parametric analysis and sorting technique (COPAS).

2. Material and Methods

2.1. Mouse work

All animal experiments were performed according to the Swiss Animal Welfare laws and approved by the local veterinary authority (Veterinäramt Zürich). Bearing and breeding of the used mouse strains (see below) were performed in the animal facility of the Institute of Anatomy at the University of Zurich. Mice were kept in ventilated cages (type II long IVC) with a regulated 12 hours day-night cycle, had free access to food and water and were fed with standard rodent chow (Kliba, Switzerland), if not stated otherwise. The following established and newly generated transgenic mouse models were used:

Established mouse lines

- **PV-eGFP** [193]
- **I1-KO** [165]
- **AS-KO** [194]
- **PV-cre (**Stock number: 008069, Jackson Laboratories)
- **PKD1** $^{flox/flox}$ [182]

Newly generated mouse lines

- **PKD1 PVcre** (PKD1 $^{flox/flox}$ x PV-cre)
- **PKD1 PVcre eGFP** (PKD1 $^{flox/flox}$ x PV-cre xPv-eGFP)

2.1.1. PV-eGFP mice

To perform COPAS (complex object parametric analysis and sorting) sorts (see below), PV-eGFP mice generated by Meyer and coworkers were used [193]. This mouse model expresses the enhanced green fluorescent protein (eGFP) under the parvalbumin (PV) promoter. Immunohistochemistry on cryosections showed that eGFP positive cells also display NCC expression, whereas β-ENaC positive cells lack the eGFP signal. Therefore, the renal eGFP expression is restricted to the DCT1 in PV-eGFP mice (Picard, Trompf et al. 2013 submitted).

2.1.2. I1 KO mice

Mice with a complete knockout of I1 were kindly provided by Dr. Paul Greengard (Rockefeller University). These mice were used to investigate the effect of I1 on DCT function.

2.1.3. PKD1 PV cre mice/ PKD1 PVcre eGFP

It is known that a complete loss of PKD1 causes embryonic lethality [182]. Therefore, we used a cre/lox strategy which allows a tissue specific deletion of PKD1. The general advantage of this system is the potential of a tissue- or cell-specific deletion of a critical part of the gene of interest by controlled homologous recombination in the genome. The cre protein is a P1 bacteriophage site-specific recombinase that catalyzes the recombination of two loxP sites. Within the gene of interest, the specific DNA sequence is flanked by 2 loxP-sites. Mating of a mouse strain that expresses cre under a tissue-specific promoter with a mouse line that carries the lox P site in the genome results in a tissue-specific knockout of the gene of interest.

Dr. Eric Olson provided PKD1$^{flox/flox}$ mice in which the loxP sites are flanking exon 12 through exon 14 of the *Prkcm* locus, which represent a part of the kinase domain of PKD1 [182]. This mouse line was crossbred with mice that express cre recombinase constitutively under the PV promoter (B6;129P2-Pvalb $^{tm1(cre)Arbr/J}$, Stock number: 008069, Jackson Laboratories) to obtain a specific PKD1 deletion in the PV-expressing DCT1. Breeding was performed so that all animals exhibited allelic homogeneity for the loxP sites in the genome. The control groups of mice in an experiment display the loxP sites only, whereas the KO groups exhibit the loxP sites and express cre under the PV promoter additionally.

In order to successfully isolate PKD1-deficient DCT1 cells by COPAS, PKD1 PVcre mice were crossbred with PV-eGFP mice. This breeding led to a mouse line with a specific deletion of PKD1 in DCT1 that also expresses eGFP in this specific tubular segment.

2.1.4. Aldosterone-synthase deficient mice (AS-KO)

AS-KO mice were kindly provided by Dr. Olivier Smithies who generated this mouse line to investigate the effect of aldosterone deficiency in the kidney [194].

2.1.5. Genotyping

PV-eGFP: Due to the fact that PV is expressed in skeletal muscles transgenic mice can be easily identified (distinguished from wildtype mice) by placing mice under an UV lamp. PV-eGFP mice reveal a strong fluorescence that can be easily detected post-partum through the hairless skin.

loxP sites, PVcre, Ppp1r1a: To isolate the DNA from either tail, ear or toe tissue of PKD1 PVcre mice and PKD1 PVcre eGFP mice or I1-KO mice, the blackPREP Rodent Tail DNA Kit (845-BP-0010250, Analytik Jena, Germany) was used. The extraction of the DNA was performed according to the manufacturer`s protocol.

The PCR reaction mix consisted of 0.8 µl of each primer (10 µM), 1.2 µl of $MgCl_2$ (25 mM, M8787, Sigma), 1.5 µl PCR reaction buffer (10X, P2317-1VL, Sigma), 0.15 µl dNTP (25 mM each, Promega), 0.75 µl DMSO (AppliChem), 0.3 µl Tag-Polymerase (250 U, D6677, Sigma) and 2 µl of the extracted DNA. PCR was performed under the following conditions using the primers listed in Table 1.

Table 1: PCR primer for genotyping

Primer	5’ ⟶ 3’
Fwd Prkcµ	ATG CTC TTA TGC CCG GTC ATC
Rev Prkcµ	TGA AAC GGA AAT GCT CAC AG
Fwd PV cre	GCG GTC TGG CAG TAA CCT GGT CG
Rev PV cre	GTG AAA CAG CAT TGC TGT CAC TT
Fwd Ppp1r1a	CCC ACG GAA GAT CCA GTT TA
Rev Ppp1r1a WT	CAC TTA GCC GGG AAA CTC TG
Rev Ppp1r1a KO	TAA AGC GCA TGC TCC AGA CT

PCR program to detect the ppp1r1a allele:

Temperature in °C	Time in Sec	
94	600	
94	30	35 cycles
56	45	
72	45	
72	600	
4	∞	

PCR program to detect the Prkcµ allele and the cre allele:

Temperature in °C	Time in Sec	
94	600	
94	30	35 cycles
56	45	
72	135	
72	600	
4	∞	

2.5 µl of loading buffer (6X, Promega) was added to the PCR solution. PCR products were separated by electrophoration in a 1.5% agarose gel (100 V, 1 h).

Product size of the Ppp1r1a allele: WT 380 bp; KO 280 bp
Product size of the floxed Prkcµ allele: 1031 bp
Product size of the PV cre allele: 100 bp

2.1.6. Metabolic cage experiments

To determine physiological parameters in mice, animals were kept in metabolic cages (Tecniplast, Buguggiate, Italy). Due to the special design of the cage, urine and faeces can be effectively separated outside the cage. Furthermore, it is possible to analyze food and water intake of individual animals. Body weight as well as water and food consumption were measured daily. After an adaptation phase of 3 days, urine and faeces of the animal were monitored. 24 h urine was collected and urinary cations (Na^+, K^+, Ca^{++}, Mg^{++}) were measured by ion chromatography (Metrohm ion chromatograph, Herisau, Switzerland). Cation concentrations in the urine were normalized to urinary creatinine concentrations determined according to a method described by Jaffé [195]. Urinary aldosterone was measured either with a radioimmunoassay kit (DPC Dade Behring, La Défense, France) or with a competitive EIA Aldosterone assay (Cayman Chemical,USA) following the manufacturer´s instructions.

2.1.7. Measurment of blood plasma parameters

Blood gas and blood ions were measured from heparinized venous blood taken from the right ventricle using an ABL505 blood gas analyzer (Radiometer, Copenhagen, Denmark) in the Zurich Integrative Rodent Physiology facility (University of Zurich). For the determination of plasma aldosterone in PKD1 PVcre mice, blood was drawn from the right ventricle, transferred into a K_2E EDTA microtainer tube (365975, BD, USA), centrifuged at 4000x g for 10 min and stored at -20°C. Plasma aldosterone analysis was performed in the University Hospital Zurich by radioimmunoassay (DRG instruments).

2.1.8. Diet experiments

For diet experiments, semi synthetic diets (Sniff, Soest, Germany) mixed 1:1.5 with water (100 g food + 150 ml water) were used. Animals were exposed to either control food (0.3% K^+; 0.3% Na^+), low Na^+ diet (0.05%Na^+), high Na^+ diet (3% Na^+) or low K^+ diet (0.05% K^+) for 3 to 14 days depending on the design of the experiment. To investigate adaptive physiological changes in the animals under the different diets, mice were kept for specific time periods in metabolic cages according to the experimental set up.

2.1.9. Hydrochlorothiazide test (HCTZ)

To assess if NCC function differs between control and KO mice, the HCTZ test was used. Animals were kept in metabolic cages and were exposed to low Na^+ or normal Na^+ diet for 14 days. After an adaptation phase in the metabolic cages, mice received a single intraperitoneal injection of 10 µl/g BW vehicle (0.9% NaCl + DMSO; 1:1) and on the second day all animals were treated with HCTZ (50 mg/g BW, dissolved in 0.9% NaCl + DMSO; 1:1, i.p). On both days urine was collected before injection, and 3 h and 6 h after the treatment. Urine was analyzed for creatinine concentrations and Na^+, K^+, Ca^{2+} and Mg^{2+}.

2.1.10. Blood pressure measurements by tail cuff method

Systolic blood pressure was recorded on conscious mice using the non-invasive tail-cuff method (BP2000, Visitech Systems, Apex, NC, USA) as described previously [196]. Mice were habituated to the instrument for 4 consecutive days. Subsequently, blood pressure was measured daily between 8 a.m. and 12 a.m. for 5 consecutive days. On each day, mice were adapted to the device during 10 blood pressure assessments before the actual start of the 20 blood pressure assessments that were used to calculate the average daily blood pressure of each mouse.

2.2. Immunohistochemistry

Deeply anesthetized animals (ketamin/xylazine; 65 mg/kg BW/13 mg/kg BW) were perfused via the abdominal aorta with 50 ml fixative (3% paraformaldehyde,Sigma, in 0.1 M phosphate buffer). After a fixation time of 5 min, the fixative was rinsed out by perfusion of 0.1 M phosphate buffer for 5 min. 2 mm to 3 mm thick kidney pieces were mounted on corks, frozen in liquid propane and stored at -80°C for later analysis.

For immunohistochemical analysis, 4 µm to 5 µm consecutive sections of fixed kidney were cut in a cryostat (Microm, Leica, Switzerland) and mounted on chrom-alun/gelantin- coated glass slides (Duran Group, Germany). Then, the slices were blocked for at least 30 min with 10% normal goat serum and incubated with primary antibodies (Table 3) diluted in PBS/ 0.5% BSA/ 0.04% sodium azide solution in a humidified chamber over night at 4°C. The next day, the slices were washed three times for 10 min in PBS and incubated with the corresponding, fluorescent labeled secondary antibodies (Tabel 3) for 2 h at RT in the dark. After another three washings with PBS, the sections were coverslipped using glycergel (DAKO, USA) containing 2.5% 1,4-diazabicyclooctane (Sigma) as fading retardant and analyzed using a Leica DM 6000 fluorescent microscope (Leica, Wetzlar, Germany).

2.3. Protein sample preparation and western blot analysis

PBS-perfused kidneys were homogenized (Polytron, Kinematica, Germany) in ice-cold K-HEPES buffer (200 mM Mannitol, 80 mM Hepes, 41 mM KOH, pH7.5) containing protease inhibitor (Complete ULTRA, Roche, Switzerland) and phosphatase inhibitor (PhosSTOP, Roche, Switzerland) and centrifuged at 2000x g at 4°C for 15 min. Supernatant, containing the proteins, was saved in a new tube. The remaining pellet was resuspended in another 400 µl K-HEPES buffer and another homogenisation step with subsequent centrifugation was performed. Both supernatants were combined (kidney lysate). To prepare the kidney membrane fraction, 400 µl of the kidney lysate were centrifuged at 100’000x g at 4°C for 1 h. The supernatant, containing an enrichment of cystosolic proteins was saved and the pellet (enrichment of membrane bound proteins) was resuspended in 400 µl K-HEPES and sonicated for 30 s on ice (Sonopuls, Bandelin, Germany).

After the measurement of protein concentration (UPF 86421, Uptima, France), electrophoretic separation of the proteins was carried out (Mini Protean Tetra Cell, Biorad, Switzerland). For COPAS sorted samples 400 tubules per lane and for kidney membrane fraction 25 µg protein were used on 8 to 12 % polyacrylamide gels. Proteins were transferred to a nitrocellulose membrane (Whatman, Bottmingen, Switzerland) by tank blotting at 100 V, 2 h (BioRad Mini-Trans-Blot Cell system). After transfer, membranes were blocked for 1 h with Odyssey blocking buffer (LI-COR, Biosciences, Germany) and incubated overnight at 4°C with the primary antibodies (see Table 3) under continuous agitation. On the subsequent day, the blots were washed 3 times for at least 10 min with PBS containing 0.1% Tween and incubated with the corresponding secondary antibodies under continuous agitation for 2 h at RT. Afterwards, the membranes were washed again as described above. For visualization and analysis of the protein bands the Odyssey IR imaging system (LI-COR, Biosciences, Germany) was used. Densitometric quantifications were performed using Odyssey V3.0 software (LI-COR, Biosciences, Germany) and were normalized to beta-actin.

2.4. RNA extraction from kidney

Total RNA was extracted using RNAspin Midi RNA isolation kit (GE Healthcare, UK) according to the manufacturer's recommendations. Quality and concentration of the isolated RNA samples were determined with a NanoDrop ND-1000 (NanoDrop Technologies Delaware, USA). Total RNA samples were stored at -80°C until further processing.

2.5. RNA extraction from COPAS sorted DCT

RNA extraction was performed with an RNAqueous-Micro RNA extraction kit (Applied Biosystems/Ambion, Switzerland). Immediately after COPAS sorting, pelleted tubules were resuspended in 50 µl of lysis buffer provided by the manufacturer and stored at -80°C until RNA extraction. RNA isolation and DNase treatment was performed according to the manufacturer's protocol. The quality of the isolated RNA was measured by NanoDrop ND 1000 (NanoDrop Technologies, Delaware, USA).

2.6. Real-time PCR

cDNA was synthesised by reverse transcription of 200 ng (COPAS sorted DCT) or 1 µg (whole kidney) of RNA using a Goscript Reverse transcription system kit (A5000, Promega, USA) according to the manufacturer's recommendation.

Real-time PCR was performed on a Roche Light Cycler 480II instrument with the Light Cycler 480 SYBR/Green Master kit (04887352001, Roche, Germany). The reaction mix consisted of 1 µl of each primer (10 µM), 10 µl Mastermix (ready-to-use), 6.5 µl water and 1.5 µl cDNA. For whole kidney expression studies, 10 ng to 20 ng of cDNA and for COPAS- sorted DCTs, 2 ng to 5 ng cDNA per well were used. Relative mRNA gene expression was determined after normalization to GAPDH gene expression: Ratio = $2^{*Ct\ (GAPDH-Target)}$. All reactions were run in triplicates.

Table 2: Primer using for qRT-PCR analysis.

Primer	5’ ⟶ 3’
Fwd NCC	TGACCTGCATTCATTCCTCA 3
Rev NCC	GAAGCGAACAGGTTCTCCAG
Fwd WNK1S	TGC TGC TGT TCT CAA AAG GAT TGT A
Rev WNK1S	TTC AGG AAT TGC TAC TTT GTC AAA ACT G
Fwd WNK1L	TGC ATG CTT GAG ATG GCT ACA T
Rev WNK1L	CTT TGT CAA AAC TGG CTG GCT T
Fwd WNK4	CGA CAG AGT TGT CGA GTG TCA
Rev WNK4	TAC AAT GAG TTC ATC CTG CCC
Fwd PV	AGG ATG AGC TGG GGT CCA TTC TGA A
Rev PV	GCT TTC AGC CAC CAG AGT GGA GA
Fwd CalbindinD28K	GCG AAA GAA GGC TGG ATT GGA GC
Rev CalbindinD28K	TGC TGG CAT CGA AAG AGC AGC AA
Fwd TRPM6	ACT CAG AGC AGT TTG GCC AGC T
Rev TRPM6	CGC AGA CCT CCA GAG ACC GC
Fwd Renin	ATC TTT GAC ACG GGT TCA GC
Rev Renin	TGA TCC GTA GTG GAT GGT GA
Fwd Prox1	GTT CAC CAG CAC ACC CAC CCA G
Rev Prox1	GAT AGC CCT TCC TGC ATT GCG CT
Fwd SIK1	CTC CGT CCG AAC TCC CCG GG
Rev SIK1	ACT GGA GCA GCC TCT GCT GGT
Fwd GAPDH	CCT GCT TCA CCA CCT TCT TGA3
Rev GAPDH	CAT GGC CTT CCG TGT TCC

RT-PCR program:

Temperature in °C	Time in Sec	
95	300	
95	10	35 cycles
60	45	
70	45	
95	5	
65	60	
40	30	

2.7. Isolation of single tubular fragments using the complex object parametric analyzer biosorter (COPAS)

For COPAS sorting, adult PV-eGFP or adult PKD1 PVcre eGFP males were used. To prepare single renal tubular fragments, mice were anesthetized with ketamin (Narketan 10, 80 mg/kg body wt, Chassot, Belp, Switzerland) and xylazine (Rompun, 33 mg/kg body wt; Bayer, Germany) or with isoflurane (Abbott, Baar, Switzerland) inhalation. Animals were perfused through the right heart with 10 ml of ice-cold PBS then with 10 ml of digestion solution (Collagenase Type-1, 1 mg/ml, Worthington, USA; 1 mg/ml hyaluronidase, Sigma, USA; 0.1 mg/ml DNaseI, Sigma, USA, prepared in ice-cold KREBS: 145 mM NaCl, 10 mM HEPES, 5 mM KCl, 1 mM NaH_2PO4, 2.5 mM $CaCl_2$, 1.8 mM $MgSO_4$, 5 mM glucose, pH 7.3). The renal cortex from both kidneys was dissected under a stereomicroscope (CLS150X, Leica, Germany). Samples were finely minced and digested in 10 ml of fresh digestion solution at 37°C for 17 min. The tubular digest was first filtered through 250 µm and 212 µm nylon sieves and afterwards the flow-through was filtered through a 100 µm and a 40 µm cell strainer (Becton Dickinson Labware, Franklin Lakes, NJ). The tubules retained by the 40-µm cell strainer were diluted with ice-cold KREBS buffer to a total volume of 50 ml.

All sorting was performed with a complex object parametric analyzer and sorter (COPAS) device (Union Biometrica, USA). As described previously [197], for sorting fluorescent renal collecting ducts, the following instrument settings were used: delay 8, width 5, photomultiplier tube (PMT) 700, sheath fluid pressure 4.2-4.5. The sample fluid pressure was set to maintain a sort frequency of 20–50 events/s (sample pressure 5.4-5.9). The mixer speed was 80%. 800 green fluorescent particles were collected directly into ice-cold KREBS containing 0.05% BSA (Sigma, USA), centrifuged at 800x g for 10 min and resuspended in either 1xLB for protein analysis or in 50 µl of RNA lysis buffer (RNAqueous-Mirco RNA isolaton kit, Ambion, Switzerland). For performing primary cell culture, COPAS-isolated DCTs were placed on ice until further processing.

2.8. Transcriptomic analysis after diuretic treatment using Agilent Microarray hybridization and analysis

To identify genes that might be important for DCT growth and function, microarray analysis (Agilent, USA) on COPAS isolated DCTs (see above) were performed. Before COPAS sorting, 5 mice per group were treated with a single intraperitoneal injection of either vehicle (0.9% saline, PEG; 1:1), furosemide (40 mg/g BW in 0.9% saline PEG solution), or hydrochlorothiazide (40 mg/g BW, in 0.9% saline PEG solution), to stimulate and inhibit DCT cell growth, respectively. After 4 h of treatment, mice were sacrificed and the DCTs were isolated by COPAS (see above). RNA was extracted (see

above) and hybridized on whole mouse genome 4x44K Oligo microarrays (Agilent, USA) as previously described in Picard, Trompf et al. (submitted). Analyses of expression values were performed using Gene-spring 10 software (Agilent Technologies, USA) and ratio analyses: I) control/hydrochlorothiazide II) control/furosemide III) furosemide/hydrochlorothizade with a cut off of 2.5 were performed. Differential regulation of certain genes was confirmed by RT-PCR as described in chapter 2.6.

2.9. Cell culture

All cells were cultured at 37°C in 5% CO_2 in a cell incubator (SANYO, USA). The medium of the primary cell culture was changed every second day and HEK cells were passed weekly.

2.9.1. Primary cell culture of COPAS- isolated DCTs

Around 1000 COPAS-isolated DCTs (see above) were harvested, resuspended in 100 µl preheated (37°C) cell culture medium (DMEM/Ham´s F12, 1:1, 12709F, 12615F, Lonza, containing 3.2% $NaHCO_3$, Gibco; 114.3 mM L-Glutamine, Gibco; non-essential amino acids, Gibco; 2 mg/ml cirpoxin, Mepha; 5 µg/ml insulin, I6634 Sigma; 5 µg/ml transferin, T1428 Sigma; 5 ng/ml prostaglandin E1, P7527, Sigma; 5 pM triodotiroxine, T5516, Sigma; 50 mM sodium selenite, 214485, Sigma; 500 nM hydrocortisone, H0888, Sigma; 2% fetal calf serum, Bioconcept) and seeded on collagen-coated (1 mg/ml collagen type I from rat tail, Millipore, USA; diluted in 0.136 % acetic acid, Sigma, USA) 24 well plates (Nunc, USA) or 12 mm polycarbonate transwell filters (3412, Coring, USA) to obtain differentiated and polarized epithelium. Resistance was measured daily by an epithelial volt-ohm meter (EVOM, USA).

2.9.2. Immunocytochemistry

COPAS-isolated DCTs were grown on collagen-coated permeable transwell filters. After 10 days, the outgrowing cells were washed with PBS (100 µl apical and 600 µl basolateral) and fixed with 3 % paraformaldehyde (Sigma, USA) in 0.1 M phosphate buffer at RT for 30 min. Subsequently, the filters were washed 3 times with PBS and cut into 3 pieces using a scalpel. The pieces were mounted on corks, frozen in liquid propane and stored at -80°C for later analysis. The following immunofluorescence staining was done as described under Immunohistochemistry (2.2).

2.9.3. RNA isolation and cDNA synthesis of DCT primary cell culture

To isolate RNA from outgrowing cells, cells were washed with ice-cold PBS. Subsequently 50 µl of RNA lysis buffer (Applied Biosystems/Ambion, Switzerland) was pipetted directly on filters or into the 24 well plates. After 30 s of incubation, the RNA solution was transferred into a test tube and RNA was extracted according to the manufacturer´s protocol.
cDNA was synthesized by reverse transcription of 150 ng RNA using random primers (Microsynth, Switzerland) and an Improm II Reverse Transcription Kit (Promega, USA) following the instructions of the manufacturer. Real-time PCR was performed on an ABI Prism 7700 cycler (Applied Biosystems, USA) with the iQ SYBR Green Supermix (Biorad, Switzerland). 4 ng of reverse transcribed RNA per well and primer as summarized in Table 2 were used.

2.9.4. Cultivation and transfection of HEK 293T cells

Human embryonic kidney cells (HEK293T) were cultivated in DMEM medium supplemented with 10% heat-inactivated fetal bovine serum (Bioconcept, Switzerland) and penicillin/streptomycin 100 U/ml (15070, Gibco, USA). For the transfection procedure, $1*10^6$ HEK293T cells were seeded in 6 well tissue culture plates (Nunc, USA) and grown until 90% confluency. The transfection-DNA-solution was prepared and applied on the cells using Metafectene (Metafectene Pro, Biontex, Switzerland) according to the manufacturer´s recommendation. After 24 h, the cells were collected for protein analysis.

2.9.5. PKD1 plasmids

To test whether PKD1 controls NCC phosphorylation *in vitro*, NCC together with wildtype PKD1, constitutively-active PKD1 mutant (PKD1 S738/744E) or kinase-dead PKD1 mutant (PKD1 K612W) were transiently transfected into HEK293Tcells. Cloning of NCC-cDNA in pCR-Script vector was done by Marianna Di Chiara.
Wildtype PKD1 and various mutants of PKD1, PKD1 K612W (kinase-dead) and PKD1 S738/744E (constitutively active) in pCDNA3 mammalian expression vectors were kindly provided by Dr. Angelika Hausser (Institute of Cell Biology and Immunology, University of Stuttgart, Germany) and generated and described by Johannes and coworkers. [198, 199].

2.9.6. Protein preparation of transfected HEK293T cells

24 h posttransfection, cells were washed 3 times with 1 ml ice-cold PBS for 10 min in the cold room. Subsequently, the cells were scraped in 1 ml ice-cold PBS and the solution mix was transferred to a sample tube and centrifuged at 11000x g at 4°C for 10 min. The cell pellet was lysed by vigorous pipetting in ice-cold radio-immuno-precipitation assay (RIPA) buffer (Thermo Scientific, USA) containing protease inhibitor cocktail (Roche, Switzerland) and phosphatase inhibitor (Roche, Switzerland) and incubated on ice for 40 min. Afterwards, another centrifugation step was performed to pellet cell debris, protein concentration of the supernatant was assessed by Bradford assay (Uptima, USA). 25-50 µg of total protein lysates in 2X Laemmli loading buffer were loaded on the SDS page and western blot analyses were performed as described in chapter 2.3.

Table 3: Antibodies for protein analysis

		Dilution		
Antibody	**Host**	**WB**	**IF**	**Source**
tNCC	rabbit	1:2000	1:2000	Pineda
pT53 NCC	rabbit	1:10000		Pineda
pT58 NCC	rabbit	1:5000		Pineda
pS71 NCC	rabbit	1:5000		Pineda
pS89 NCC	rabbit	1:2000		Pineda
αENAC	rabbit	1:2000		Pineda
βENaC	rabbit	1:20000		Pineda
γENaC	rabbit	1:5000		Pineda
β actin	rabbit	1:5000		Sigma
Calbindin D28k	mouse		1:50000	Swant
NaPiIIa	rabbit	1:5000		J.Biber
NKCC2	rabbit	1:5000	1:10000	J.Loffing
tPKD1	rabbit	1:500	1:1000	Cell signalling
pS744/748 PKD1	rabbit	1:500		Cell signalling
pS916 PKD1	rabbit	1:500		Cell signalling
Pendrin	rabbit	1:5000		C.Wagner
I1	rabbit	1:500		Epitomics
pSPAK	rabbit	1:500		Cell signalling

PV	rabbit		1:1000	Swant
Cre	rabbit		1:10000	S.Berger
Goat-anti-mouse Alexa Fluor 680-conjugated IgG	mouse	1:20000		Licor-Bioscience
Goat-anti-rabbit Alexa Fluor 680-conjugated IgG	rabbit	1:20000		Licor-Bioscience
Donkey-anti-sheep Alexa Fluor 800-CW-conjugated IgG	donkey	1:20000		Licor-Bioscience
Donkey-anti-rabbit Cy3	donkey		1:1000	Jackson Immuno Research Laboratories
Goat anti-mouse IgG FITC-conjugated	mouse		1:1000	Jackson Immuno Research Laboratories

3. Results

Ppp1r1a and Prkcμ were first identified by Dr. Nicolas Picard in our laboratory to be DCT enriched gene-transcripts (Picard, Trompf et al. 2013, submitted). To perform his analysis, Dr. Picard used kidneys of mice with eGFP expression under the PV promoter. He sorted the eGFP positive DCT1 by COPAS and performed comparative gene expression analyses using Whole Mouse Genome Microarrays (Agilent).

To assess the impact of Ppp1r1a and Prkcμ on the DCT, and thus on the renal control of whole body homeostasis a series of in vivo and in vitro experiments were performed. The results are described in the following chapters Project 1 and Project 2.

3.1. Project 1: Investigating the role of the Ppp1r1a-transcript (I1) for NCC regulation

3.1.1. Localization of I1 in the kidney

To localize I1 in the mouse kidney, fluorescent immunohistochemistry was performed. I1 (Figure 1B) was highly expressed in the cytoplasm of the NCC- and Calbindin D28k-positive DCT cells (Figure 1A). In addition a strong signal for I1 was also found in the preceding, NCC- and CalbindinD28k-negative, cortical TAL (Figure 1B) as well as in the medullary TAL (data not shown).

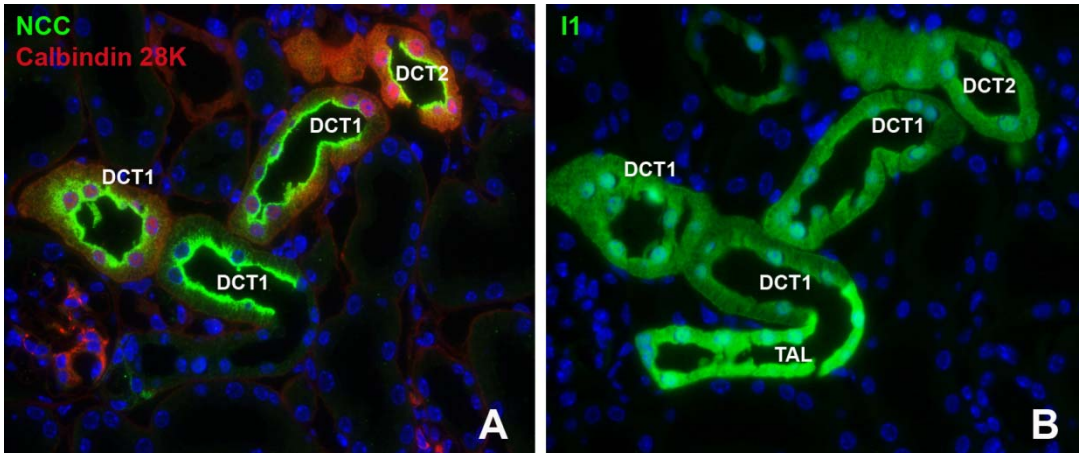

Figure 9: Expression of I1 in mouse kidney. Immunohistochemical detection of I1 revealed an intense cytoplasmatic staining for I1 along the DCT as well the preceding TAL. Analysis were performed on consecutive cryosections of mouse kidneys stained (A) for NCC (red) and CaBPD28k (green), to identify the DCT, and (B) for I1 (green). Cell nuclei were labeled with DAPI (blue).

3.1.2. I1 regulates phosphorylation and activity of NCC in vitro

To determine the impact of I1 on NCC phosphorylation, knockdown experiments of Ppp1r1a by siRNA were performed in HEK293 cells overexpressing NCC using the Tet-on expressions system. (Figure 10A). These experiments were done in collaboration with Prof. Dr. Ellison (Portland, OR, USA).

This cell line exhibits high levels of endogenous I1 and its target PP1a. NCC expression could not be detected by western blot as long as the cells were not stimulated with tetracycline (Figure 10A; lane 0). After stimulation with tetracycline (1 μg/ml), total NCC and NCC phosphorylated at threonine 53 (pT53 NCC) become well detectable in mock-transfected cells (no siRNA) and cells transfected with randomized siRNA (Control siRNA) respectively. Knockdown of I1 protein by specific siRNA (Ppp1ra siRNA) transfection resulted in a dramatic reduction of NCC phosphorylation at position T53, while the abundance of total NCC and PP1a remained unchanged (Figure 10A).

To get further insights into the effect of I1 on NCC activity, thiazide-dependent ^{22}Na uptake experiments on *Xenopus laevis* oocytes were performed. Co-injection of mRNA for NCC and a constitutively active mutant of I1 (Ppp1r1aT35D) resulted in a slight increase of thiazide-dependent ^{22}Na uptake. Nevertheless, when NCC was co-injected with Ppp1r1aT35D and its target PP1A, the thiazide-dependent ^{22}Na uptake was two times as high as seen for Ppp1r1aT35D only. In contrast, PP1A alone did not have any significant effect on thiazide-dependent ^{22}Na uptake (Figure 10B).

Taken together, these data suggest that I1 represents a novel regulator controlling NCC phosphorylation and thus its function *in vitro*.

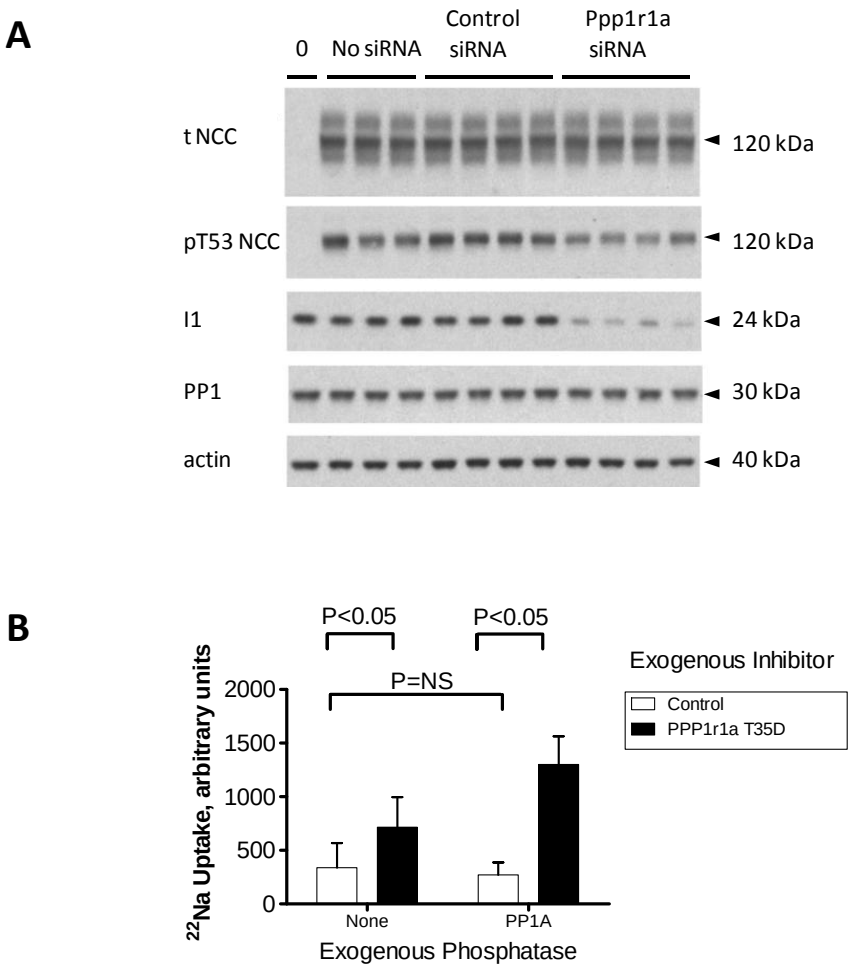

Figure 10: I1 promotes NCC phosphorylation and activity *in vitro*. (A) I1 was down-regulated in tetracycline-inducible NCC stable expressing HEK 293 cell line by siRNA. Western blot analysis revealed that this cell line expresses high levels of endogenous I1 and PP1. In addition, NCC and pT53 NCC were detectable when cells were treated with 1 µg/ml tetracycline. Knockdown of I1 led to a reduction of the NCC phosphorylation at pT53, whereas total NCC and PP1 expression were not changed. (B) Regulation of NCC activity by PP1 and I1 was assessed by ^{22}Na uptake experiments in *Xenopus laevis* oocytes. Co-injection of NCC with a constitutively active mutant of I1 (Ppp1r1a T35D) slightly increased NCC activity while additionally injected PP1A increased Na^+ influx to an even greater extent. Mean ± SEM, n = 3 for each condition. Statistical significance was calculated by one-way ANOVA (* p<0.05).

3.1.3. I1 regulates phosphorylation of NCC *in vivo*

Since the *in vitro* experiments pointed to a role of I1 in the control of NCC phosphorylation and function, we investigated the role of I1 *in vivo*. Mice with a complete knockout of I1 (kindly provided by Dr. Paul Greengard) were analyzed. Immunofluorescent staining on cryosections of mouse kidneys confirmed the complete I1-deficiency in the KO mice (Figure 11A). The immunohistochemical results were supported by western blot analysis of total kidney preparations that revealed a 28 kDa band representing I1 in wildtype mice (WT), but not in I1-KO mice (KO) (Figure 11B).

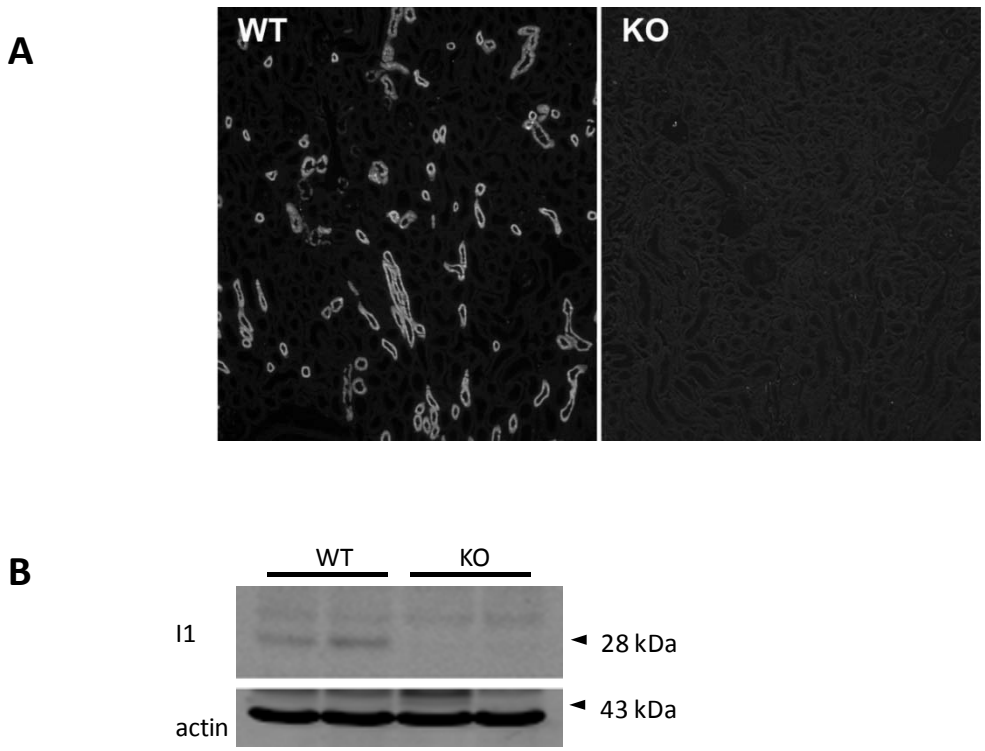

Figure 11: Loss of I1 protein abundance in I1 knockout mice. (A) Immunohistochemistry and (B) Immunoblot analysis were used to confirm the successful knockout of I1 in the kidney of I1-deficient mice.

In order to investigate the role of I1 in the control of NCC phosphorylation *in vivo*, western blot analyses were performed on kidneys of WT and I1-deficient mice. We used a novel set of rabbit antibodies directed against NCC phosphorylated at threonine 53 (pT53 NCC), threonine 58 (pT58 NCC), serine 71 (pS71 NCC) and serine 89 (pS89 NCC), respectively (Picard, Trompf 2013, submitted). The total abundance of NCC was assessed using an antibody directed against an amino acid sequence in the third extracellular loop of NCC (Sorensen, Grossmann, 2012, in press). In accordance with the *in vitro* results, immunoblotting of membrane preparations of mouse kidney showed no difference in the total abundance of NCC between the two genotypes, whereas NCC phosphorylation in I1-KO

mice was significantly reduced at all four analyzed phosphorylation sites (Figure 12). Thus, the I1 dependent phosphorylation of NCC seen in the previous *in vitro* studies could be confirmed *in vivo.*

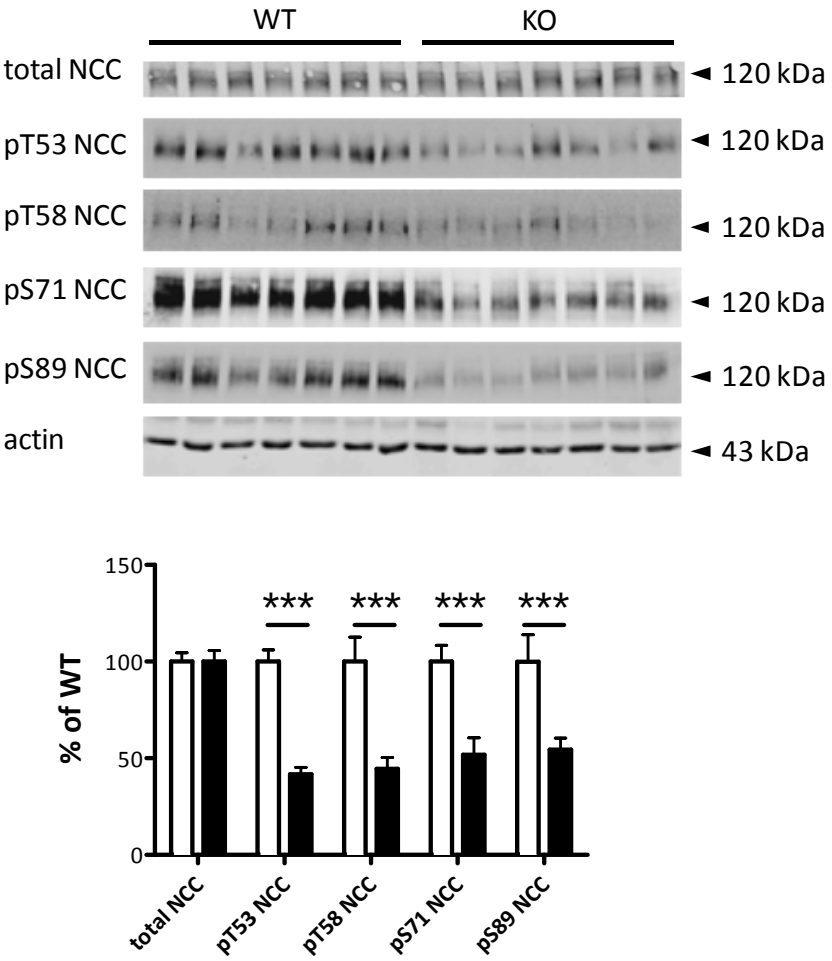

Figure 12: I1 is required for NCC phosphorylation *in vivo*. Western blot experiments were performed using membrane preparation of kidney homogenates from wildtype (WT) and I1-deficient (KO) mice. Expression of total NCC and its phosphorylated forms at threonine 53 (pT53 NCC), threonine 58 (pT58 NCC), serine 71 (pS71 NCC) and serine 89 (pS89 NCC) were analyzed. Densitometric analysis of the western blots revealed a significant down-regulation of all four analyzed phosphorylation sites of NCC. In contrast, total abundance of NCC was not changed. The relative intensities of the bands of interest were normalized against beta-actin. Relative measurements were calculated with the averages of the WT group set at 100%. Results are mean ± SEM, n=7, Statistical Significance was calculated by student t-test (***=p<0.001).

3.1.4. Lower blood pressure in I1-deficient mice

From previous studies it is known that a decrease in NCC phosphorylation is associated with a reduced arterial blood pressure [123, 200]. Therefore, we measured by tail-cuff arterial blood pressure in I1-deficient female and male mice and their corresponding wildtype littermates. Independent of gender, I1 deficiency decreased systolic blood pressure by approximately 10 mmHg, when mice were kept on standard diet (Figure 13A and B). To investigate if I1-deficient mice manifest salt dependent changes of arterial blood pressure, female I1-KO mice and their wildtype littermates were placed for 2 weeks on either a low (0.05 % Na^+) or a high (3 % Na^+) Na^+ diet. On low Na^+ diet, I1-KO animals displayed a significantly reduced blood pressure (Figure 13C), whereas on high salt diet, the differences in blood pressure between the genotypes was abolished (Figure 13D).

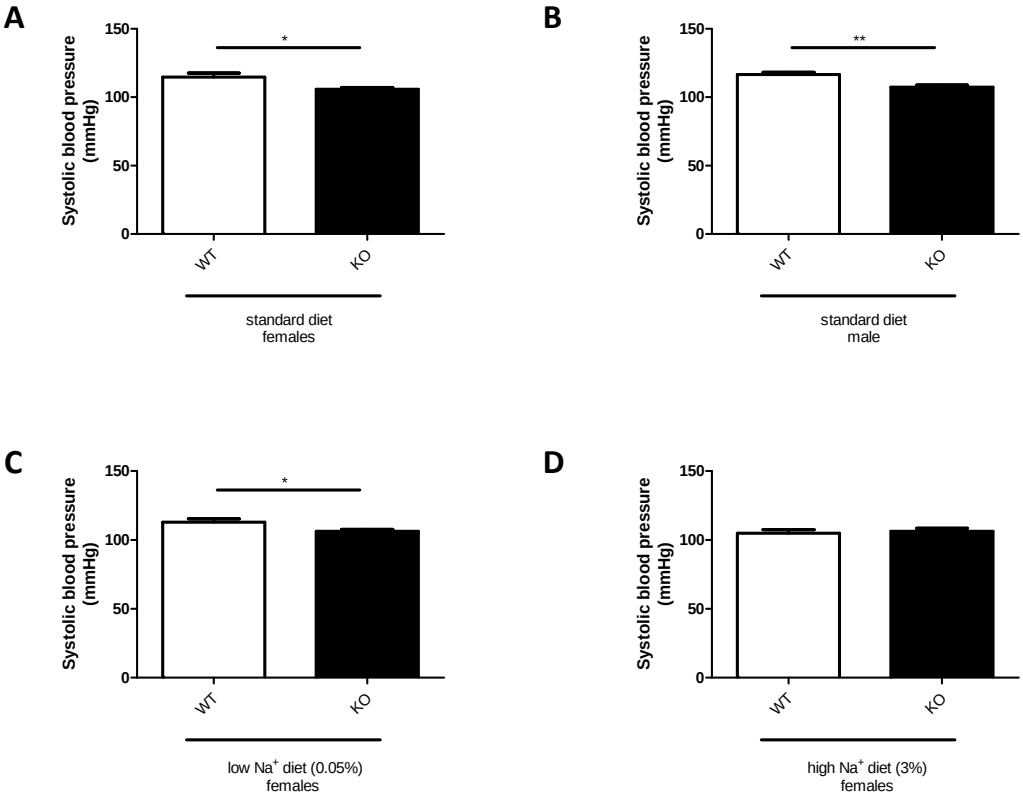

Figure 13: I1-deficient mice display a reduced blood pressure. Systolic blood pressure measurements by tail-cuff-method were performed in wildtype (WT) and I1-KO (KO) mice on normal diet ((A) 0.3% Na^+, females n=10 for each genotype, (B) males n=8 for each genotype), (C) low Na^+ diet (0.05% Na^+, n=10 for each genotype), and (D) high Na^+ diet (3% Na^+, n=10 for each genotype). Each bar depicts the average values of 4 days. Values are means ± SEM. Statistical significance was calculated by student t-test (*=p<0.05, **=p<0.01).

3.1.5. I1-KO mice show no overt Gitelman syndrome phenotype

To obtain further insights into the physiological impact of I1 deficiency on sodium balance, metabolic cage experiments as well as blood gas analysis of mice on standard diet and on chronically low Na^+ diet (0.05% Na^+) were performed (Tables 4 and 5). I1-KO mice showed a tendency for an enhanced fractional excretion of Na^+ on standard diet compared to wildtype littermates (WT: 28.19 ± 1.39 UNa^+/UCreat, I1-KO: 32.22 ± 1.45 UNa^+/UCreat,p=0.062). This genotype dependent difference in urinary sodium loss was even more prominent, when the mice were placed on low Na^+ diet (WT: 1.83 ± 1.03 UNa^+/UCreat, I1-KO: 4.17 ± 1.65 UNa^+/UCreat, p=0.2906). Parallel to the elevated Na^+ excretion, I1 deficient mice exhibited a slight increase in urinary K^+ excretion on both diets (standard diet: WT: 165.48 ± 27.56 UK^+/UCreat, I1-KO: 181.76 ± 27.22 UK^+/UCreat, p=0.6799; low Na diet: WT: 118.01 ± 19.86 UK^+/UCreat, I1-KO: 138.15 ± 22.39 UK^+/UCreat, p=0.514). However, no hypocalciuria was seen in the I1-deficient mice (WT: 0.289 ± 0.058 UCa^+/UCreat, I1-KO: 0.320 ± 0.045 UCa^+/UCreat, p=0.6784). In line with the elevated urinary potassium levels, blood gas analysis showed a weak decrease in blood K^+ ion concentration in I1-deficient mice compared to their wildtype littermates on both diets (standard diet: WT: 3.4 ± 0.14 K^+ mM, I1-KO: 3.3 ± 0.11 K^+ mM, p=0.5894; low Na diet: WT: 3.98 ± 0.25 K+ mM, I1-KO: 3.56 ± 0.19 K+ mM, p=0.2062). On the low Na^+ diet, I1-KO animals showed a weak increase in blood bicarbonate compared to wildtype animals (WT: 19.74 ± 0.67 $HCO3^-$ mM, I1 KO: 20.44 ± 0.63 $HCO3^-$ mM, p=0.4598). Although, the genotype dependent differences of the analyzed metabolic parameters were not significant, neither for urinary ion excretion nor for blood parameters, the findings would be consistent with partial loss of NCC function. Complete loss of NCC function in Gitelman syndrome goes along with arterial hypotension, renal Na^+ and K^+ loss, metabolic alkalosis as well as hypocalciura [36].

Table 4: Metabolic parameters of wildtype (WT) and I1-KO (KO) littermates on standard diet and on low Na^+ diet

	Standard diet					**Low Na^+ diet**				
	WT	n	***KO***	n	p	***WT***	n	***KO***	n	p
Food intake (g)	3.48 ± 0.32	9	4.02 ± 0.39	8	ns	5.58 ± 0,55	10	5.54± 0.61	9	ns
Water intake (ml)	2.59 ± 0.23	9	2.76 ± 0.17	8	ns	1.98 ± 0,26	10	2.03 ± 0.3	10	ns
Urine volume (ml)	1.44 ± 0.15	9	1.53 ± 0.21	9	ns	1.26 ± 0.21	10	1.6 ± 0.22	9	ns
UNa^+/UCreat	28.19 ± 1.39	9	32.22 ± 1.45	9	ns	1.83 ± 1.03	6	4.17 ± 1.65	8	ns
UK^+/UCreat	165.48 ± 27.56	9	181.76 ± 27.22	9	ns	118.01 ± 19.86	9	138.15 ± 22.39	10	ns
UCa^+/UCreat	0.289 ± 0.058	9	0.32 ± 0.045	9	ns	ND		ND		
UAldo/UCreat	14.93± 1.53	8	11.31 ± 1.79	7	ns	17.79 ± 3.52	8	13. 16± 1.99	9	

Values are ± SEM, n= number of animals, ns= not significant, ND= not determined. Statistical significance was calculated by student t-test.

Table 5: Physiological blood gas parameters of wildtype (WT) and I1-KO (KO) littermates on standard diet and on low Na^+ diet.

	Standard diet					**Low Na^+ diet**				
	WT	n	***KO***	n	p	***WT***	n	***KO***	n	p
pH	7.15 ± 0.02	9	7.16 ± 0.02	8	ns	7.15 ± 0.02	10	7.17 ± 0.02	9	ns
pCO_2 (mmHg)	56.74 ± 2.31	9	55.16 ± 3.72	8	ns	58.70 ± 2.23	10	58.10 ± 1.75	9	ns
$HCO3^-$ (mM)	18.97 ± 0.54	9	18.71 ± 0.71	8	ns	19.74 ± 0.67	10	20.44 ± 0.63	9	ns
K^+ (mM)	3.4 ± 0.14	9	3.3 ± 0.11	8	ns	3.98 ± 0.25	10	3.56 ± 0.19	9	ns
Na^+ (mM)	142.57 ± 0.57	9	142.22 ± 0.52	8	ns	148.60 ± 0.70	10	148.89 ± 0.54	9	ns
Cl^- (mM)	106.86 ± 1.10	9	106.00 ± 1.36	8	ns	112.40 ± 0.99	10	110.67 ± 0.53	9	ns
Ca^+ (mM)	0.73 ± 0.06	9	0.73 ± 0.08	8	ns	0.74 ± 0.06	10	0.70 ± 0.06	9	ns
Mg^+ (mM)	0.88 ± 0.12	4	0.87 ± 0.03	4	ns	ND		ND		
Haematocrit (%)	44.7 ± 9	9	43.8 ± 0.8	8	ns	45.6 ± 0.9	10	46.3 ± 1.0	9	ns

Values are means ± SEM, n= number of animals, ns= not significant, ND= not determined. Statistical significance was calculated by student t-test.

While exhibiting many features of Gitelman syndrome, NCC KO animals do not show hypokalemia as long as the mice are kept on standard food intake [37]. However, when placed on a K^+ restricted diet, NCC KO mice become hypokalemic [39]. Thus, we placed wildtype and I1-KO mice on a low K^+ (0.05 % K) diet for 5 days. In the course of these 5 days, food and water intake increased slightly in all animals on the low K^+ diet (Figure 14A and B). Furthermore, urine volumes were similar in I1-KO animals and wildtype animals on low K^+ diet (Figure 14C). As expected, on the low K^+ diet urinary K^+ excretion decreased in both genotypes (Figure 14D), whereas urinary Na^+ concentration did not differ in respect to the decreased dietary K^+ intake or the genotype (Figure 14E). The low dietary K^+ intake nevertheless had impact on urinary aldosterone levels that decreased to equally low values in both genotypes (Figure 14G). However, on day 5 on low K^+ diet, I1-deficient mice showed significantly lower blood K^+ levels than wildtype animals (Figure 14F).

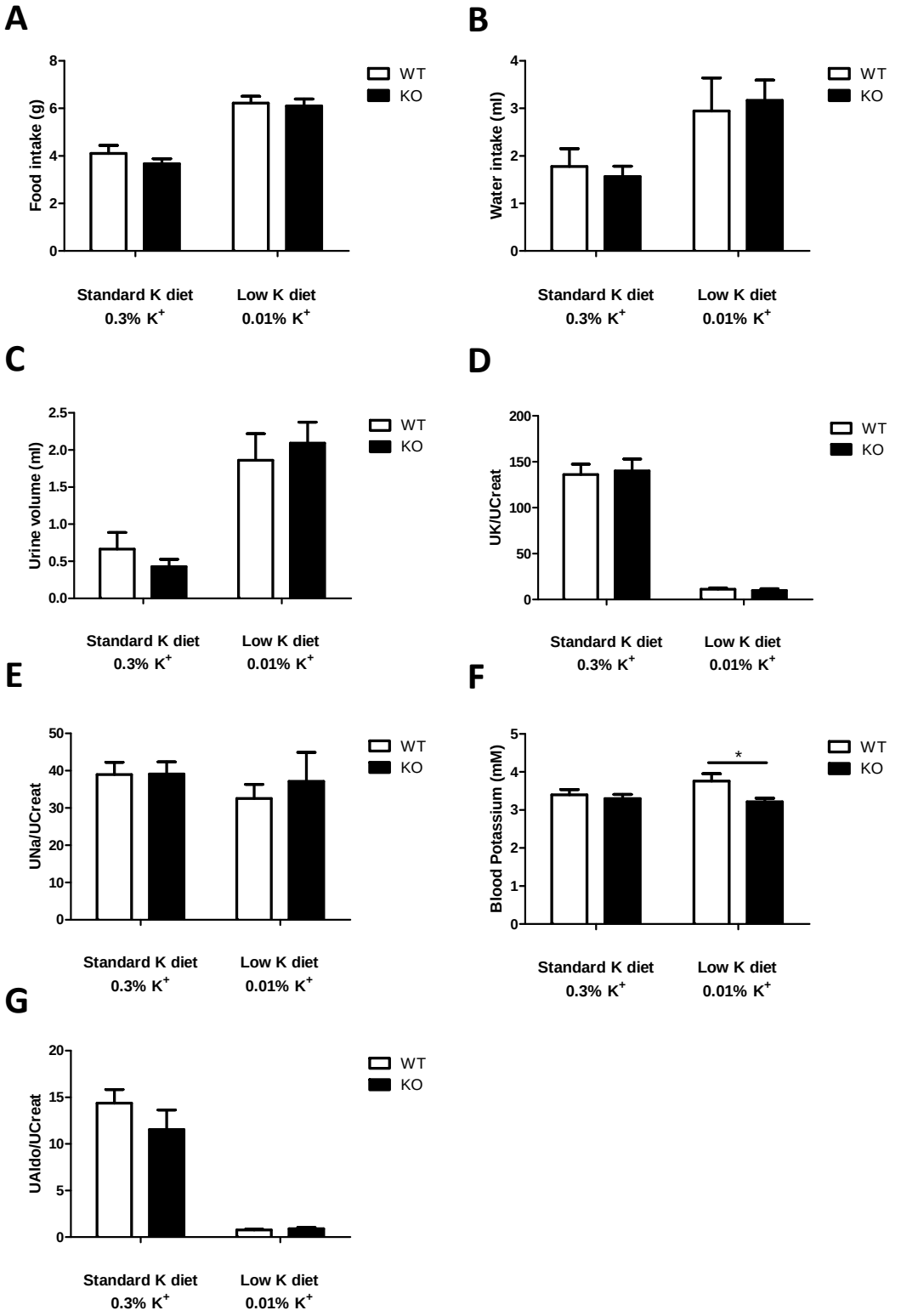

Figure 14: Hypokalemia in I1 deficient mice on low K^+ diet. Mice were kept in metabolic cages and fed with low K^+ diet (0.05%) for 5 days. (A) Food intake, (B) water intake and (C) urine volume were measured on standard diet and on low K^+ diet. Furthermore, (D) urinary K^+ excretion, (E) Na^+ excretion and (F) aldosterone concentration on standard diet and on low K^+ diet were analyzed and normalized against creatinine (WT: n=8 for standard diet and n=8 for low K^+ diet; KO: n=7 for standard diet and n=8 for low K^+ diet). (G) The effect of I1-deficiency on blood K^+ was measured on standard and on low K^+ diet (WT: n=7 for standard diet and n= 8 for low K diet; KO: n=9 for standard diet and n=6 for low K^+ diet). Values are means ± SEM. Statistical significance was calculated by student t-test (*= $p<0.05$).

3.1.6. Thiazide response and fractional cortical tubular volume in wildtype and I1-deficient mice

Some [122, 123], but not all mouse models ([123], Picard, Trompf et al. 2013 submitted and unpublished observation) with reduced NCC activity have a reduced diuretic and natriuretic response to thiazide and show a reduced fractional volume of the DCT. Therefore we analyzed the thiazide response and fractional cortical tubular volume of the DCT in wildtype and I1-KO mice.

I1-KO animals and their corresponding wildtype littermates were either fed with normal Na^+ diet or, to maximally activate NCC, with low Na^+ diet (0.05% Na^+) for 2 weeks before the animals were placed in metabolic cages. To see if the subcutaneous injection of 10 µl/g BW vehicle per se has any natriuretic effect, mice of both genotypes were injected with vehicle only. Analysis of various urine parameters did not reveal any differences between both genotypes (data not shown). On the subsequent day, all animals received a subcutaneous injection of HCTZ (50 mg/kg BW) and urinary Na^+ excretion was measured for the subsequent 6 h. HCTZ-induced natriuresis on normal diet as well as on low Na diet was not significantly different between both genotypes (Figure 15A). However, on low Na^+ diet, I1-KO mice had a tendency for a decreased HCTZ response (WT: 158.3 ± 10.8, n=8; KO: 118.5 ± 18.2, n=8, p=0.081).

To get insights about the effect of I1 depletion on the renal morphology we used immunofluorescence on fixative-perfused kidneys of wildtype and I1-KO animals. The fractional cortical tubular volume of NCC expressing DCTs was determined. No detectable effects of I1 deficiency on neither the fractional cortical tubule volume or the length of the DCT were found (Figure 15B).

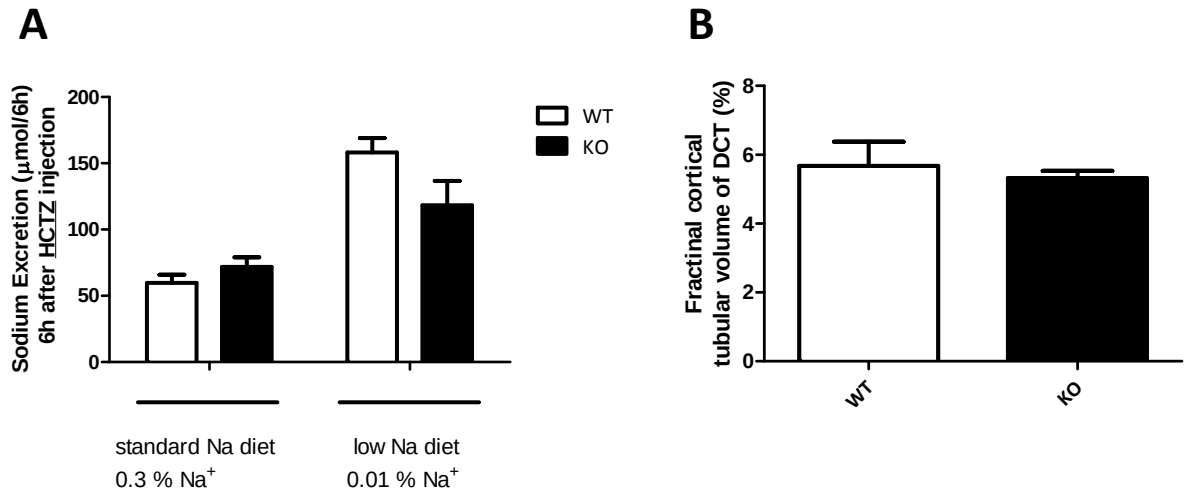

Figure 15: Effect of hydrochlorothiazide injection on urinary Na^+ excretion and morphometry of the DCT in I1-deficient mice. (A) Mice kept on normal Na^+ diet (0.3% Na^+) or low Na^+ diet (0.05% Na^+) were injected subcutaneously with HCTZ (50 mg/kg of body weight). Urines from wildtype (WT) and I1-KO mice were collected 6 h after injection (WT n=9 and KO n= 8 on standard diet; WT n=9 and KO n=8 on low Na^+ diet). (B) Immunofluorescence labeling with NCC on renal cortex was used to investigate the morphometry of DCT in I1-deficient mice (n=5 for both genotypes). Values are means ± SEM. Statistical significance was calculated by student t-test.

3.1.7. I1-deficient mice do not show alterations of the RAA-system

To assess the activity of the RAA-system, renal renin mRNA expression and urinary aldosterone excretion were determined in wildtype and I1-KO mice. Neither renin mRNA (Figure 16) nor urinary aldosterone excretion (Table 4) were different between genotypes.

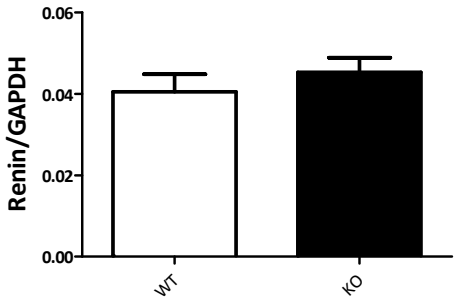

Figure 16: Expression of renin in WT and I1-KO animals. mRNA expression of renin in whole kidneys from wildtype (WT) and I1-KO mice was normalized against GAPDH. Values are means ± SEM, n=6.

3.1.8. I1-deficient mice show no changes in mRNA expression of DCT specific proteins

To investigate if I1 loss impacts on the mRNA-expression of other DCT-specific proteins, RNA from whole kidneys of wildtype and I1-KO mice was extracted and qRT-PCR analysis was performed. I1-KO mice do not show any alteration in the mRNA level of NCC, NCC-regulating WNK kinases (WNK1S, WNK1L or WNK4) or TRPM6 when compared to WT animals (Table 6).

Table 6: Renal gene expression in wildtype (WT) and I1-KO littermates on standard diet (0.3% Na^+).

	WT	n	***KO***	n	p
NCC	0.600± 0.018	6	0.550 ± 0.017	6	ns
WNK1S	0.0531 ± 0.0027	6	0.0482 ± 0.0018	6	ns
WNK1L	0.0338 ± 0.0028	6	0.0364 ± 0.0010	6	ns
WNK4	0.0516 ± 0.0029	6	0.0511 ± 0.0020	6	ns
TRPM6	0.0141 ± 0.001	6	0.0127 ± 0.0007	6	ns

Gene expressions are relative to GAPDH gene expression. Values are means ± SEM, n=number of mice, ns=not significant. Statistical significance is assessed by student t-test.

3.1.9. Compensatory up-regulation of pendrin in I1 deficient mice

Despite the reduction in NCC phosphorylation by approximately 50%, I1-deficient mice did not show a reduced thiazide-response or DCT atrophy compared with their wildtype littermates. Potential compensatory molecular mechanisms might explain the rather mild phenotype of I1-deficient mice. Hence, immunoblot analyses of the known renal sodium transporters along the nephron were performed (Figure 17). Protein abundance of DCT upstream localized renal sodium transporters NaPiIIa (expressed in the PT) and NKCC2 (expressed in the TAL) did not show significant changes in I1-KO animals. Furthermore, protein expression of all three subunits of ENaC (expressed along DCT2, CNT and CD) as well as NDCBE (Na^+-driven $Cl^-/HCO3^-$ exchanger expressed in the collecting duct) were not altered in I1-deficient mice compared to wildtype mice. However, the renal protein expression of pendrin was significantly up-regulated in the I1-KO mice.

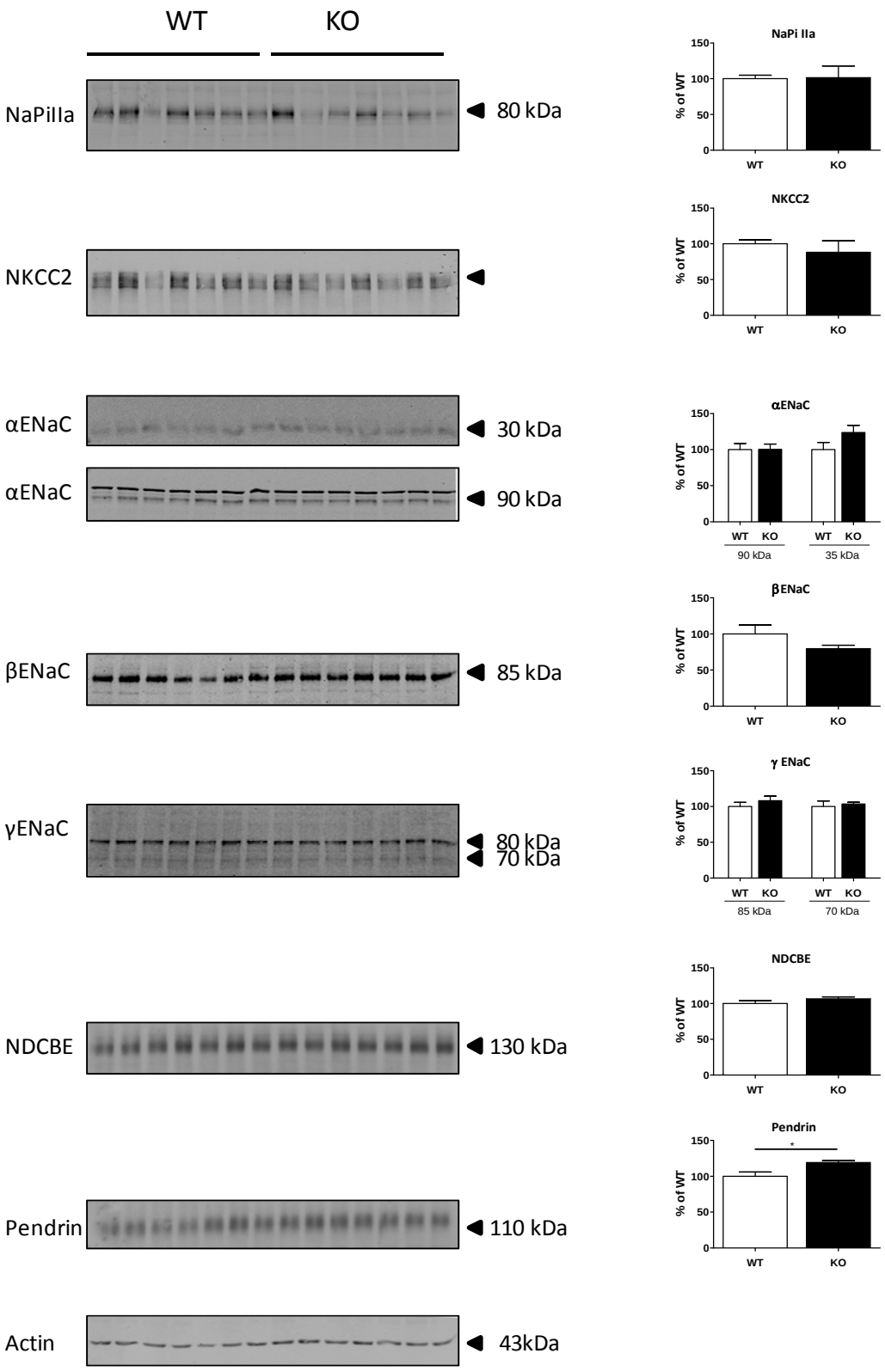

Figure 17: I1 deficiency causes a significant up-regulation of pendrin in the kidney. Western blot experiments were performed using membrane preparations from kidneys of wildtype (WT) and I1-deficient (KO) mice to determine the abundance of NaPi IIa, NKCC2, αENaC, βENaC, γENaC, NDCBE and pendrin. Densitometric values for each protein were normalized against actin. Densitometric analysis revealed a significant up-regulation of pendrin in I1-KO mice, whereas all other renal Na^+ transporters were unchanged. Relative measurements were calculated with the average of the WT group set at 100%. Results are means ± SEM, n=7. Statistical significance was calculated by student t-test (*=$p<0.05$).

3.1.10. Unaltered SPAK phosphorylation in I1-deficient mice

To examine whether the reduction in NCC phosphorylation in the I1-deficient mice is mediated by changes in WNK/SPAK signaling, immunoblot analysis of I1-KO mice and their corresponding wildtype littermates were performed using antibodies directed against total SPAK and SPAK phosphorylated at serine 373. The phospho-specifity of the pSPAK antibody was tested in total kidney protein homogenates treated with Calf Intestinal Phosphatase (+CIP). A ~ 70 kDa band representing pSPAK was seen in COPAS-sorted DCTs and also in whole kidney preparation. Dephosphorylation of the total kidney homogenate (+CIP) completely abolished the band at ~ 70kDa (Figure 18A). Compared to wildtype littermates, I1-deficient mice did not show any difference in the abundance of total SPAK and phosphorylated SPAK (Figure 18B).

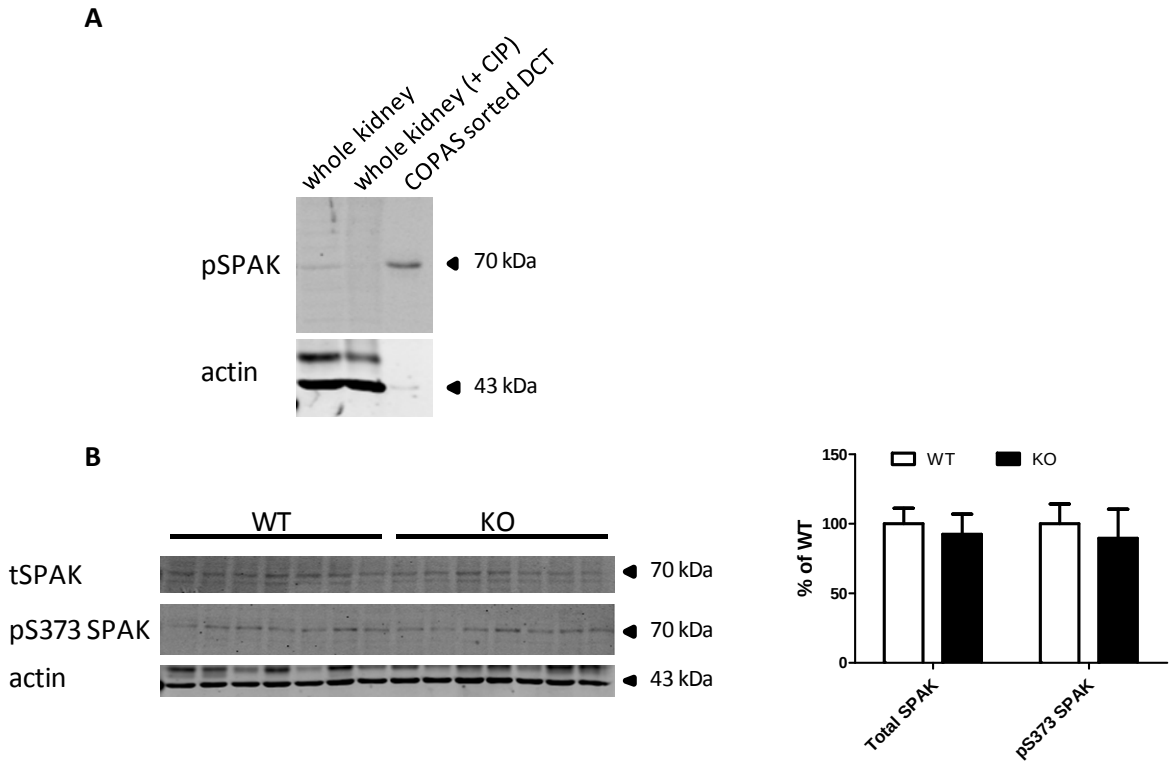

Figure 18: I1 deficiency does not affect SPAK phosphorylation. (A) The specificity of pSPAK was confirmed using total kidney protein lysates from wildtype (WT) that were either treated with or without Calf Intestinal Phosphatase for 1 h at 37°C. In addition, 400 DCT were also transferred to the membrane to prove the strong expression of pSPAK in the DCT. (B) Immunoblotting for total SPAK (tSPAK) and SPAK phosphorylated at serine 373 (pS373 SPAK) in the total membrane fraction of kidneys from WT and I1-KO animals did not reveal differences between genotypes. All densitometric data were normalized against actin. Relative measurements were calculated with the average of the WT group set at 100%. Results are means ± SEM, n=7. Statistical significance was calculated by student t-test.

3.2. Project 2: Investigating the role of PKD1 for NCC regulation

3.2.1. Localization of PKD1 in the kidney

To localize PKD1 in the mouse kidney, fluorescent immunohistochemistry was performed on cryosections of PFA-fixed mouse kidneys. High expression levels of PKD1 could be detected in the cytoplasma of NCC expressing DCT1 and DCT2 cells as well as in the preceding, NKCC2 positive, TAL (Figure 19).

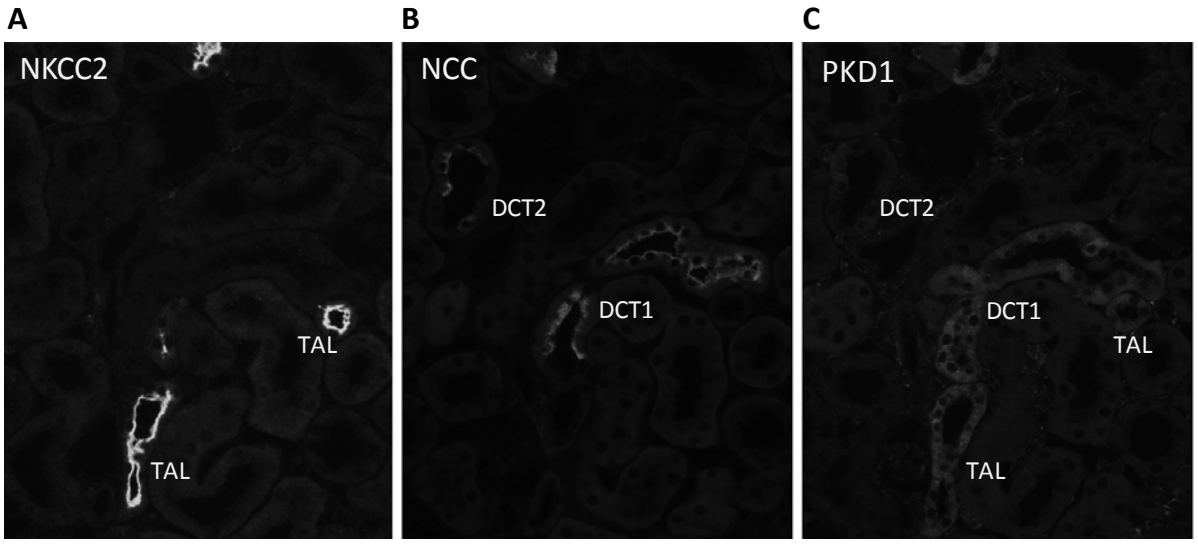

Figure 19: Expression of PKD1 in mouse kidney. Consecutive cryosections of mouse kidney cortex stained with antibodies against (A) NKCC2, (B) NCC and (C) PKD1. PKD1 is highly expressed in the cytoplasm of NKCC2-positive TAL and NCC-positive DCT1 and DCT2.

3.2.2. Aldosterone regulates PKD1 in vivo

In vitro experiments of McEneaney and coworkers showed that aldosterone regulates PKD1 in the collecting duct cell line M1 [181]. To test if aldosterone has impact on PKD1 expression and phosphorylation *in vivo*, we analyzed archived kidneys from adrenalectomized rats that were treated with a single injection of aldosterone (0.5 µg/g BW, i.p.), or vehicle only [21]. Renal PKD1 expression and phosphorylation at position serine 918 was examined by immunohistochemistry in kidneys that have been harvested 2 h and 4 h after injection (Figure 20).

2 h after aldosterone injection, a dramatic increase of total PKD1 protein abundance along the DCT could be observed, that persisted and was still visible 4 h after injection. In addition, PKD1 trafficking from cytoplasmatic compartments to the apical cell membrane of the DCT cells could be observed already 2 h after aldosterone injection. Additionally phosphorylated PKD1 at serine 918 was exclusively detectable in the apical membrane of DCT cells 2 h and even more prominent 4 h after

aldosterone injection. These findings for PKD1 run parallel with the findings for the phosphorylation of NCC at position threonine 58 that was strongly up-regulated 2 h and 4 h after aldosterone injection. In contrast the expression of total NCC protein along the DCT remained unchanged.

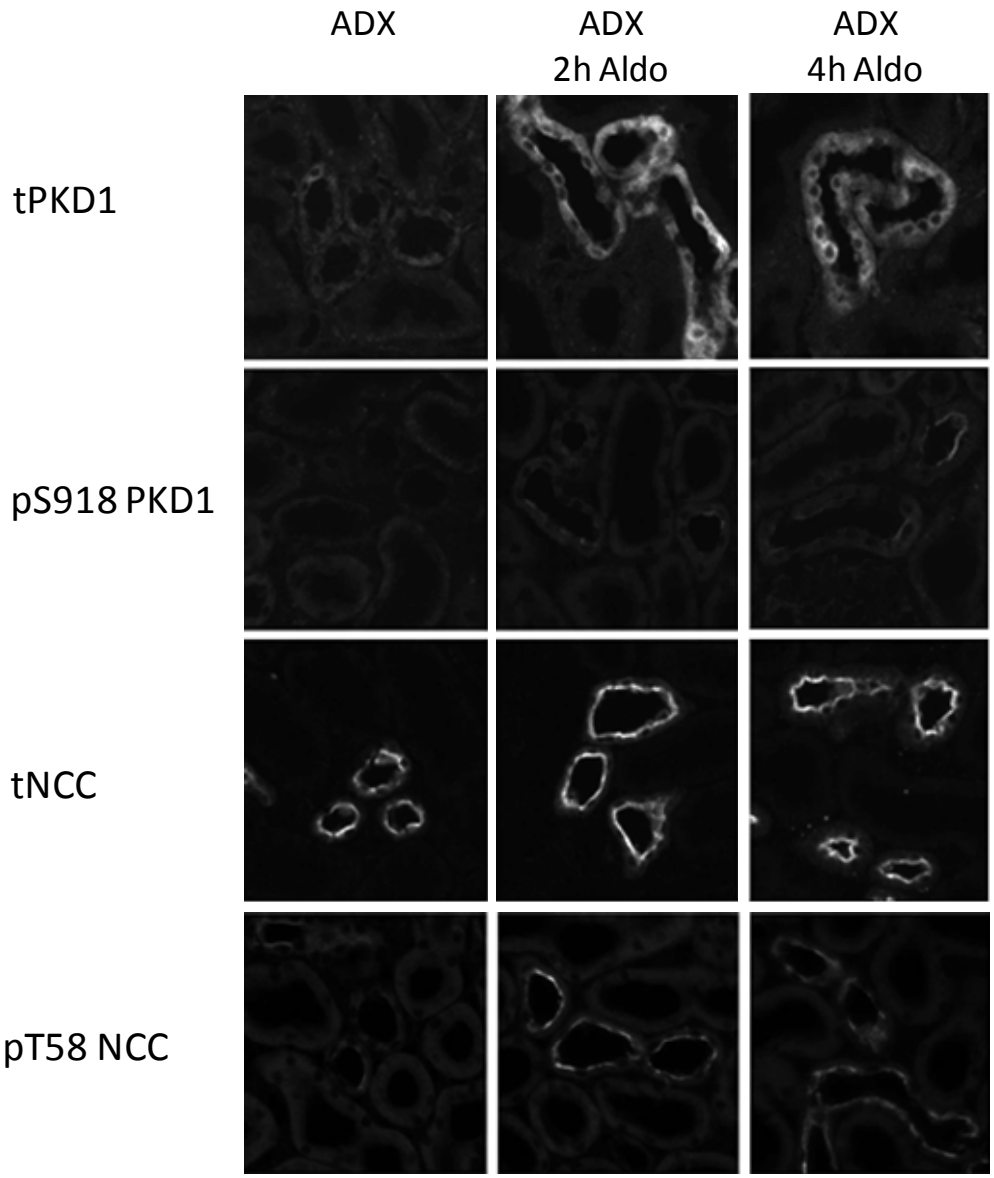

Figure 20: Effect of aldosterone on PKD1 in kidneys of adrenalectomized rats. Immunohistochemistry of kidneys from adrenalectomized (ADX) rats 2 h or 4 h after a single dose of vehicle or aldosterone injection (0.5 µg/gBW). Immunostainings using applying antibodies against total PKD1 (tPKD1), PKD1 phosphorylated at serine 918 (pS918 PKD1), total NCC (tNCC) and NCC phosphorylated at threonine 58 (pT58 NCC). In all aldosterone-injected animals, a rapid up-regulation of total PKD1 and phosphorylated PKD1 at serine 918 is accompanied by an enhanced phosphorylation of NCC, which is visible already 2 h after aldosterone injection. Note the predominant intracellular and predominant subapical localization of total and phosphorylated PKD1, respectively.

3.2.3. Reduced total PKD1 expression and phosphorylation levels in AS-deficient mice

To further investigate the impact of aldosterone on PKD1, aldosterone synthase-deficient mice (AS-KO) were analyzed. Immunoblot analysis of membrane preparation of kidneys of wildtype and AS-KO animals revealed a significant decrease of total PKD1 expression as well as a significant reduction of PKD1 phosphorylated at serine 916 (Figure 21A). qRT-PCR analysis showed that PKD1 is decreased already at the mRNA level (Figure 21B).

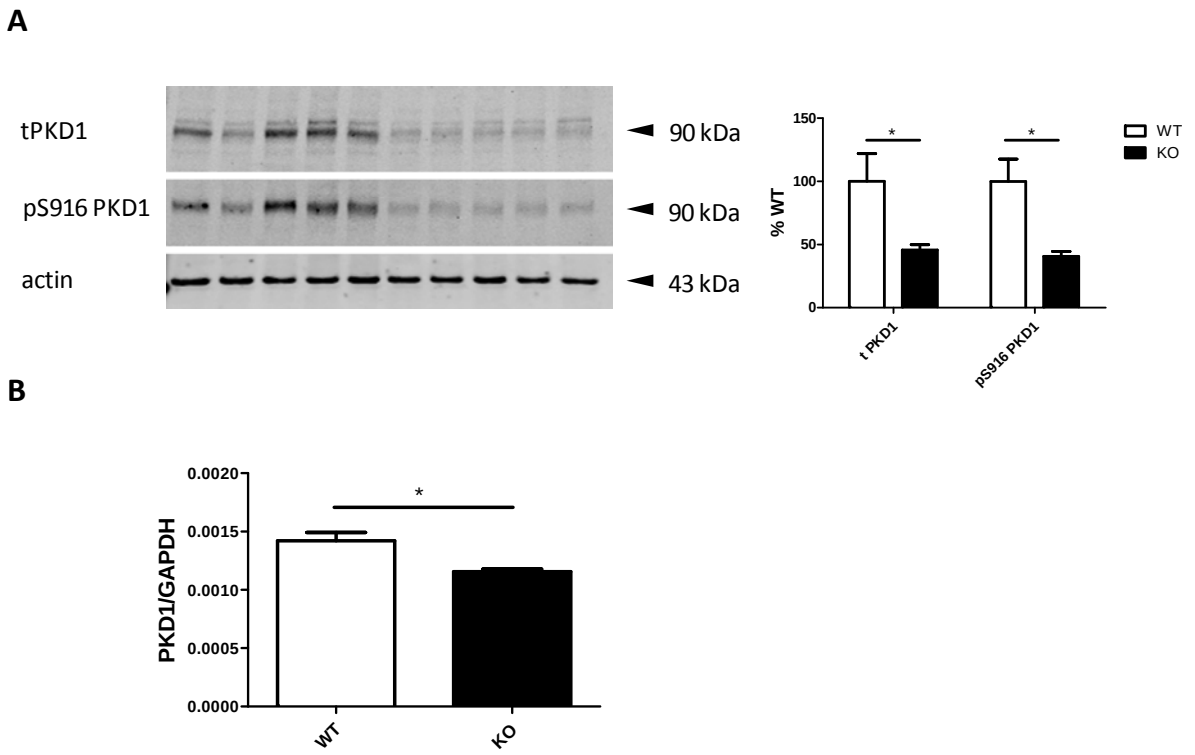

Figure 21: Reduced PKD1 abundance in AS KO animals. A) Western blot experiments were performed using membrane preparations from kidneys of wildtype (WT) and AS-KO animals to determine the expression of total PKD1 (tPKD1) and PKD1 phosphorylation site at serine 916 (pS916 PKD1). Densitometric analyses showed a significant decrease of tPKD1 and pS916 PKD1. All densitometric data were normalized against actin. Relative measurements were calculated with the average of the WT group set at 100%, Data are means ± SEM, n=5. (B) PKD1 mRNA expression in whole kidney preparations of WT and AS-KO animals was assessed by qRT-PCR. Data are means ± SEM, n=3. Statistical significance was calculated by student t-test (*=p<0.05).

3.2.4. Mice with DCT1-specific deletion of PKD1

To investigate the role of renal PKD1 in more detail, mice with a specific deletion of PKD1 in the DCT1 (PKD1-KO mice) were generated by cross-breeding floxed PKD1 mice (PKD1 $^{flox/flox}$ mice) with mice expressing cre under the parvalbumin promoter (PV-cre mice). To confirm the successful deletion of PKD1 in the DCT1, immunohistochemistry on serial kidney sections were performed. To discriminate between DCT1 and DCT2 segments, antibodies against PV, expressed in DCT1 only (Figure 22A) and Calbindin D28k, strongest signal in DCT2 (Figure 22B), were used. Cre-expression could exclusively be detected along the PV-positive DCT1. Cre-immunostaining ceased at the transition to the DCT2 (Figure 22C). Consistently, PKD1 expression was absent from the PV- and cre-positive DCT1 but was still detectable in the PV- and cre-negative DCT2 (Figure 22D).

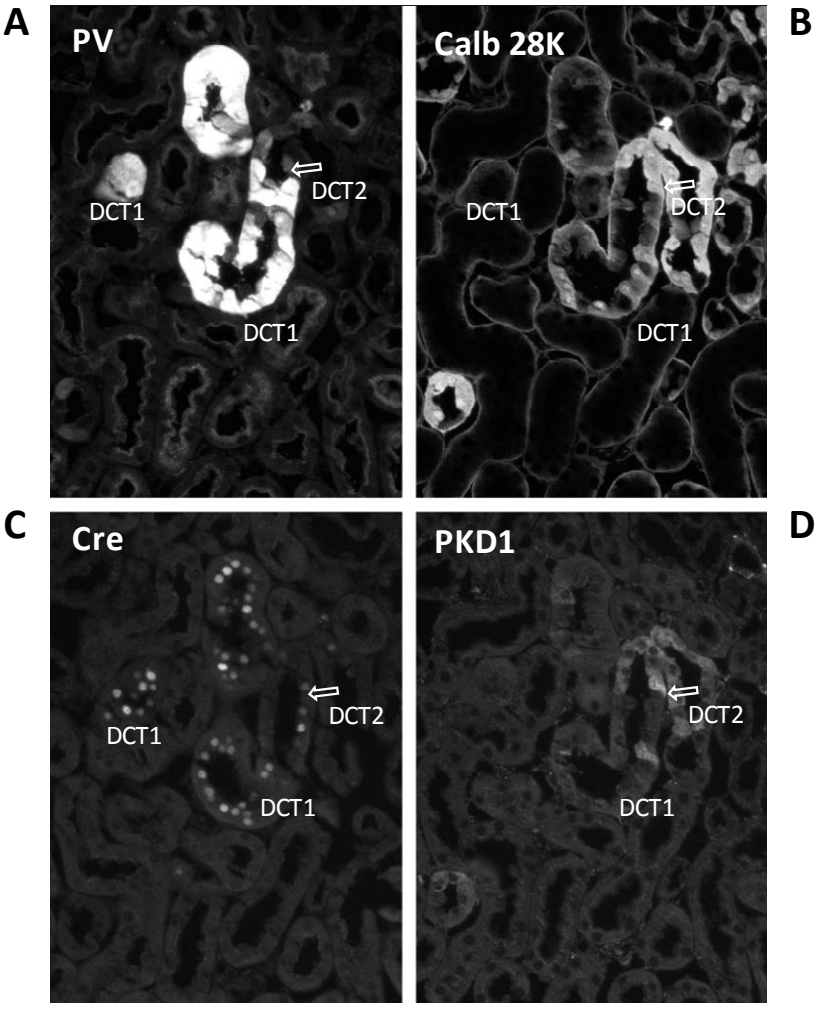

Figure 22: Successful knockout of PKD1 in the DCT1 of PKD1-KO mice. Consecutive cryosections of a kidney from a PKD1$^{flox/flox}$ X PVcre mouse stained with antibodies against (A) parvalbumin (PV), (B) calbindin 28K (Calb 28K), (C) cre and (D) PKD1 confirm the absence of PKD1 abundance in DCT1.

These findings were further confirmed by western blot analyzes of COPAS-sorted DCTs from PKD1 PVcre PVeGFP mice (Figure 23). While PKD1 was well detectable in DCT of control animals, PKD1 was barely seen in DCT preparations from PKD1-KO animals (KO). The weak band is likely explained by slight contamination by the preceding PKD1-expressing TAL or the DCT2.

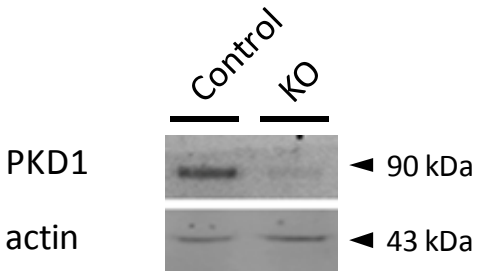

Figure 23: Detection of PKD1 in COPAS-sorted DCTs from control and PKD1 KO mice. DCT1 were isolated with COPAS from kidneys of PKD1 PVcre eGFP mice (control and PKD1 KO). Immunoblot of 400 DCTs from each mouse showed a high level of PKD1 in the control animal, but only a very weak band in the PKD1 KO mouse. Actin served as a loading control.

3.2.5. PKD1 regulates the phosphorylation of NCC in vivo

To test the effect of PKD1 deficiency on total NCC expression and NCC phosphorylation in the kidney *in vivo*, immunoblots of membrane preparations of kidneys from control mice and PKD1-KO mice were performed. Total abundance of NCC was determined using an antibody against the extracellular epitope of NCC (total NCC). The phosphorylation level of NCC was assessed using phosphoform-specific antibodies against the phosphorylation sites threonine 53 (pT53 NCC), threonine 58 (pT58 NCC) and serine 71 (pS71 NCC). While the total NCC abundance was not changed, the phosphorylation of all tested phosphorylation sites was significantly reduced in the kidneys of PKD1-KO mice, compared to control littermates (Figure 24A). Likewise, immunoblots of COPAS-isolated DCTs from PKD1 PVcre PVeGFP control mice and PKD1 PVcre PVeGFP KO mice revealed that total NCC abundance was not changed, but NCC phosphorylation at threonine 53 was reduced in DCT1 from PKD1 deficient mice (Figure 24B).

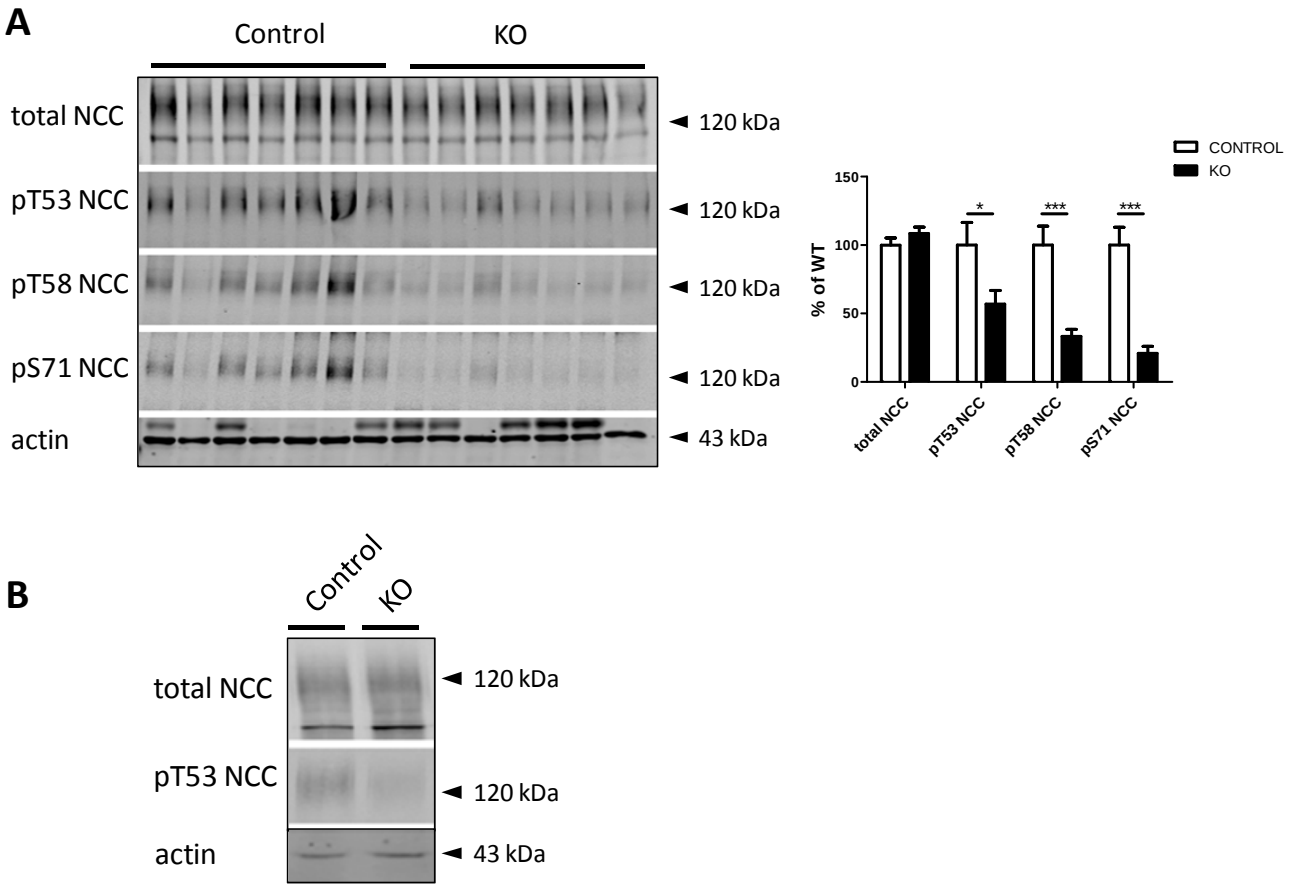

Figure 24: Loss of PKD1 reduces NCC phosphorylation *in vivo*. (A) Immunoblots for total NCC abundance and NCC phosphorylated forms at threonine 53 (pT53 NCC), threonine 58 (pT58 NCC) and serine (pS71 NCC) in total membrane fraction from mouse kidneys of control mice and PKD1-KO mice (KO). Densitometric analysis revealed a significant down-regulation of all tested NCC phosphorylation sites in PKD1-KO mice, whereas the total NCC expression was not altered. All membranes were normalized against actin. Relative measurements were calculated with the averages of the control group set at 100%. Results are means ± SEM, n=7. Statistical significance was calculated by student t-test (*=p≤0.05, ***=p≤0.001.). (B) Detection of total NCC and NCC phosphorylated site threonine 53 (pT53 NCC) in COPAS-isolated DCTs from kidneys of PKD1 PV-cre PV-eGFP control mouse and PKD1 PV-cre PV-eGFP KO mouse. Actin served as a loading control.

3.2.6. Mice with DCT1-specific deletion of PKD1 show a reduction in blood pressure

Lack of PKD1 in the DCT1 leads to a significant reduction all tested phosphorylation site of NCC *in vivo*. To see if this significantly lower NCC phosphorylation causes lower arterial blood pressure, systolic blood pressure was monitored by the tail-cuff method in PKD1-deficient males and their corresponding control littermates on standard diet (0.3% Na^+) and on low Na^+ diet (0.05% Na^+). On standard diet there were no significant changes in systolic blood pressure between control mice and PKD1-KO animals. However, a clear tendency towards lower blood pressure in PKD1-KO animals could be observed (day 5: Control: 100.12 ± 6.25 mmHg, PKD1-KO: 92.14 ± 1.51 mmHg; p= 0.2745; Figure 25A). When animals were fed chronically with the low Na^+ diet, PKD1-KO mice showed a significant reduction in systolic blood pressure on day 2 and a tendency towards reduced blood pressure was observable during the whole experiment (Figure 25B).

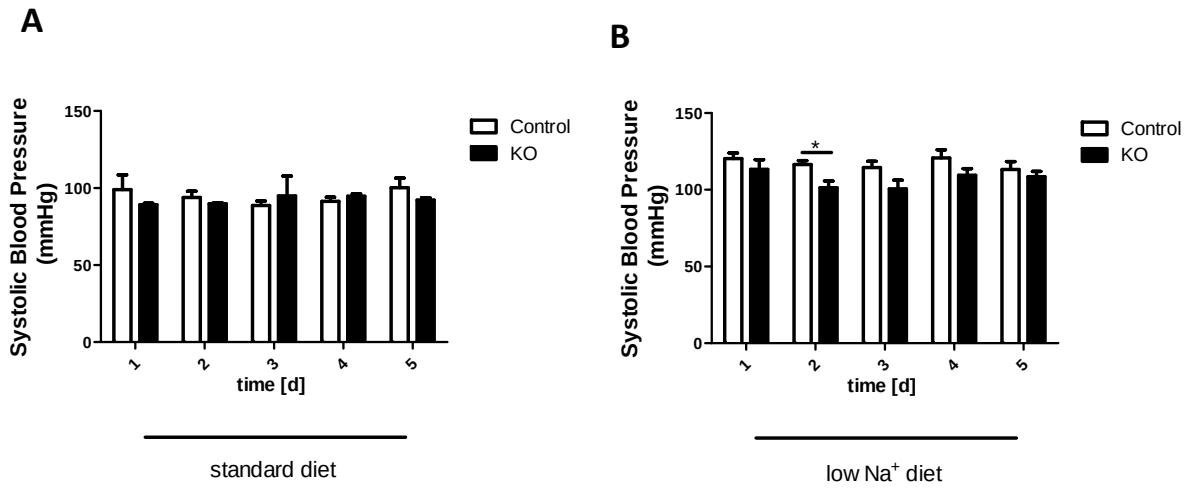

Figure 25: PKD1-KO animals show a reduced blood pressure under low Na^+ diet. Arterial blood pressure was measured by tail-cuff method in control and PKD1-KO animals on (A) normal diet (0.3% Na^+) and (B) low Na^+ diet (0.05% Na^+). Values are means ± SEM, control animals: n=3 to 7, PKD1-KO animals n=4-7 on standard diet; control animals: n=5 to 7, PKD1-KO animals n=4-8 on low Na^+ diet. Statistical significance was calculated by student t-test (*=p<0.05).

3.2.7. No evidence for disturbed HCTZ-response in PKD1-KO mice

As presented above, PKD1-KO animals display a significantly lower NCC phosphorylation that might lead to a reduced NCC activity. Therefore, HCTZ tests in control mice and PKD1-KO mice on standard diet (0.3% Na^+) and on low Na^+ diet (0.05% Na^+) were performed. Urine was collected 6 h after intraperitoneal injection of HCTZ (40 mg/kgBW) and analyzed for Na^+, K^+ and Cl^- excretion. On standard diet as well as on low Na^+ diet, Na^+, K^+ and Cl^- concentrations did not differ between genotypes (Figure 26 A-C).

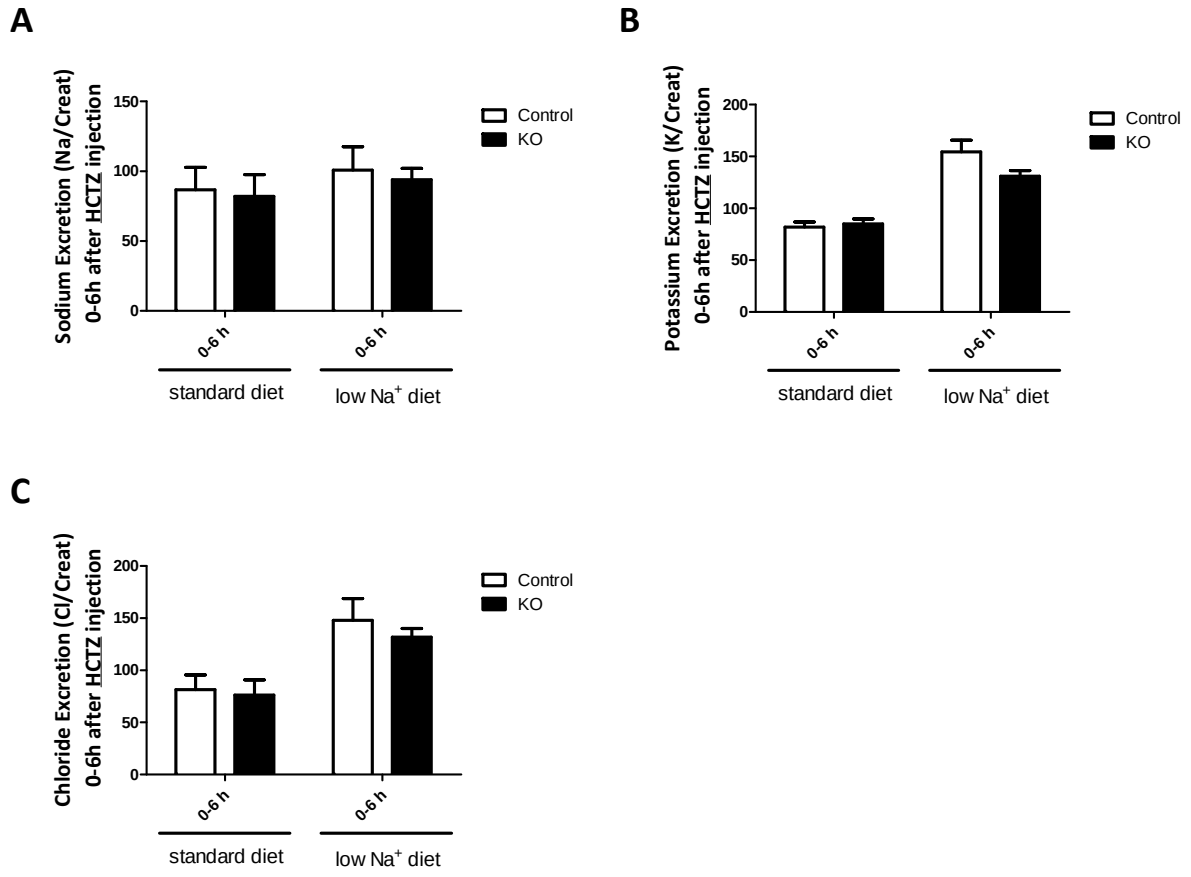

Figure 26: Testing the functional activity of NCC in PKD1-KO mice on standard and low Na^+ diet. (A) Urinary Na^+-, (B) K^+-, and (C) Cl^--excretion 6 h after HCTZ treatment (40 mg/kgBW). Values are means ± SEM, n=5 to 7 in both genotypes for standard diet, n= 4 to 6 in both genotypes for low Na^+ diet. Statistical significance was calculated by student t-test.

3.2.8. PKD1-KO mice show no overt Gitelman syndrom

To determine physiological urine and blood gas parameters on normal diet (0.3% Na^+) and on chronic low Na^+ diet (0.05% Na^+), control and PKD1-KO mice were placed in metabolic cages. Interestingly, despite the significantly lower NCC phosphorylation, PKD1-KO mice showed no fully developed Gitelman-like phenotype. Compared with control mice, PKD1-KO mice did not show any significant differences for urinary ion excretion (Table 7) and blood ion concentration, blood pH or blood bicarbonate (Table 8) on both diets. However, there was a slight tendency for a higher renal Mg^+ excretion (Controls: 4.67 ± 0.73 Mg/Creatinine, PKD1-KO: 5.69 ± 0.85 Mg/Creatinine, p=0.3841) and lower plasma K^+ level (Controls: 4.93 ± 0.21 mM K^+; PKD1-KO: 4.4 ± 0.33 mM K^+, p=0.1941) on standard diet. Also on a low Na^+ diet (0.3% Na^+ for 14 days) no statistical difference for the analyzed urine and plasma parameters were observed (Table 9 and Table 10).

Table 7: Physiological urinary parameters of control and PKD1-KO female mice on standard diet.

	Control	n	PKD1-KO	n	p
Water intake (ml)	1.50 ± 0.40	6	1.85 ± 0.49	6	ns
Urine volume (ml)	1.32 ± 0.58	6	1.22 ± 0.15	6	ns
Na^+/Creat	55.52 ± 9.73	6	58.25 ±12.36	6	ns
K^+/Creat	72.22 ± 4.56	5	77.70 ±7.22	6	ns
Mg^+/Creat	4.67 ± 0.73	6	5.69 ± 0.85	6	ns
Osmolaritiy (mosmol)	2560 ± 215.1	9	2640 ± 148.52	9	ns

Values are means ± SEM, n=number of animals, ns= not significant. Statistical significance was calculated by student t-test.

Table 8: Physiological blood gas parameters of control and PKD1-KO female mice on standard diet.

	Control	n	ko	n	p
pH	7.23 ± 0.015	6	7.2 ± 0.023	5	ns
pCO_2 (mmHg)	49.82 ± 1.3	6	51.5 ± 3.25	5	ns
HCO_3^- (mM)	20.37 ± 0.63	6	19.32 ± 0.46	5	ns
K^+ (mM)	4.93 ± 0.21	6	4.4 ± 0.33	5	ns
Na^+ (mM)	148.17 ± 1.14	6	149.4 ± 1.47	5	ns
Cl^- (mM)	112.67 ± 0.92	6	113.8 ± 0.58	5	ns

Ca^{2+} (mM)	1.28 ± 0.01	6	1.31 ± 0.019	5	ns
Hematocrit (%)	45.35 ± 0.68	6	44.18 ± 0.53	5	ns

Values are means ± SEM, n=number of animals, ns= not significant. Statistical significance was calculated by student t-test.

Table 9: Physiological urinary parameters of control and PKD1-KO male mice on low Na^+ diet.

	Control	n	ko	n	p
Water intake (ml)	1.55 ± 0.29	7	1.26 ± 0.13	7	ns
Urine volume (ml)	1.15 ± 0.12	7	1.06 ± 0.21	7	ns
Na^+/Creat	9.87 ± 0.99	6	8.46 ± 2.19	6	ns
K^+/Creat	67.82 ± 18.13	6	68.33 ± 6.68	6	ns
Mg^+/Creat	7.89 ± 1.49	6	6.78 ± 1.17	6	ns

Values are means ± SEM, n=number of animals, ns= not significant. Statistical significance was calculated by student t-test.

Table 10: Physiological blood gas parameters of control and PKD1-KO male mice on low Na^+ diet.

	Control	n	ko	n	p
pH	7.32 ± 0.013	7	7.28 ± 0.011	7	ns
pCO_2 (mmHg)	43.9 ± 1.67	7	46.8 ± 0.94	7	ns
HCO_3^- (mM)	22.37 ± 0.58	7	21.44 ± 0.54	7	ns
K^+ (mM)	4.8 ± 0.1	7	4.58 ± 0.17	6	ns
Na^+ (mM)	148.43 ± 0.48	7	148.57 ± 0.2	7	ns
Cl^- (mM)	111.86 ± 0.55	7	111.86 ± 0.51	7	ns
Ca^{2+} (mM)	1.25 ± 0.011	7	1.26 ± 0.01	7	ns
Hematocrit (%)	47.82 ± 0.92	7	46.77 ± 0.86	7	ns

Values are means ± SEM, n=number of animals, ns= not significant. Statistical significance was calculated by student t-test.

3.2.9. PKD1-KO mice display significantly elevated aldosterone levels but unaltered renin expression

PKD1-deficient mice exhibited a significant increase in urinary aldosterone excretion in comparison to control animals (Figure 27A). In addition, analysis of plasma aldosterone confirmed higher aldosterone levels in PKD1 KO mice compared to their control littermates (Figure 27B). Nevertheless, testing renal renin mRNA expression in kidneys of control mice versus PKD-1 KO mice with qRT-PCR revealed no differences between the genotypes (Figure 27C).

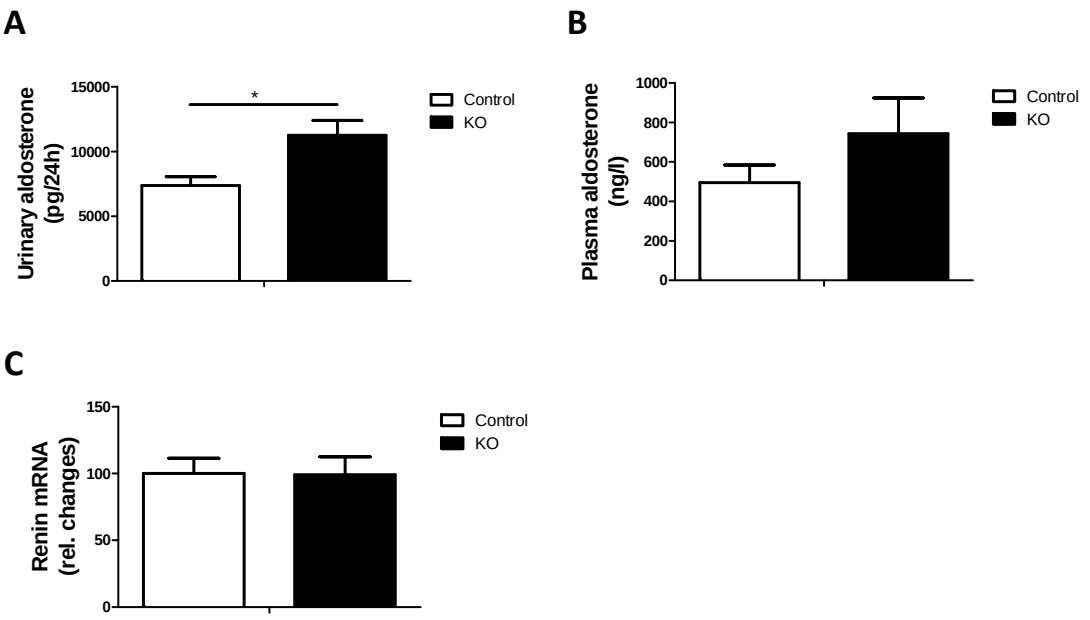

Figure 27: Aldosterone measurements and renin expression in control and PKD1-KO mice. Aldosterone concentration was measured in (A) urine and (B) plasma of control (n=6 and n=5 respectively) and PKD1-KO mice (n=7 and n=6 respectively). (C) Renin expression was assessed by qRT-PCR, n=5 for each group. Values are means ± SEM. Statistical significance was calculated by student t-test (*=p≤0.05).

3.2.10. PKD1-KO mice do not show no an altered expression of NCC, WNK kinases and other distal tubule marker mRNAs

Quantitative mRNA analyses by qRT-PCR was used to test for the altered expression of distal tubule marker mRNA. Neither NCC, WNK kinases, TRPM6, PV, Calbindin D28k, NKCC2 was differently expressed in kidneys of PKD1-KO mice when compared to kidneys of control mice (Table 11).

Table 11: Renal gene expression in control and PKD1-KO littermates on standard diet.

	Control	n	KO	n	p
NCC	0.609± 0.004	6	0.587 ± 0.006	6	ns
WNK1S	0.013 ± 0.0006	6	0.012 ± 0.001	6	ns
WNK1L	0.02 ± 0.002	6	0.022 ± 0.002	6	ns
WNK4	0.021 ± 0.0016	6	0.016 ± 0.0009	6	ns
TRPM6	0.006 ± 0.0004	6	0.005 ± 0.0006	6	ns
PV	0.008 ± 0.0006	6	0.006 ± 0.0008	6	ns
Calbindin D28K	0.093 ± 0.0064	6	0.094 ± 0.0138	6	ns
NKCC2	0.0062 ± 0.0015	6	0.0057 ± 0.0014	6	ns

Gene expressions are relative to GAPDH gene expression. Values are means ± SEM, n=number of mice, ns=not significant. Statistical significance is assessed by student t-test.

3.2.11. Compensatory up-regulation of ENaC in PKD1 KO mice

To test whether up-regulation of other ion transporters along the nephron may compensate for the reduced phosphorylation of NCC in PKD1-KO mice, western blot analyses using total membrane preparations from kidneys of control and PKD1-KO mice were performed (Figure 28). Expression of sodium transporters located in the PT (NaPiIIa) or in the TAL (NKCC2) showed no differences between the genotypes. However, all three subunits (α, β, γ) of ENaC, expressed in nephron portions localized downstream of the DCT1 (DCT2, CNT, CD), were significantly up-regulated in PKD1-KO mice when compared to control animals. Renal abundance of pendrin, expressed in intercalated cells [201], did not differ between the genotypes.

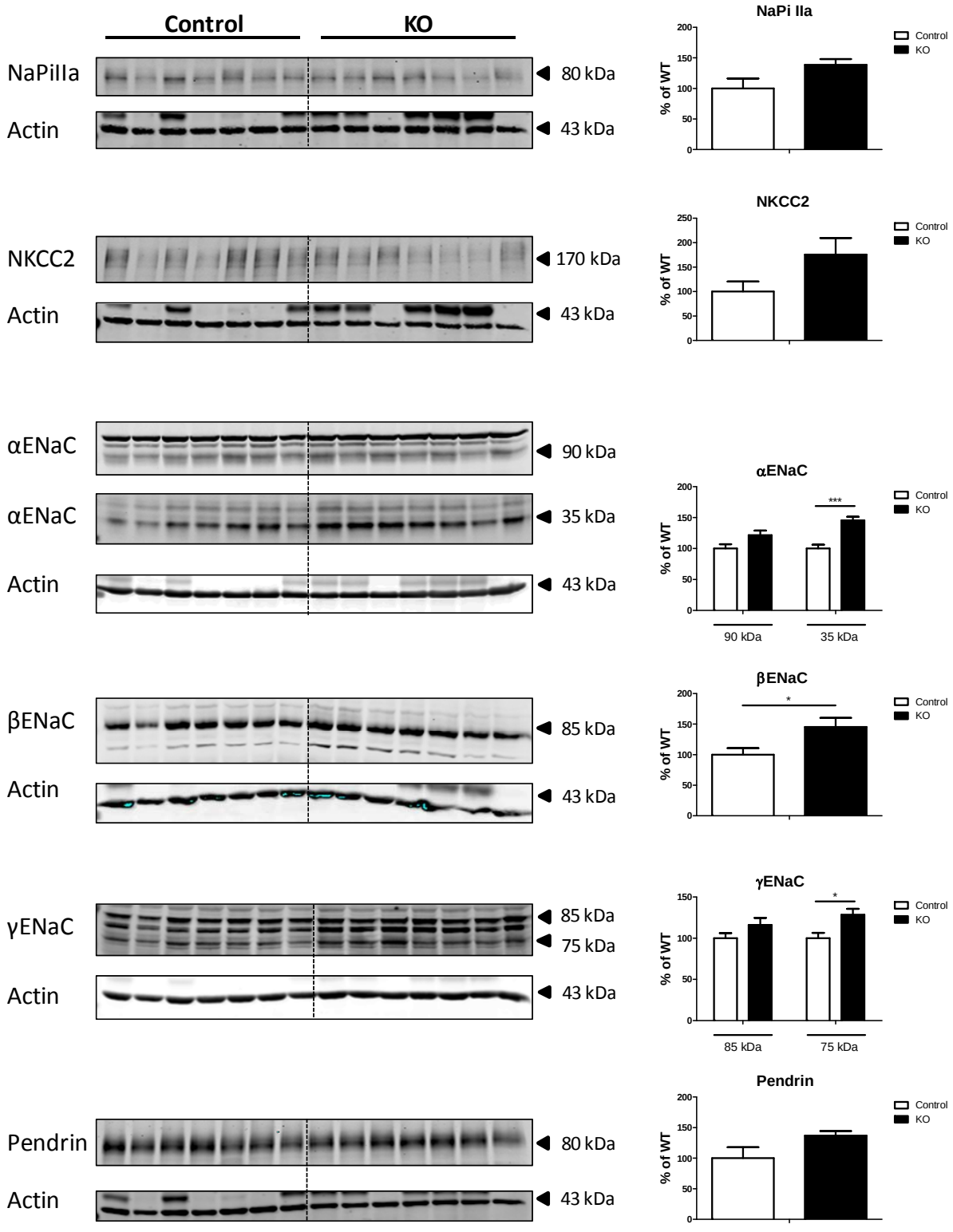

Figure 28: PKD1–KO mice display significant up-regulation of ENaC in the kidney. Westernblot experiments were performed using total membrane preparations from kidneys of control and PKD1-KO mice to determine the protein abundance of NaPi IIa, NKCC2, αENaC, βENaC, γENaC, and pendrin. Densitometric analysis revealed a significant up-regulation of all subunits of ENaC, whereas all other renal Na^+ transporters were not affected. Densitomitric data were normalized against actin. Relative measurements were calculated with the averages of the control group set at 100%. Results are mean ± SEM, n=7. Statistical significance was calculated by student t-test (*=p≤0.05, **=p≤0.01, ***=≤0.001).

3.2.12. Preliminary data: PKD1 increases the abundance of total NCC in transiently transfected HEK293T cells

The *in vivo* experiments supported the assumption that PKD1 is involved in the regulation of NCC activity. Hence, to obtain further insight into underlying mechanisms, *in vitro* experiments using HEK293T cells transfected with NCC together with either PKD1 wildtype (PKD1 WT), kinase dead PKD1 mutant (PKD1 K612W) or constitutive active PKD1 mutant (PKD1 S738/744E) were performed (Figure 29). In contrast to the kinase-dead PKD1 mutant (PKD1 K612W), the constitutively active mutant of PKD1 (PKD1 S738/744E) increased the expression of total NCC when compared to the transfection with wildtype PKD1 (PKD1 WT) or with NCC alone.

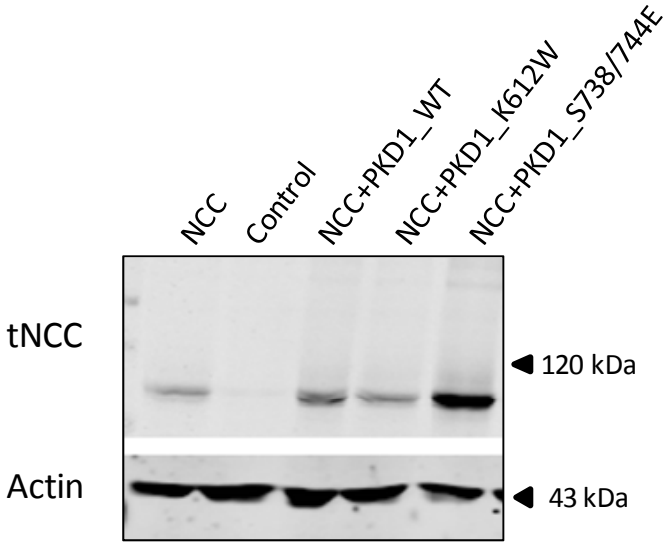

Figure 29: PKD1 increases the expression of total NCC abundance in transiently transfected HEK293T cells. HEK293T cells were transiently transfected with NCC together with either PKD1 (PKD1 WT), a kinase dead PKD1 mutant (K612W) or a constitutive active PKD1 mutant (S738/744E). After 24 h, the cells were collected and protein extractions for immunoblot analysis of total NCC were performed. Actin served as a loading control.

3.3. Project 3: Using transcriptomic analysis to identify mediators of DCT cell growth

The data obtained in projects 1 and 2 corroborated the assumption that the identification of DCT-enriched genes by transcriptomic mRNA analysis may reveal novel regulatory pathways for NCC and DCT function. A characteristic feature of the DCT is its structural plasticity. Alterations in its ion transport activity induced by diuretic treatment (e.g. furosemide) or genetic manipulation (e.g., Gitelman syndrome) induce marked structural and functional changes in the DCT [18, 38, 50]. However, the molecular mechanisms that control DCT growth are largely unknown. To gain further insight into the underlying molecular processes, transcriptomic mRNA analysis on COPAS-isolated DCTs from mice with stimulated or inhibited DCT cell growth were performed.

3.3.1. Identification of potential mediators of DCT cell growth

To identify genes that might be important for DCT growth and function, comparative transcriptome analysis of COPAS-isolated DCTs from PV eGFP mice that were either treated with vehicle, furosemide (50 mg/gBW, to stimulate DCT growth), or HCTZ (50 mg/gBW, to inhibit DCT cell growth) were performed. Ratio analysis of I) Control/HCTZ; II) Control/furosemide and III) furosemide/HCTZ for each gene product were determined. In response to hydrochlorothiazide, 112 genes were down-regulated and 121 genes were up regulated. In response to furosemide, 153 genes were down-regulated and 80 genes were up-regulated. In order to further restrict the discovered gene pool, only genes with an average raw intensity above 200 in all three conditions (Control, furosemide, HCTZ) were considered (Table 12).

Table 12: Potentially mediators of DCT cell growth found by transcriptomic analysis.

Gene Symbole	Gene Name	Average Raw Intensity [CTR]	Average Raw Intensity [FURO]	Average Raw Intensity [HCTZ]	Ratio HCTZ/CTR	Ratio FURO/CTR	Ratio HCTZ/FURO
Ptprz1	protein tyrosine phosphatase, receptor type Z, polypeptide 1	216829,6	300022,5	335620,2	1,548	1,384	1,119
Txnip	thioredoxin interacting protein	27772,6	21427,3	58857,8	2,119	0,772	2,747
Timp3	tissue inhibitor of metalloproteinase 3	22123,8	57745,8	31959,0	1,445	2,610	0,553
Angptl4	angiopoietin-like 4	13012,9	3518,1	27202,7	2,090	0,270	7,732
Hnrnpk	heterogeneous nuclear ribonucleoprotein K	11724,2	763,5	861,7	0,073	0,065	1,129

Pisd-ps3	phosphatidylserine decarboxylase, pseudogene 3	10926,3	4748,1	5744,2	0,526	0,435	1,210
Nuak2	NUAK family, SNF1-like kinase, 2	8170,1	21881,2	15221,7	1,863	2,678	0,696
Pdk4	pyruvate dehydrogenase kinase, isoenzyme 4	7420,5	5508,6	16811,6	2,266	0,742	3,052
Tnfrsf12a	tumor necrosis factor receptor superfamily, member 12a	5762,7	20177,6	8023,0	1,392	3,501	0,398
Acot1	acyl-CoA thioesterase 1	3963,9	1533,7	9028,7	2,278	0,387	5,887
Trpm6	transient receptor potential cation channel, subfamily M, member 6	3556,5	3990,4	1605,2	0,451	1,122	0,402
Fnip2	folliculin interacting protein 2	2705,4	2728,1	938,8	0,347	1,008	0,344
Adora2b	adenosine A2b receptor	1884,4	1599,8	721,6	0,383	0,849	0,451
Insig2	insulin induced gene 2	1705,3	1808,5	1745,1	1,023	1,061	0,965
Txnip	thioredoxin interacting protein	1620,6	1306,1	3392,5	2,093	0,806	2,598
Frmd4a	FERM domain containing 4A	1529,0	1821,9	832,3	0,544	1,192	0,457
Snn	stannin	1084,3	1147,7	1408,4	1,299	1,058	1,227
Plin4	perilipin 4	1032,6	814,3	306,2	0,297	0,789	0,376
Hbegf	heparin-binding EGF-like growth factor	997,0	2379,5	3386,5	3,397	2,387	1,423
Rnf183	ring finger protein 183	813,3	607,0	295,8	0,364	0,746	0,487
Ren1	renin 1 structural	748,0	377,6	285,8	0,382	0,505	0,757
Sik1	salt inducible kinase 1	635,6	1008,5	398,0	0,626	1,587	0,395
Thsd1	thrombospondin, type I, domain 1	630,5	516,8	273,7	0,434	0,820	0,530
		454,1	510,1	584,9	1,288	1,123	1,147
Mex3a	mex3 homolog A (C. elegans)	420,1	459,6	196,6	0,468	1,094	0,428
Prox1	prospero-related homeobox 1	407,2	348,3	984,2	2,417	0,855	2,825
4931408A02Rik	RIKEN cDNA 4931408A02 gene	367,0	383,2	139,9	0,381	1,044	0,365
Fgfbp1	fibroblast growth factor binding protein 1	354,5	1162,9	530,3	1,496	3,281	0,456
Sclt1	sodium channel and clathrin linker 1	349,6	238,9	236,2	0,676	0,683	0,989
Fgd3	FYVE, RhoGEF and PH domain containing 3	283,5	795,2	786,4	2,774	2,805	0,989
Fbxl18	F-box and leucine-rich repeat protein 18	270,2	262,4	315,6	1,168	0,971	1,203
Pggt1b	protein geranylgeranyltransferase type I, beta subunit	267,0	271,3	303,8	1,138	1,016	1,120
Nktr	natural killer tumor recognition sequence	258,6	233,6	263,1	1,017	0,903	1,126
Maff	v-maf musculoaponeurotic fibrosarcoma oncogene family, protein F (avian)	233,7	644,4	210,1	0,899	2,758	0,326
Adamtsl3	ADAMTS-like 3	218,4	204,1	90,8	0,415	0,934	0,445
Ankrd61	ankyrin repeat domain 61	205,4	124,4	447,5	2,179	0,606	3,597

Lmo1	LIM domain only 1	203,5	117,0	526,3	2,586	0,575	4,497
Slc47a1	solute carrier family 47, member 1	203,0	247,4	206,4	1,016	1,218	0,834
Ren2	renin 2 tandem duplication of Ren1	200,9	110,0	79,1	0,394	0,548	0,719
Lifr	leukemia inhibitory factor receptor	198,8	219,1	207,3	1,042	1,102	0,946
Chac1	ChaC, cation transport regulator-like 1 (E. coli)	184,4	72,1	524,7	2,845	0,391	7,280
Odz4	odd Oz/ten-m homolog 4 (Drosophila)	179,8	81,1	272,0	1,512	0,451	3,355
		179,0	154,9	214,5	1,198	0,865	1,385
Cxcl16	chemokine (C-X-C motif) ligand 16	178,8	427,8	143,2	0,801	2,392	0,335
Ace2	angiotensin I converting enzyme (peptidyl-dipeptidase A) 2	172,4	379,1	505,9	2,935	2,199	1,335
AI118078	expressed sequence AI118078	162,8	110,5	301,5	1,852	0,679	2,728
S100a14	S100 calcium binding protein A14	153,7	150,3	65,8	0,428	0,978	0,438
Sorbs2	sorbin and SH3 domain containing 2	144,2	112,3	337,6	2,342	0,779	3,005
Nrg1	neuregulin 1	125,1	381,1	225,3	1,801	3,046	0,591
Nrg1	neuregulin 1	106,4	321,4	194,9	1,831	3,020	0,606
9630033C03Rik	RIKEN cDNA 9630033C03 gene	82,3	56,1	456,0	5,543	0,682	8,122
Mylip	myosin regulatory light chain interacting protein	76,0	819,0	35,5	0,467	10,779	0,043
Sprr1a	small proline-rich protein 1A	74,2	245,8	48,4	0,653	3,312	0,197
1300002K09Rik	RIKEN cDNA 1300002K09 gene	35,4	3310,1	29,4	0,829	93,428	0,009
Igh-VJ558	immunoglobulin heavy chain (J558 family)	22,8	149,4	202,3	8,880	6,558	1,354
Igh-VJ558	immunoglobulin heavy chain (J558 family)	12,3	164,5	217,6	17,658	13,347	1,323
Igh-VJ558	immunoglobulin heavy chain (J558 family)	4,2	309,8	427,9	102,926	74,535	1,381

Microarray analysis of COPAS-isolated DCT from mice that were either treated with Control (CTR), furosemide (FURO; 50 mg/gBW), or HCTZ (HCTZ; 50 mg/gBW), for 4 h. Average raw intensity and ratio analyses Control/HCTZ; Control/furosemide; furosemide/HCTZ with a cut off of 2.5 were performed. In a subsequent selection step, genes with an average raw intensity above 200 in all three conditions (Control, furosemide, HCTZ) were considered for further analysis.

3.3.2. Confirmation of potential mediators of DCT cell growth by qRT-PCR

The transient receptor potential melastatin 6 channel (TRPM6), the salt inducible kinase 1 (SIK1), the cation transport regulator (Chac1), and the transcription factor Prox1 were chosen from the gene pool (highlighted in table 12). Using the same RNA samples as analyzed by microarray, we confirmed the differential transcription of the four genes of interest by qRT-PCR (Figure 30).

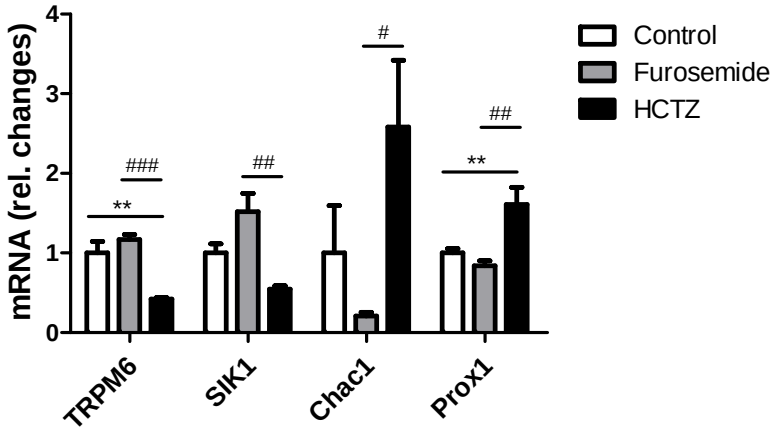

Figure 30: Confirmation by qRT-PCR analysis of 4 potential mediators of DCT growth. mRNA expression of transient receptor potential melastatin 6 channel (TRPM6), salt inducible kinase 1 (SIK1), cation transport regulator (Chac1) and transcription factor Prox1 in COPAS isolated DCT from mice that were either treated with Control, furosemide or HCTZ. Data are mean ± SEM, n=5. Statistical significance was calculated by one-way ANOVA test (**= $p<0.005$ for Control vs HCTZ; # = $p<0.05$, ## = $p<0.05$, ## = $p<0.001$ for Control vs furosemide).

3.4. Project 4: Establishing ex vivo DCT cell culture as a tool to study DCT cell function

In addition to the *in vivo* experiments, studies on DCT function require *ex vivo* systems which allow a higher level of experimental control than experiments in living animals. Therefore, primary DCT cell cultures, derived from PV eGFP mice, were established using the complex object parametic analysis and sorting technique (COPAS).

3.4.1. Outgrowing cells form a polarized epithelium

Around 1000 COPAS-sorted DCTs were grown in cell culture dishes or on collagen-coated permeable filter supports. After 8 days in culture the outgrowing cells on the filter formed a polarized epithelium with an electrical transepithelial resistance of more than 560 ± 92.38 Ohm/cm^2 (Table 13).

Table 13: Measurments of transepithelial resistance on primary DCT cell culture.

Time after seeding (d)	Resistance (Ohm/cm^2)
3	110 ± 5
4	130 ±0
6	330 ± 66.58
8	560 ± 92.38

Around 1000 COPAS-isolated DCTs were grown on transwell filters for 8 days. 3, 4, 6 and 8 days after seeding the transepithelia resistance was measured by EVOM. Data are means ± SEM, n=3.

3.4.2. Characterization of DCT primary cell culture

After 8 days of culturing, DCT cells were harvested and characterized by qRT-PCR and immunocytochemistry. qRT-PCR analysis revealed that DCT cells that were grown on filters had a 10 fold higher NCC expression compared to DCT cells that were grown on plastic support (Figure 31A). However, qRT-PCR analysis revealed also that during the cultivation procedure, the mRNA-expression of NCC and WNK4 decreased more than 100-fold and the mRNA-level of WNK1s was more than 1000-fold lower when compared to native DCTs collected immediately after sorting (Figure 31A, B and C).

Consistent with the high transepithelial resistance (Table 13), immunocytochemistry revealed that cultivated DCT cells formed a polarized epithelial monolayer and showed the presence of NCC in the apical membrane of the cells. Moreover, the DCT cells maintained GFP expression under the control of the parvalbumin promoter, suggesting that the cells maintained a rather differentiated DCT-like phenotype (Figure 31D).

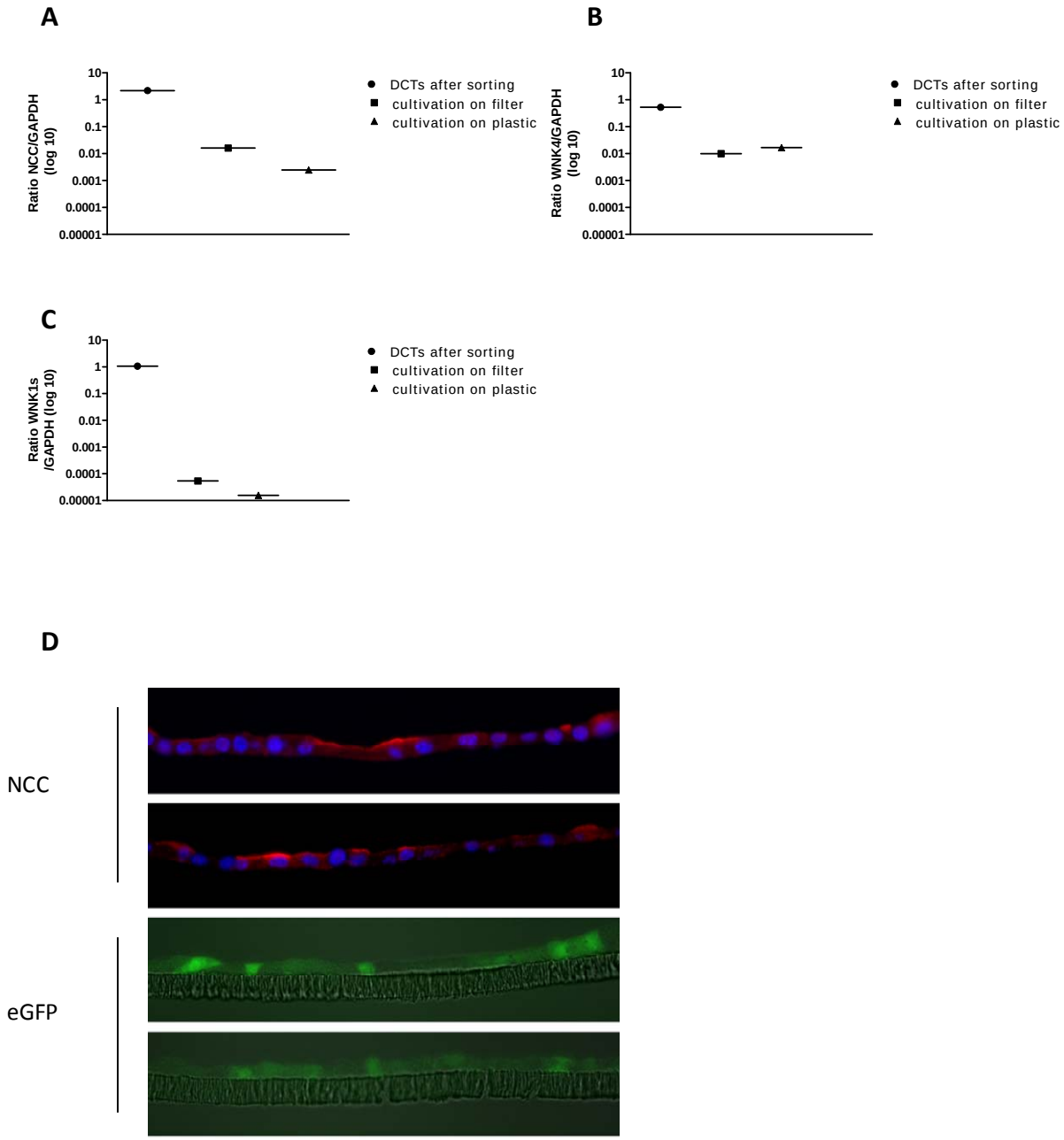

Figure 31: Characterization of primary DCT cell culture. Around 1000 COPAS-sorted DCTs were grown on collagen-coated plastic support or transwell filters for 8 d. mRNA expression of (A) NCC, (B) WNK4 and (C) WNK1S of cultivated DCTs cell or DCT cells collected immediately after sorting was assessed by qRT-PCR. (D) Immunocytochemstriy revealed NCC expression in the apical membrane of the cells that were cultivated on filters. Furthermore, eGFP signal could also be detected.

4. Discussion

The distal convoluted tubule (DCT) plays an important role in the regulation of Na^+ homeostasis and blood pressure. The thiazide-sensitive Na^+Cl^- co-transporter (NCC) is the major apical Na^+ transport pathway in the DCT1. In the late DCT (DCT 2), NCC expression overlaps with the expression of the amiloride-sensitive epithelial Na^+ channel (ENaC). Only little is known about the underlying molecular mechanisms that control NCC function. Based on the fact that many of the so far described NCC regulating proteins (e.g., KS-WNK1, WNK4, SPAK, Klhl3, PV) are enriched in the DCT, we hypothesized that the DCT expresses a specific repertoire of regulatory proteins that control its function. In a recent screen for DCT-specific genes, two gene products were found to be highly expressed in the DCT, i.e., the Ppp1r1a gene encoding for the protein phosphatase inhibitor 1 (I1) and the Prkcμ gene encoding for protein kinase D1 (PKD1). The experiments presented in this thesis provide evidence that I1 and PKD1 may be novel molecular players in the control of NCC function. Moreover, using microarray analysis of COPAS-isolated DCTs, we identified a set of genes regulated under conditions known to impact DCT growth. Furthermore, we established *ex vivo*-DCT cell cultures as a tool to study DCT function.

4.1. I1 controls phosphorylation of NCC *in vitro* and *in vivo*

Protein phosphorylation occurs post-translationally and is relevant for nearly all cellular events, including transcription, translation, cell metabolism, cell-cycle progression, protein-protein interactions, protein turnover, cell migration, and apoptosis. The phosphorylation of proteins is regulated by protein kinases which transfer a phosphate group to a serine, threonine or tyrosine residue, and by protein phosphatases which catalyze the removal of these phosphate groups. Approximately 500 protein kinases and around 150 protein phosphatases are known to be expressed by the human genome. This complex network can shift the balance between phosphorylation and dephosphorylation and thus modulate activity of the target protein.

The most extensively studied serine/threonine kinases in the DCT are WNK and SPAK. After phosphorylation of SPAK by WNK, SPAK in turn directly phosphorylates NCC on conserved serine/threonine residues, leading to the activation of NCC [2]. Furthermore, Glover and coworkers showed that phosphatase 4 is able to dephosphorylate and thereby deactivate NCC [78]. In general, protein phosphatases interact with a wide range of substrates, so that a network of regulatory and inhibitory proteins is necessary that modulates the specificity and catalytic activity of protein

phosphates. In this thesis, we found that I1 and PKD1 are novel players in the complex network of kinases and phosphatases that control NCC phosphorylation and activity.

As outlined above, NCC is the major Na^+ pathway in the DCT and can be activated and deactivated by phosphorylation and dephoshorylation mechanisms, respectively. Here, we suggest that I1 is a novel regulator in the control of NCC phosphorylation and function. I1 was the first described endogenous inhibitor of protein phosphatase 1 [164]. I1 is a cytosolic protein and can be found in many organs including brain, muscle and heart [1]. Furthermore, Higuchi and coworkers could show that I1 is also localized in the kidney, with higher expression of I1 in the medulla than in the cortex [202]. In accordance with this study, we also found I1 expression in the kidney. Using immunohistochemistry, we could show that I1 is expressed in the cytoplasma of NCC- and Calbindin 28K-positive DCTs. In addition, I1 was also abundant in the preceding NCC- and Calbindin 28K-negative cortical and medullary TAL.

In collaboration with Prof. Ellison we could show that the experimental knockdown of I1 in HEK292 cells causes a dramatic reduction of the conserved NCC phosphorylation site threonine 53, whereas the total expression of NCC is not changed. Furthermore, ^{22}Na uptake experiments in NCC-injected *Xenopus laevis oocytes* revealed that Na^+ uptake is slightly increased when co-expressed with the constitutively active mutant of I1, suggesting that an endogenously expressed phosphatase is inhibited by I1. This effect is even more pronounced when I1 is co- injected with the catalytic subunit of PP1. A possible explanation for this result is that the inhibitory effect of human I1 is not as strong on *Xenopus lavevis*-phosphatases as on the human PP1, and that co- injection with human I1 and human PP1 results in a stronger interaction with NCC leading to enhanced Na^+ uptake. In contrast, we could not show that PP1 inhibits the Na^+ uptake in NCC- injected *Xenopus laevis oocytes*. Recently, Lin and colleagues used co-immunoprecipitation and western blot analysis to show that PP1 is associated with WNK4 [163]. Similar experiments could help to explore whether PP1 directly interacts with NCC. In accordance with the *in vitro* results, mice with a complete knockout of I1 show a reduction of approximately 50% in NCC phosphorylation at threonine 53, threonine 58, serine 71 and serine 89 whereas the total abundance of NCC is not affected. The similarities between the *in vitro* and *in vivo* data clearly indicate that reduced NCC phosphorylation is a cell-autonomous effect of I1-deficiency.

4.2. I1-mediated phosphorylation of NCC is independent of the SPAK/WNK4 pathway

We demonstrate that I1 deficiency leads to a significant dephosphorylation of NCC *in vivo*. *In vivo* and *in vitro* experiments under standard conditions have revealed that WNK4 likewise reduces the phosphorylation level of NCC as well as its activity [35]. The phenotype of mice with two additional copies of wildtype WNK4 ($WNK4^{wt}$) supports the assumption that WNK4 is a negative regulator of NCC. $WNK4^{wt}$ animals exhibit lower blood pressure, hypocalciuria, hypoplasia of the DCT and are predisposed to hypokalemia. Indeed, protein-protein interactions between WNK4 and NCC could be observed *in vitro* [133], but it is not clear whether WNK4 directly interacts with NCC. So far, only SPAK/OSR1 kinases were found to directly phosphorylate NCC [80]. The importance of the SPAK kinase in the phosphorylation of NCC has been underlined by investigations in the phenotypes of SPAK Thr243Ala knockin mice [121] and SPAK knockout mice [119, 123]. The abnormal physiology of these gene-modified mice (hypotension, hypokalemia, hypomagnesemia and hypocalciuria) is similar to the effect of loss of NCC function in humans [36] and mice [37, 38]. Since both the commercial phosphoform-specific-WNK4 antibodies as well as antibodies produced in-house failed to yield satisfactory western blots results, it was not possible to investigate whether I1-deficiency leads to any difference in WNK4-protein expression. However, qRT-PCR analysis did not reveal any changes in WNK4 mRNA levels in I1-deficient mice when compared to their wildtype littermates. Furthermore, western blot analysis did not reveal any differences in total SPAK-expression as well as in its phosphorylation status at serine 373 in I1-deficient mice. In conclusion, our findings suggest that I1 regulates the phosphorylation of NCC through a SPAK/WNK4-independent pathway. Given the fact that SPAK is also expressed in TAL we cannot formally exclude that I1-deficiency caused altered SPAK phosphorylation in DCT that we may have missed when analyzing whole kidney homogenates. Additional experiments on COPAS sorted DCT are needed to address the specific SPAK regulation in DCT. COPAS-sorted DCT may also provide enough material for co-immunoprecipitation experiments to test for direct molecular interaction between I1 and perhaps PP1 and NCC and perhaps other proteins.

4.3. I1 knockout mice show features of NCC-deficiency

Loss-of-function mutations in the gene encoding NCC can lead to the salt-losing Gitelman syndrome, an autosomal-recessive disorder with hypokalemic alkalosis, hypocalciuria, hypokalemia, hypomagnesemia and hypotension [36]. Appropriate mouse models to study this disease are NCC-KO mice [37, 38], NCC knock-in mice with a Gitelman mutation (Ser707/X) [203] and SPAK-deficient mice [119, 123]. These three transgenic mouse models show a Gitelman-like phenotype with renal salt wasting, secondary hyperaldosteronism, hypomagnesemia and hypocalciuria. In contrast, I1-KO mice display urinary ion and aldosterone excretion comparable to their wildtype littermates. Furthermore, no hypomagnesemia or hypokalemic alkalosis is observed in these animals. I1-KO mice neither show any signs of a structural atrophy of the DCT, nor a different thiazide response on standard diet when compared to wildtype littermates. A possible explanation for this rather mild phenotype in I1-deficient mice could be residual NCC phosphorylation. We showed that I1 causes an approximately 50% decrease in the phosphorylation of NCC at threonine 53, threonine 58, serine 71 and serine 89. It is possible that under standard conditions partial NCC phosphorylation is still sufficient for proper regulation of plasma and urine electrolytes. Furthermore, unchanged urinary aldosterone levels and unaltered renin mRNA levels suggest that the RAA-system is not activated.

When I1-KO animals are challenged with low Na^+ diet to maximally activate NCC, mice show a tendency to a slightly higher fractional sodium excretion rate and display a lower response to HCTZ, suggesting a dysfunction of NCC in this mouse model. Mice with a complete deletion of NCC do not show hypokalemia on standard diet [37], but become hypokalemic when challenged with K^+ restriction [39]. This was seen in I1-deficient mice. On standard diet, I1-KO mice exhibit normal plasma K^+ contents. However, after 5 days on a low K^+ diet, I1-deficient mice develop hypokalemia, suggesting that under certain conditions I1-deficiency leads to a phenotype with some characteristics of the Gitelman syndrome.

Another important finding supporting our hypothesis that I1-deficient mice have a Gitelman-like phenotype is that despite the rather mild effect on urinary Na^+ and Ca^+ regulation and the lack of changes in the RAAS-system, I1-deficient mice have a significantly lower blood pressure on standard and on low Na^+ diet. This phenotype is similar to that found in $SPAK^{+/-}$ mice, which also display a decrease in NCC phosphorylation levels and arterial hypotension without significant abnormalities regarding plasma aldosterone and urine and plasma electrolytes [123]. In accordance, $NCC^{+/-}$ mice also show less NCC abundance and phosphorylation than wildtype mice that go along with lower blood pressure. We found in another set of experiments that these mice have unchanged urinary ion excretion levels. Moreover, unchanged urinary aldosterone and renin mRNA levels suggest that also these mice do not have any activation of the RAA-system (unpublished observation). Interestingly,

patients heterozygote for NCC mutations do also show lower blood pressure without any overt Gitelman-syndrome [204]. Moreover, thiazides often reduce arterial pressure without provoking obvious extracellular volume depletion [205]. Given the fact that I1 is also expressed in TAL and in other organs including heart and blood vessels, we cannot exclude that effects independent form DCT. We could not formally test whether NKCC2 phosphorylation is affected, because all pNKCC2 antibodies (R.Fenton, O. Devuyst) that we obtained and tested recognized pNCC and not pNKCC2 as revealed by using kidneys from $NCC^{-/-}$ mice. However, total NKCC2 abundance was not changed. Moreover, I1 deficient mice had urine volumes and urinary concentration abilities similar to wildtype mice suggesting normal NKCC2 function. Furthermore, it cannot be excluded that the decrease in blood pressure in I1-deficient mice originates from non-renal tissue inasmuch as I1 is also expressed in the heart [1, 167] and the arterial smooth muscles [174]. Although previous studies have shown that I1 deficiency has little or no impact on cardiac and arterial contractility [1, 174]. Nevertheless, further experiments are necessary to conclude that the hypotensive phenotype in I1-KO mice is of DCT and/or renal origin. Kidney cross-transplantation between wildtype and I1-deficient mice or a kidney-specific knockout of I1 using the cre/lox approach (e.g. tetracycline-inducible Pax8 promoter [206] would be helpful to obtain further insight into the role of renal I1 loss in blood pressure regulation.

4.4. I1 deficiency in the kidney is compensated by up-regulation of pendrin

We show that I1-deficient mice exhibit a significant down-regulation of NCC phosphorylation in combination with hypotension and an enhanced susceptibility to lowered plasma K^+ levels when dietary K^+ is restricted. Although these findings point to a Gitelman-like phenotype in I1-KO mice, loss of I1 apparently does not lead to any other symptoms seen in Gitelman-disease like hypocalciuria, hypomagnesemia and secondary hyperaldosteronism. In addition to the possible mediators discussed above this rather mild phenotype of I1-KO mice, could also be due to compensatory effects of up-regulation of other ion transporting pathways along the nephron.

It is known that NCC-KO mice do not show severe salt-wasting under baseline conditions [37]. Loffing et al. have suggested that NCC-KO mice compensate the Na^+ defect in the DCT with an aldosterone-dependent up-regulation of ENaC [38]. Furthermore, Vallet et al. found increased expression of the bicarbonate-chloride co-transporter pendrin in NCC-KO mice [207]. Interestingly, pendrin KO-mice do not display any dramatic salt-wasting under standard conditions [208]. However, double knockout of pendrin and NCC in mice causes severe salt-wasting, volume depletion and renal failure, suggesting that under baseline conditions each transporter compensates at least in part for

the dysfunction of the other [209]. Pendrin, together with the Na^+-driven $Cl^-/HCO3^-$-exchanger (NDCBE), moreover contributes to apical Na^+Cl^+ uptake in the CD [210]. This newly identified pathway suggests an important role for pendrin in compensatory salt reabsorption after NCC inactivation.

We could show that I1-KO mice exhibit unchanged alpha ENaC, beta ENaC and gamma ENaC protein expression. This finding is consistent with the observation of unaltered urinary aldosterone levels, suggesting that I1 deficiency in mice is not compensated via the ENaC-dependent salt reabsorption pathway as observed in NCC-KO mice [38]. However, we found that in I1-deficient mice pendrin expression is slightly but significantly up-regulated which could have contributed to the compensated phenotype. In contrast, since we did not observe any changes in NDCBE protein abundance, it may be possible that this novel NDCBE-pathway in the CCD is not involved in the compensatory mechanism of salt reabsorption in I1-deficient mice.

4.5. Further directions

It is known that I1 is phosphorylated and activated by protein kinase A upon cAMP stimulation [202]. This cAMP-induced activation of I1 has been proposed to be relevant for the beta-adrenergic and dopaminergic stimulation of Na^+/K^+-ATPase activity in the renal tubules [202]. Morel [160] demonstrated that the DCT responds with enhanced cAMP-production to various hormones (e.g., AVP, angiotensin II, isoproterenol). Since NCC is likewise regulated by hormones such as AVP [87, 159], angiotensin II [137, 139] and norepinephrine [211], it might be worthwhile to investigate whether I1 is involved in the regulation of NCC by these hormones.

Of particular interest are the beta-adrenergic receptors in the DCT. Several studies have shown the presence of these receptors in the DCT *in vitro* [212, 213]. It is well established that adrenalin (epinephrine), noradrenalin (norepinephrine) and isoproterenol (a specific beta-adrenergic analog of noradrenalin) bind to beta-adrenergic receptors and increase intracellular cAMP activity [5]. Moreover, it was demonstrated that the DCT responds to isoproterenol with enhanced cAMP production [160] and increased sodium reabsorption [214]. Recently, Mu and coworkers have demonstrated that isoproterenol stimulates NCC activity, leading to salt-sensitive hypertension in mice [142]. Neuman and colleagues demonstrate that I1 is also phosphorylated by isoproteronol [215] and is involved in beta-adrenergic signaling in skeletal and heart muscle [167],[1]. Furthermore, it was shown that I1-deficient mice are partly protected against isoprenaline-induced cardiac remodeling and arrhythmia, an effect that was suggested to be due to reduced sensitivity to beta-adrenergic stimulation in I1 deficiency [173]. Moreover, already in 1979, Foulkes and Cohen showed that adrenalin infusion phosphorylates I1 *in vivo* [170]. Terker and coworkers showed that chronic norepinephrine treatment increases the phosphorylation of NCC [211]. Therefore it would be

interesting to examine to which extent I1 contributes to isoproterenol- and norepinephrine-dependent NCC activation.

A further interesting observation is that calcineurin dephosphorylates I1 in response to stimuli that increase the concentration of intracellular Ca^{++} in the renal medulla [202]. Calcineurin is a calcium- and calmodulin-dependent serine/theronine protein phosphatase also known as protein phosphatase 2B [216] or protein phosphatase 3 [217]. It is involved in many cellular processes [216], but it is best known for its role in the activation of T cells [218]. The clinical relevance is underlined by the fact that calcineurin is the target of immunosuppressive drugs namely calcineurin inhibitors (CNIs) which includes cyclosporine and tacrolimus. CNIs are efficient to prevent rejection of transplanted organs and to treat autoimmune disease. However, several studies have shown that patients with CNIs therapy develop a FHHt-like phenotype including hypertension, hyperkalemia and hypercalciura [219, 220] in which the underlying molecular mechanism are largely unknown. Recently, Hoorn and colleagues have reported that the administration of the calcineurin inhibitor tacrolimus increases blood pressure due to an up-regulation of phosphorylated NCC [143]. After tacrolimus infusion, wildtype mice display enhanced NCC phosphorylation as well as an increased WNK3-, WNK4- and SPAK-expression [143]. While we demonstrate that I1 does not affect the WNK/SPAK pathway, it would be interesting to investigate whether I1 is involved in the tacrolimus-induced stimulation of NCC. It is conceivable that tacrolimus inhibits the calcineurin-induced dephosphorylation of I1, leading to an enhancement of I1 activity, which in turn would result in enhanced inhibition of PP1 and increased phosphorylation of NCC.

4.6. PKD1 is an aldosterone-induced protein

The steroid hormone aldosterone is released by the adrenal gland in response to activation of the RAA-system as well as increases in plasma K^+ levels. It is involved in the regulation of ion transport in the kidney and hence contributes to whole-body electrolyte balance and blood pressure control. Aldosterone exerts its effects via the mineralocorticoid receptor (MR) that is expressed in TAL, DCT, CNT and CD [41], but also binds with low affinity to the glucocorticoid receptor [221]. However, it is generally assumed that aldosterone acts exclusively via the MR on the so-called “aldosterone-sensitive distal nephron” that extends from the late DCT (DCT2) inasmuch as 11-beta-hydroxysteroid dehydrogenase type II (11β-HSD) is not expressed in DCT1 and TAL [128]. 11β-HSD converts cortisol into cortisone, resulting in a reduction of the cortisol/aldosterone ratio in the cell and higher affinity of aldosterone to the MR. In the ASDN, ENaC is the major effector of aldosterone. The aldosterone-dependent activation of ENaC is achieved by serum-glucocorticoid-kinase 1 (SGK1) [222] that in turn interacts with other regulatory proteins such as Ned4-2 [223] and WNK4 [224] to increase Na^+

reabsorption in the ASDN. However, several studies have shown that NCC is also affected by aldosterone [139, 225, 226]. So far, the underlying molecular mechanisms linking aldosterone and NCC remain unclear. Rozansky and colleagues have suggested that SGK1 reverses the inhibitory effect of WNK4, leading to enhanced NCC activity and, therefore, increased Na^+ reabsorption [150] in the DCT. However, Loffing and coworkers detected high expression of SGK1 in the CNT and CD but not in the DCT of aldosterone-treated andrenalectomized rats [21].

Protein kinase D1 (PKD1) also seems to be affected by aldosterone. Data from Tsybouleva and colleagues indicate that PKD1 is involved in aldosterone-induced cardiac hypertrophy [227]. Furthermore, McEneaney showed that aldosterone stimulates PKD1 activation and promotes ENaC translocation in cortical collecting duct cells [181]. Moreover, suppression of PKD1 in this cell line inhibits aldosterone-induced SGK1-expression [228]. However, it has to be considered that these experiments were performed *in vitro*. Here, we show that aldosterone impacts PKD1 expression and phosphorylation *in vivo*. Interestingly, these effects occur predominantly in DCT and not in CNT/CD suggesting that PKD1 in the kidney regulates predominantly NCC rather than ENaC. Consistently with this notion PKD1 appears to be a DCT-enriched transcript and protein as revealed by our microarray data and immunohistochemistry-experiments. Interestingly, the immunohistochemistry-experiments showed also a shift of PKD1 to the apical membrane in DCT cells of aldosterone-injected rats. The shift goes along with enhanced phosphorylation of PKD1 at serine 916 that is the autophosphorylation site of active PKD1 [189] . The increase in tPKD1 and pPKD1 correlates with enhanced level of NCC phosphorylation, suggesting an activation of NCC by PKD1 at the apical membrane of the cell. Based on these observations we suggest that PKD1 is involved in the aldosterone-dependent activation of NCC. Interestingly, WNK4 and SPAK also seem to participate in the aldosterone-mediated control of NCC [139]. We found a conserved consensus PKD1 phosphorylation site in WNK4, leading us to hypothesize that aldosterone acts on NCC via the PKD1/WNK4 pathway.

Our conclusion that PKD1 is an aldosterone-induced protein is supported by the down-regulation of PKD1 in aldosterone-synthase-deficient mice. AS-KO mice display significantly decreased total PKD1 expression as well as a significant reduction of PKD1 phosphorylation at serine 916. Furthermore, PKD1-mRNA is strongly down-regulated in AS-KO mice.

4.7. Mice with PKD1 loss in the DCT1 show features of Gitelman-sydrome

The data mentioned above are consistent with the idea that PKD1 controls NCC phosphorylation. Support for this notion comes from our observation in PKD1-KO mice. These mice revealed a significant reduction in NCC phosphorylation at threonine 53, threonine 58 and serine 71, whereas total NCC expression was not changed. In contrast to I1-KO mice, which show a reduction by about 50% NCC phosphorylation, PKD1-KO mice display a respective decrease by more than 75%, suggesting that NCC phosphorylation is more strongly affected by PKD1 than I1 deficiency.

In contrast to the I1-deficient mice, PKD1-KO mice have elevated plasma aldosterone levels and signs for an increased proteolytic activation of ENaC. Likewise, mice with a complete deletion of NCC do also have increased aldosterone levels and, as a consequence, higher ENaC activity in the aldosterone-sensitive distal nephron [38]. The compensatory up-regulation of ENaC in PKD1-KO mice might explain in PKD1-KO mice the absence of overt salt-wasting and the absence of major effects on blood pressure as long mice are kept on standard diet. However, under conditions of Na^+-depletion, PKD1-KO mice do also become hypotensive. This phenomenon has also been observed in $NCC^{-/-}$ mice [37] and in $SPAK^{-/-}$ mice [122].

As described above, Gitelman syndrome is associated with renal salt wasting, secondary hyperaldosteronism, hypocalciuria, hypokalemia, hypomagnesemia and hypotension [36]. Mouse models with a genetic disruption of either NCC [37, 38] or SPAK [119, 123] partly mimic this phenotype. PKD1-KO mice show some features of the Gitelman syndrome (e.g. hyperaldosteronism), they have no significant defects in urinary calcium, magnesium and potassium excretion, though plasma K^+ tended to be lower in PKD1-KO than in wildtype mice. However, it has to be considered that PKD1 deficiency in this model is exclusively restricted to the DCT1. Compensatory effects that might take place in the DCT2 may obscure effects on DCT1 at the whole-organ/mouse level. Thus, with a complete PKD1 knockout in the DCT (DCT1 and DCT2), NCC phosphorylation might be even more severely diminished leading to a more prominent phenotype. In fact, preliminary immunofluorescent data indicate that PKD1-KO mice lack almost completely NCC phosphorylation in the DCT1, but show pronounced up-regulation of NCC-phosphorylation in DCT2. Therefore, a mouse model expressing cre along the entire DCT (e.g. mice with cre expression under the NCC promoter) is needed to further assess the role of PKD1 in DCT function.

4.8. Further directions

We provide evidence that PKD1 is regulated by aldosterone in the DCT. Aldosterone-injected adrenalectomized rats show a rapid up-regulation of total PKD1 expression as well as a dramatic increase in serine 916 phosphorylation which correlates with increased PKD1 activity. In addition, NCC phosphorylation but not total NCC expression was highly elevated after aldosterone treatment. To investigate if PKD1 is involved in aldosterone-induced up-regulation of NCC, PKD1-KO mice could be treated with aldosterone. However, angiotensin II stimulates adrenal aldosterone secretion and it would be difficult to modulate angiotensin II signaling *in vivo* without confounding effects due to concomitant changes in plasma aldosterone levels. This problem might be prevented by using adrenalectomized PKD1-KO mice.

Furthermore, it is well established that WNK4 via SPAK is involved in the control of NCC phosphorylation and function [35, 105]. We found a conserved consensus PKD1 phosphorylation site in WNK4, suggesting that NCC phosphorylation is controlled by the PKD1/WNK4 pathway. Experiments in *Xenopus laevis* oocytes would be useful to test this hypothesis. In such experiments, NCC could be co-expressed together with wildtype PKD1, constitutively active or kinase-dead PKD1. Furthermore, wildtype, constitutively active and kinase-dead WNK4 could be used to analyze whether PKD1 affects NCC phosphorylation via WNK4. Moreover, our hypothesis might be confirmed by mutations of the PKD1 consensus motif in WNK4 that is expected to diminish the effect of PKD1 on NCC.

4.9. TRPM6, Chac1, SIK1 and Prox1 are differently regulated in DCT cells in response to diuretic treatment that alters DCT cell growth

The DCT reveals a remarkable structural plasticity in response to altered salt transport [50]. This is most apparent under diuretic treatment. It is known that enhanced Na^+ transport (e.g., due to treatment with furosemide) is associated with epithelial hypertrophy and hyperplasia [18, 47, 48, 50, 229], whereas impaired transport (e.g., due to treatment with thiazide) leads to atrophy or even apoptosis of the DCT [50, 51]. Knowledge about the molecular mechanisms that control DCT growth is scarce but would be important for a proper understanding of normal DCT function and might also lead to new insights into pathological renal growth and renal cell proliferation as occurring in diabetic nephropathy, polycystic kidney disease and renal cancer. Microarray mRNA analysis of COPAS-sorted DCTs had revealed two novel regulators of NCC and, hence, DCT function, i.e., I1 and PKD1. Here, we used a similar approach to identify genes that might be relevant for DCT growth and function. Microarray analyses of COPAS-isolated DCTs from mice with furosemide- or HCTZ-manipulated DCT

cell growth and from control mice with un-stimulated cell growth were performed. Ratio analysis of the three different groups with a cut-off of 2.5 revealed that 256 genes were differently regulated. Under conditions known to induce DCT growth (treatment with furosemide), 153 genes were down-regulated and 80 genes were up-regulated. Under conditions known to suppress DCT growth (treatment with HCTZ), 112 genes were down-regulated and 121 genes were up-regulated. Based on their molecular functions and physiological roles in the body, four potentially interesting genes were selected and their differential regulation was confirmed by quantitative RT-PCR (i.e, the transient receptor potential melastatin 6 channel (TRPM6), the salt inducible kinase 1 (SIK1), the cation transport regulator (Chac1), and the transcription factor Prox1). **TRPM6** belongs to the transient receptor potential (TRP) channel family characterized by six transmembrane segments and intracellularly located N- and C-terminus domains [230]. It is localized in the early DCT and is significantly involved in the fine-tuning of Mg^+ excretion [33]. Mutations in TRPM6 cause autosomal recessive hypomagnesemia with secondary hypocalcemia [231, 232]. Previous studies showed that prolonged thiazide-treatment reduces TRPM6 expression, which may explain thiazide-induced hypomagnesemia in patients under chronic thiazide treatment [233]. However, in these previous studies it remained unclear whether the down-regulation of TRPM6 was due to a direct down-regulation of TRPM6 at the cellular level or simply due to the thiazide-induced structural atrophy of the DCT. Now, our data suggest that the down-regulation occurs very rapidly and even before major structural changes to the DCT occur. **SIK1** was first discovered by Wang and coworkers who performed cDNA subtraction hybridization on adrenocortical tissue from salt-treated rats [234]. It is a member auf the AMPK family and has a conserved kinase and ubiquitin domain and a regulatory site that can be recognized by various kinases (e.g., cAMP-dependent kinase, calmodulin kinase or LKB) [235]. SIK1 plays an important role in the regulation of Na^+K^+-ATPase activity in response to changes in intracellular sodium concentration [236]. Moreover, SIK1 was implicated in controlling the phosphorylation and function of the histone-deacytylases and hence gene transcription and growth [237]. Thus, SIK1 might be involved in both the functional and the structural adaptation of the DCT in response to altered salt transport. **Chac1** is a cytosolic protein and its expression is induced in response to accumulation of unfolded proteins in the endoplasmatic reticulum, pointing to a role in the unfolded protein response (UPR) pathway [238]. Furthermore, in *Escherichia coli* the chac-gene is assumed to code for a cation transport protein [239], making it another candidate that could take part in the adaptive response of the DCT. **Prox1** is a highly conserved transcription factor that belongs to the homeobox family [240]. Its C-terminus is responsible for DNA binding and the N-terminus exhibits two nuclear receptor boxes that enable Prox1 two interact with various nuclear receptors [241]. Prox1 is involved in the development of various organs such as the central nervous system, lymphatic system, eye, liver, pancreas and heart [241]. Furthermore, it is involved in human

tumor development including colon cancer, brain tumors, Kaposi sarcoma, hematological malignancies, breast cancer, pancreatic cancer, liver cancer, biliary carcinoma and esophageal cancer [241]. Thus, several interesting candidate genes have been identified. The regulation and the functional significance of these genes for DCT function and growth will need to be addressed in future studies by using for example appropriate knock-out models.

4.10. Ex vivo DCT cell cultures as a tool to study DCT function

There is increasing need for an *ex vivo* system that allows studying the molecular regulation of NCC in native DCT epithelia. Until now, only two native DCT cell lines are available, i.e., mpkDCT [242] and mDCT cells [243]. mpkDCT cells have been derived from microdissected DCTs of a transgenic mouse carrying the SV-40 large T and small t antigens under the control of the L-pyruvate kinase promoter [242]. These cells form a polarized epithelium and, similar to native mouse DCTs, show transcellular Ca^{++} transport [244]. However, NCC expression in mpkDCT cells is extremely low and requires 60 cycles of RT-PCR to be detected [244]. mDCT cells have been derived from immunodissected DCT and TAL cells and immortalized by SV-40 transfection [243]. These cells show detectable amiloride-sensitive Na^{+} uptake and thiazide-sensitive NaCl uptake [245] and have been used mainly to analyze Ca^{++} and Mg^{++} transport mechanisms [246-248]. However, mDCT cells do not develop tight junctions and their NCC expression is too low to enable functional studies. Thus, none of the available cell lines are suitable for studies on the regulation of NCC. Therefore, we established primary mouse DCT cell cultures from COPAS-sorted DCTs. Green fluorescent DCTs were grown in cell culture dishes and on permeable filter support. After eight days of growth on permeable supports, DCT cells formed a polarized epithelium with a transepithelial electrical resistance of around 560 Ohm/cm^2. RT-PCR confirmed that outgrown DCT cells maintained DCT cell characteristics such as NCC and WNK1s expression. Moreover, immunocytochemistry revealed that cultivated DCT cells grow as a monolayer and maintain NCC expression at the apical membrane of the cell. Thus, we successfully established primary DCT cells cultures with detectable NCC expression in a polarized epithelium. However, although some of the DCT cells retained rather strong NCC abundance, most of the cultivated DCT cells lost NCC expression. Hence, further optimization of the cell culture conditions is necessary before the primary cell culture system can be used for biochemical studies. Based on the recommendation by the thesis committee, optimization of the cell culture conditions was abandoned and our approach was continued by Markadieu and colleagues to establish a DCT primary cell culture system for functional analysis [249].

4.11. General conclusion

By identifying DCT-enriched genes, the present thesis contributes to the characterization of novel regulators of thiazide-sensitive NCC and, hence, DCT function. The discovery of novel regulatory pathways in the control of NCC function is of particular interest because NCC is critically involved in blood pressure regulation. This is indicated not only by the observation that loss-of-function mutations of NCC can lead to the salt-losing Gitelman syndrome comprising symptoms like hypokalemic alkalosis, hypocalciuria and hypotension, but also by the fact that thiazide-based diuretics are first-line agents in the treatment of arterial hypertension. Furthermore, thiazide administration reduces urinary Ca^{2+} excretion and thereby diminishes the risk of urolithiasis and osteoporosis. However, administering thiazide diuretics can also lead to metabolic side effects like hypokalemia, impairments in glucose tolerance and increases in serum uric acid. Therefore, there is need for non-thiazide inhibitors of NCC function that might show an improved clinical profile. I1 and PKD1 are more recently described molecular players in the control of NCC function and respective inhibitors are already considered potential agents in cancer and cardiac therapy. It is therefore essential to investigate the underlying molecular mechanisms of I1 and PKD1 effects on DCT function and to characterize the therapeutic potential as well as side effect profile of PKD1 and I1 inhibitors. The analysis of these and other potential regulators of NCC function will enable a deeper understanding of the regulatory pathways that control renal ion transport and, on the long run, may contribute to the development of new drugs to treat hypertension.

5. Bibliography

1. Wittkopper, K., et al., *Phosphatase-1 inhibitor-1 in physiological and pathological beta-adrenoceptor signalling.* Cardiovasc Res, 2011. **91**(3): p. 392-401.
2. Richardson, C. and D.R. Alessi, *The regulation of salt transport and blood pressure by the WNK-SPAK/OSR1 signalling pathway.* J Cell Sci, 2008. **121**(Pt 20): p. 3293-304.
3. Jaggi, M., et al., *Protein kinase D1: a protein of emerging translational interest.* Front Biosci, 2007. **12**: p. 3757-67.
4. McCormick, J.A. and D.H. Ellison, *The WNKs: atypical protein kinases with pleiotropic actions.* Physiol Rev, 2011. **91**(1): p. 177-219.
5. Boron, W.F.a.B., E.L., *Medical Physilogy*, ed. ed. 2009: Saunders Elsevier.
6. Reilly, R.F. and D.H. Ellison, *Mammalian distal tubule: physiology, pathophysiology, and molecular anatomy.* Physiol Rev, 2000. **80**(1): p. 277-313.
7. Hoenderop, J.G., B. Nilius, and R.J. Bindels, *Calcium absorption across epithelia.* Physiol Rev, 2005. **85**(1): p. 373-422.
8. McDonough, *Mechanisms of proximal tubule sodium transport regulation that link extracellular fluid volume and blood pressure.* Am J Physiol Regul Integr Comp Physiol., 2010.
9. Moral, Z., et al., *Regulation of ROMK1 channels by protein-tyrosine kinase and -tyrosine phosphatase.* J Biol Chem, 2001. **276**(10): p. 7156-63.
10. Wang, W.H., et al., *A potassium channel in the apical membrane of rabbit thick ascending limb of Henle's loop.* Am J Physiol, 1990. **258**(2 Pt 2): p. F244-53.
11. Simon, D.B., et al., *Genetic heterogeneity of Bartter's syndrome revealed by mutations in the K+ channel, ROMK.* Nat Genet, 1996. **14**(2): p. 152-6.
12. Fremont, O.T. and J.C. Chan, *Understanding Bartter syndrome and Gitelman syndrome.* World J Pediatr, 2012. **8**(1): p. 25-30.
13. Simon, D.B., et al., *Mutations in the chloride channel gene, CLCNKB, cause Bartter's syndrome type III.* Nat Genet, 1997. **17**(2): p. 171-8.
14. Birkenhager, R., et al., *Mutation of BSND causes Bartter syndrome with sensorineural deafness and kidney failure.* Nat Genet, 2001. **29**(3): p. 310-4.
15. Mancilla, E.E., F. De Luca, and J. Baron, *Activating mutations of the Ca2+-sensing receptor.* Mol Genet Metab, 1998. **64**(3): p. 198-204.
16. Simon, D.B., et al., *Bartter's syndrome, hypokalaemic alkalosis with hypercalciuria, is caused by mutations in the Na-K-2Cl cotransporter NKCC2.* Nat Genet, 1996. **13**(2): p. 183-8.
17. Ares, G.R., P.S. Caceres, and P.A. Ortiz, *Molecular regulation of NKCC2 in the thick ascending limb.* Am J Physiol Renal Physiol, 2011. **301**(6): p. F1143-59.
18. Kaissling, B., S. Bachmann, and W. Kriz, *Structural adaptation of the distal convoluted tubule to prolonged furosemide treatment.* Am J Physiol, 1985. **248**(3 Pt 2): p. F374-81.
19. Bachmann, S., et al., *Sodium transport-related proteins in the mammalian distal nephron - distribution, ontogeny and functional aspects.* Anat Embryol (Berl), 1999. **200**(5): p. 447-68.
20. Loffing, J. and B. Kaissling, *Sodium and calcium transport pathways along the mammalian distal nephron: from rabbit to human.* Am J Physiol Renal Physiol, 2003. **284**(4): p. F628-43.
21. Loffing, J., et al., *Aldosterone induces rapid apical translocation of ENaC in early portion of renal collecting system: possible role of SGK.* Am J Physiol Renal Physiol, 2001. **280**(4): p. F675-82.
22. Harris, M., et al., *A novel neutrophil elastase inhibitor prevents elastase activation and surface cleavage of the epithelial sodium channel expressed in Xenopus laevis oocytes.* J Biol Chem, 2007. **282**(1): p. 58-64.
23. Loffing, J., et al., *Differential subcellular localization of ENaC subunits in mouse kidney in response to high- and low-Na diets.* Am J Physiol Renal Physiol, 2000. **279**(2): p. F252-8.

24. Rossier, B.C., *The epithelial sodium channel: activation by membrane-bound serine proteases.* Proc Am Thorac Soc, 2004. **1**(1): p. 4-9.
25. Schild, L., *The epithelial sodium channel and the control of sodium balance.* Biochim Biophys Acta, 2010. **1802**(12): p. 1159-65.
26. Verrey, F., *Sodium reabsorption in aldosterone-sensitive distal nephron: news and contributions from genetically engineered animals.* Curr Opin Nephrol Hypertens, 2001. **10**(1): p. 39-47.
27. Lifton, R.P., *Molecular genetics of human blood pressure variation.* Science, 1996. **272**(5262): p. 676-80.
28. Rossier, B.C., et al., *Epithelial sodium channel and the control of sodium balance: interaction between genetic and environmental factors.* Annu Rev Physiol, 2002. **64**: p. 877-97.
29. Ellison, D.H., H. Velazquez, and F.S. Wright, *Thiazide-sensitive sodium chloride cotransport in early distal tubule.* Am J Physiol, 1987. **253**(3 Pt 2): p. F546-54.
30. Lourdel, S., et al., *A chloride channel at the basolateral membrane of the distal-convoluted tubule: a candidate ClC-K channel.* J Gen Physiol, 2003. **121**(4): p. 287-300.
31. Uchida, S., *In vivo role of CLC chloride channels in the kidney.* Am J Physiol Renal Physiol, 2000. **279**(5): p. F802-8.
32. Loffing, J., et al., *Distribution of transcellular calcium and sodium transport pathways along mouse distal nephron.* Am J Physiol Renal Physiol, 2001. **281**(6): p. F1021-7.
33. Voets, T., et al., *TRPM6 forms the Mg2+ influx channel involved in intestinal and renal Mg2+ absorption.* J Biol Chem, 2004. **279**(1): p. 19-25.
34. Gamba, G., *Molecular physiology and pathophysiology of electroneutral cation-chloride cotransporters.* Physiol Rev, 2005. **85**(2): p. 423-93.
35. Gamba, G., *The thiazide-sensitive Na+-Cl- cotransporter: molecular biology, functional properties, and regulation by WNKs.* Am J Physiol Renal Physiol, 2009. **297**(4): p. F838-48.
36. Simon, D.B., et al., *Gitelman's variant of Bartter's syndrome, inherited hypokalaemic alkalosis, is caused by mutations in the thiazide-sensitive Na-Cl cotransporter.* Nat Genet, 1996. **12**(1): p. 24-30.
37. Schultheis, P.J., et al., *Phenotype resembling Gitelman's syndrome in mice lacking the apical Na+-Cl- cotransporter of the distal convoluted tubule.* J Biol Chem, 1998. **273**(44): p. 29150-5.
38. Loffing, J., et al., *Altered renal distal tubule structure and renal Na(+) and Ca(2+) handling in a mouse model for Gitelman's syndrome.* J Am Soc Nephrol, 2004. **15**(9): p. 2276-88.
39. Morris, R.G., E.J. Hoorn, and M.A. Knepper, *Hypokalemia in a mouse model of Gitelman's syndrome.* Am J Physiol Renal Physiol, 2006. **290**(6): p. F1416-20.
40. Lifton, R.P., A.G. Gharavi, and D.S. Geller, *Molecular mechanisms of human hypertension.* Cell, 2001. **104**(4): p. 545-56.
41. Bostanjoglo, M., et al., *11Beta-hydroxysteroid dehydrogenase, mineralocorticoid receptor, and thiazide-sensitive Na-Cl cotransporter expression by distal tubules.* J Am Soc Nephrol, 1998. **9**(8): p. 1347-58.
42. Lalioti, M.D., et al., *Wnk4 controls blood pressure and potassium homeostasis via regulation of mass and activity of the distal convoluted tubule.* Nat Genet, 2006. **38**(10): p. 1124-32.
43. McCormick, J.A., et al., *Overexpression of the sodium chloride cotransporter is not sufficient to cause familial hyperkalemic hypertension.* Hypertension, 2011. **58**(5): p. 888-94.
44. Yu, Z., et al., *Sodium retention in rats with liver cirrhosis is associated with increased renal abundance of NaCl cotransporter (NCC).* Nephrol Dial Transplant, 2005. **20**(9): p. 1833-41.
45. Bickel, C.A., et al., *Increased renal Na-K-ATPase, NCC, and beta-ENaC abundance in obese Zucker rats.* Am J Physiol Renal Physiol, 2001. **281**(4): p. F639-48.
46. Song, J., et al., *Increased renal ENaC subunit and sodium transporter abundances in streptozotocin-induced type 1 diabetes.* Am J Physiol Renal Physiol, 2003. **285**(6): p. F1125-37.

47. Ellison, D.H., H. Velazquez, and F.S. Wright, *Adaptation of the distal convoluted tubule of the rat. Structural and functional effects of dietary salt intake and chronic diuretic infusion.* J Clin Invest, 1989. **83**(1): p. 113-26.
48. Kaissling, B. and B.A. Stanton, *Adaptation of distal tubule and collecting duct to increased sodium delivery. I. Ultrastructure.* Am J Physiol, 1988. **255**(6 Pt 2): p. F1256-68.
49. Loffing, J., M. Le Hir, and B. Kaissling, *Modulation of salt transport rate affects DNA synthesis in vivo in rat renal tubules.* Kidney Int, 1995. **47**(6): p. 1615-23.
50. Kaissling, B. and J. Loffing, *Cell growth and cell death in renal distal tubules, associated with diuretic treatment.* Nephrol Dial Transplant, 1998. **13**(6): p. 1341-3.
51. Loffing, J., et al., *Thiazide treatment of rats provokes apoptosis in distal tubule cells.* Kidney Int, 1996. **50**(4): p. 1180-90.
52. Wagner, C.A., et al., *Mouse model of type II Bartter's syndrome. II. Altered expression of renal sodium- and water-transporting proteins.* Am J Physiol Renal Physiol, 2008. **294**(6): p. F1373-80.
53. Lorenz, J.N., et al., *Impaired renal NaCl absorption in mice lacking the ROMK potassium channel, a model for type II Bartter's syndrome.* J Biol Chem, 2002. **277**(40): p. 37871-80.
54. Renfro, J.L., *Water and ion transport by the urinary bladder of the teleost Pseudopleuronectes americanus.* Am J Physiol, 1975. **228**(1): p. 52-61.
55. Renfro, J.L., *Interdependence of Active Na+ and Cl- transport by the isolated urinary bladder of the teleost, Pseudopleuronectes americanus.* J Exp Zool, 1977. **199**(3): p. 383-90.
56. Stokes, J.B., *Sodium chloride absorption by the urinary bladder of the winter flounder. A thiazide-sensitive, electrically neutral transport system.* J Clin Invest, 1984. **74**(1): p. 7-16.
57. Gamba, G., et al., *Primary structure and functional expression of a cDNA encoding the thiazide-sensitive, electroneutral sodium-chloride cotransporter.* Proc Natl Acad Sci U S A, 1993. **90**(7): p. 2749-53.
58. Mastroianni, N., et al., *Molecular cloning, expression pattern, and chromosomal localization of the human Na-Cl thiazide-sensitive cotransporter (SLC12A3).* Genomics, 1996. **35**(3): p. 486-93.
59. Gagnon, K.B., R. England, and E. Delpire, *Volume sensitivity of cation-Cl- cotransporters is modulated by the interaction of two kinases: Ste20-related proline-alanine-rich kinase and WNK4.* Am J Physiol Cell Physiol, 2006. **290**(1): p. C134-42.
60. Kunchaparty, S., et al., *Defective processing and expression of thiazide-sensitive Na-Cl cotransporter as a cause of Gitelman's syndrome.* Am J Physiol, 1999. **277**(4 Pt 2): p. F643-9.
61. Velazquez, H., et al., *Rabbit distal convoluted tubule coexpresses NaCl cotransporter and 11 beta-hydroxysteroid dehydrogenase II mRNA.* Kidney Int, 1998. **54**(2): p. 464-72.
62. Cutler, C.P. and G. Cramb, *Differential expression of absorptive cation-chloride-cotransporters in the intestinal and renal tissues of the European eel (Anguilla anguilla).* Comp Biochem Physiol B Biochem Mol Biol, 2008. **149**(1): p. 63-73.
63. Bachmann, S., et al., *Expression of the thiazide-sensitive Na-Cl cotransporter by rabbit distal convoluted tubule cells.* J Clin Invest, 1995. **96**(5): p. 2510-4.
64. Plotkin, M.D., et al., *Localization of the thiazide sensitive Na-Cl cotransporter, rTSC1 in the rat kidney.* Kidney Int, 1996. **50**(1): p. 174-83.
65. Hoover, R.S., et al., *N-Glycosylation at two sites critically alters thiazide binding and activity of the rat thiazide-sensitive Na(+):Cl(-) cotransporter.* J Am Soc Nephrol, 2003. **14**(2): p. 271-82.
66. De Jong, J.C., et al., *Functional expression of mutations in the human NaCl cotransporter: evidence for impaired routing mechanisms in Gitelman's syndrome.* J Am Soc Nephrol, 2002. **13**(6): p. 1442-8.
67. Dimke, H., *Exploring the intricate regulatory network controlling the thiazide-sensitive NaCl cotransporter (NCC).* Pflugers Arch, 2011. **462**(6): p. 767-77.
68. Bazzini, C., et al., *Thiazide-sensitive NaCl-cotransporter in the intestine: possible role of hydrochlorothiazide in the intestinal Ca2+ uptake.* J Biol Chem, 2005. **280**(20): p. 19902-10.

69. Dvorak, M.M., et al., *Thiazide diuretics directly induce osteoblast differentiation and mineralized nodule formation by interacting with a sodium chloride co-transporter in bone.* J Am Soc Nephrol, 2007. **18**(9): p. 2509-16.
70. Deng, L. and G. Chen, *Cyclothiazide potently inhibits gamma-aminobutyric acid type A receptors in addition to enhancing glutamate responses.* Proc Natl Acad Sci U S A, 2003. **100**(22): p. 13025-9.
71. Calder, J.A., M. Schachter, and P.S. Sever, *Direct vascular actions of hydrochlorothiazide and indapamide in isolated small vessels.* Eur J Pharmacol, 1992. **220**(1): p. 19-26.
72. Bernstein, S.L., D.E. Borst, and P.W. Wong, *Isolation of differentially expressed human fovea genes: candidates for macular disease.* Mol Vis, 1995. **1**: p. 4.
73. Abuladze, N., et al., *Peripheral blood mononuclear cells express mutated NCCT mRNA in Gitelman's syndrome: evidence for abnormal thiazide-sensitive NaCl cotransport.* J Am Soc Nephrol, 1998. **9**(5): p. 819-26.
74. Cremaschi, D., et al., *Apical Na+-Cl- symport in rabbit gallbladder epithelium: a thiazide-sensitive cotransporter (TSC).* J Membr Biol, 2000. **176**(1): p. 53-65.
75. Drewnowska, K. and C.M. Baumgarten, *Regulation of cellular volume in rabbit ventricular myocytes: bumetanide, chlorothiazide, and ouabain.* Am J Physiol, 1991. **260**(1 Pt 1): p. C122-31.
76. Kahle, K.T., A.M. Ring, and R.P. Lifton, *Molecular physiology of the WNK kinases.* Annu Rev Physiol, 2008. **70**: p. 329-55.
77. McCormick, J.A., C.L. Yang, and D.H. Ellison, *WNK kinases and renal sodium transport in health and disease: an integrated view.* Hypertension, 2008. **51**(3): p. 588-96.
78. Glover, M., et al., *The activity of the thiazide-sensitive Na(+)-Cl(-) cotransporter is regulated by protein phosphatase PP4.* Can J Physiol Pharmacol, 2010. **88**(10): p. 986-95.
79. Pacheco-Alvarez, D., et al., *The Na+:Cl- cotransporter is activated and phosphorylated at the amino-terminal domain upon intracellular chloride depletion.* J Biol Chem, 2006. **281**(39): p. 28755-63.
80. Richardson, C., et al., *Activation of the thiazide-sensitive Na+-Cl- cotransporter by the WNK-regulated kinases SPAK and OSR1.* J Cell Sci, 2008. **121**(Pt 5): p. 675-84.
81. Lin, S.H., et al., *Phenotype and genotype analysis in Chinese patients with Gitelman's syndrome.* J Clin Endocrinol Metab, 2005. **90**(5): p. 2500-7.
82. Shao, L., et al., *Novel SLC12A3 mutations in Chinese patients with Gitelman's syndrome.* Nephron Physiol, 2008. **108**(3): p. p29-36.
83. Yang, S.S., et al., *Molecular pathogenesis of pseudohypoaldosteronism type II: generation and analysis of a Wnk4(D561A/+) knockin mouse model.* Cell Metab, 2007. **5**(5): p. 331-44.
84. Gonzales, P.A., et al., *Large-scale proteomics and phosphoproteomics of urinary exosomes.* J Am Soc Nephrol, 2009. **20**(2): p. 363-79.
85. Feric, M., et al., *Large-scale phosphoproteomic analysis of membrane proteins in renal proximal and distal tubule.* Am J Physiol Cell Physiol, 2011. **300**(4): p. C755-70.
86. Rosenbaek, L.L., et al., *Characterization of a novel phosphorylation site in the sodium chloride cotransporter, NCC.* J Physiol, 2012.
87. Mutig, K., et al., *Short-term stimulation of the thiazide-sensitive Na+-Cl- cotransporter by vasopressin involves phosphorylation and membrane translocation.* Am J Physiol Renal Physiol, 2010. **298**(3): p. F502-9.
88. Zhou, B., et al., *WNK4 enhances the degradation of NCC through a sortilin-mediated lysosomal pathway.* J Am Soc Nephrol, 2009. **21**(1): p. 82-92.
89. Subramanya, A.R., et al., *WNK4 diverts the thiazide-sensitive NaCl cotransporter to the lysosome and stimulates AP-3 interaction.* J Biol Chem, 2009. **284**(27): p. 18471-80.
90. Sandberg, M.B., et al., *ANG II provokes acute trafficking of distal tubule Na+-Cl(-) cotransporter to apical membrane.* Am J Physiol Renal Physiol, 2007. **293**(3): p. F662-9.

91. Lee, D.H., et al., *Acute hypertension provokes acute trafficking of distal tubule Na-Cl cotransporter (NCC) to subapical cytoplasmic vesicles.* Am J Physiol Renal Physiol, 2009. **296**(4): p. F810-8.
92. Rotin, D. and O. Staub, *Role of the ubiquitin system in regulating ion transport.* Pflugers Arch, 2010. **461**(1): p. 1-21.
93. Flores, S.Y., C. Debonneville, and O. Staub, *The role of Nedd4/Nedd4-like dependant ubiquitylation in epithelial transport processes.* Pflugers Arch, 2003. **446**(3): p. 334-8.
94. Rotin, D. and S. Kumar, *Physiological functions of the HECT family of ubiquitin ligases.* Nat Rev Mol Cell Biol, 2009. **10**(6): p. 398-409.
95. Glickman, M.H. and A. Ciechanover, *The ubiquitin-proteasome proteolytic pathway: destruction for the sake of construction.* Physiol Rev, 2002. **82**(2): p. 373-428.
96. Schwartz, A.L. and A. Ciechanover, *Targeting proteins for destruction by the ubiquitin system: implications for human pathobiology.* Annu Rev Pharmacol Toxicol, 2009. **49**: p. 73-96.
97. Ko, B., et al., *RasGRP1 stimulation enhances ubiquitination and endocytosis of the sodium-chloride cotransporter.* Am J Physiol Renal Physiol, 2010. **299**(2): p. F300-9.
98. Arroyo, J.P., et al., *Nedd4-2 modulates renal Na+-Cl- cotransporter via the aldosterone-SGK1-Nedd4-2 pathway.* J Am Soc Nephrol, 2011. **22**(9): p. 1707-19.
99. Hossain Khan, M.Z., et al., *Phosphorylation of Na-Cl cotransporter by OSR1 and SPAK kinases regulates its ubiquitination.* Biochem Biophys Res Commun, 2012. **425**(2): p. 456-61.
100. Faresse, N., et al., *Inducible kidney-specific Sgk1 knockout mice show a salt-losing phenotype.* Am J Physiol Renal Physiol, 2012. **302**(8): p. F977-85.
101. Boyden, L.M., et al., *Mutations in kelch-like 3 and cullin 3 cause hypertension and electrolyte abnormalities.* Nature, 2012. **482**(7383): p. 98-102.
102. Louis-Dit-Picard, H., et al., *KLHL3 mutations cause familial hyperkalemic hypertension by impairing ion transport in the distal nephron.* Nat Genet, 2012. **44**(4): p. 456-60, S1-3.
103. Pintard, L., A. Willems, and M. Peter, *Cullin-based ubiquitin ligases: Cul3-BTB complexes join the family.* EMBO J, 2004. **23**(8): p. 1681-7.
104. Petroski, M.D. and R.J. Deshaies, *Function and regulation of cullin-RING ubiquitin ligases.* Nat Rev Mol Cell Biol, 2005. **6**(1): p. 9-20.
105. Hoorn, E.J. and D.H. Ellison, *WNK kinases and the kidney.* Exp Cell Res, 2012. **318**(9): p. 1020-6.
106. Uchida, S., *Pathophysiological roles of WNK kinases in the kidney.* Pflugers Arch, 2010. **460**(4): p. 695-702.
107. Wang, Z., C.L. Yang, and D.H. Ellison, *Comparison of WNK4 and WNK1 kinase and inhibiting activities.* Biochem Biophys Res Commun, 2004. **317**(3): p. 939-44.
108. Xu, B.E., et al., *Regulation of WNK1 by an autoinhibitory domain and autophosphorylation.* J Biol Chem, 2002. **277**(50): p. 48456-62.
109. Yang, C.L., X. Zhu, and D.H. Ellison, *The thiazide-sensitive Na-Cl cotransporter is regulated by a WNK kinase signaling complex.* J Clin Invest, 2007. **117**(11): p. 3403-11.
110. Lenertz, L.Y., et al., *Properties of WNK1 and implications for other family members.* J Biol Chem, 2005. **280**(29): p. 26653-8.
111. Hoorn, E.J., et al., *The WNK kinase network regulating sodium, potassium, and blood pressure.* J Am Soc Nephrol, 2011. **22**(4): p. 605-14.
112. Xie, J., et al., *Endothelial-specific expression of WNK1 kinase is essential for angiogenesis and heart development in mice.* Am J Pathol, 2009. **175**(3): p. 1315-27.
113. Shekarabi, M., et al., *Mutations in the nervous system--specific HSN2 exon of WNK1 cause hereditary sensory neuropathy type II.* J Clin Invest, 2008. **118**(7): p. 2496-505.
114. Greenman, C., et al., *Patterns of somatic mutation in human cancer genomes.* Nature, 2007. **446**(7132): p. 153-8.
115. Qiao, Y., et al., *Autism-associated familial microdeletion of Xp11.22.* Clin Genet, 2008. **74**(2): p. 134-44.

116. Xiao, P., et al., *In vivo genome-wide expression study on human circulating B cells suggests a novel ESR1 and MAPK3 network for postmenopausal osteoporosis.* J Bone Miner Res, 2008. **23**(5): p. 644-54.
117. Vitari, A.C., et al., *The WNK1 and WNK4 protein kinases that are mutated in Gordon's hypertension syndrome phosphorylate and activate SPAK and OSR1 protein kinases.* Biochem J, 2005. **391**(Pt 1): p. 17-24.
118. Vitari, A.C., et al., *Functional interactions of the SPAK/OSR1 kinases with their upstream activator WNK1 and downstream substrate NKCC1.* Biochem J, 2006. **397**(1): p. 223-31.
119. Delpire, E. and K.B. Gagnon, *SPAK and OSR1: STE20 kinases involved in the regulation of ion homoeostasis and volume control in mammalian cells.* Biochem J, 2008. **409**(2): p. 321-31.
120. Mercier-Zuber, A. and K.M. O'Shaughnessy, *Role of SPAK and OSR1 signalling in the regulation of NaCl cotransporters.* Curr Opin Nephrol Hypertens, 2011. **20**(5): p. 534-40.
121. Rafiqi, F.H., et al., *Role of the WNK-activated SPAK kinase in regulating blood pressure.* EMBO Mol Med, 2010. **2**(2): p. 63-75.
122. McCormick, J.A., et al., *A SPAK isoform switch modulates renal salt transport and blood pressure.* Cell Metab, 2011. **14**(3): p. 352-64.
123. Yang, S.S., et al., *SPAK-knockout mice manifest Gitelman syndrome and impaired vasoconstriction.* J Am Soc Nephrol, 2010. **21**(11): p. 1868-77.
124. Yang, C.L., et al., *Mechanisms of WNK1 and WNK4 interaction in the regulation of thiazide-sensitive NaCl cotransport.* J Clin Invest, 2005. **115**(5): p. 1379-87.
125. Liu, Z., et al., *Downregulation of NCC and NKCC2 cotransporters by kidney-specific WNK1 revealed by gene disruption and transgenic mouse models.* Hum Mol Genet, 2011. **20**(5): p. 855-66.
126. Yang, C.L., et al., *WNK kinases regulate thiazide-sensitive Na-Cl cotransport.* J Clin Invest, 2003. **111**(7): p. 1039-45.
127. Subramanya, A.R., et al., *Dominant-negative regulation of WNK1 by its kidney-specific kinase-defective isoform.* Am J Physiol Renal Physiol, 2006. **290**(3): p. F619-24.
128. Gamba, G., *Regulation of the Renal Na+:Cl- Cotransporter by Phosphorylation and Ubiquitylation.* Am J Physiol Renal Physiol, 2012.
129. Zambrowicz, B.P., et al., *Wnk1 kinase deficiency lowers blood pressure in mice: a gene-trap screen to identify potential targets for therapeutic intervention.* Proc Natl Acad Sci U S A, 2003. **100**(24): p. 14109-14.
130. Hadchouel, J., et al., *Decreased ENaC expression compensates the increased NCC activity following inactivation of the kidney-specific isoform of WNK1 and prevents hypertension.* Proc Natl Acad Sci U S A, 2010. **107**(42): p. 18109-14.
131. Glover, M., A.M. Zuber, and K.M. O'Shaughnessy, *Renal and brain isoforms of WNK3 have opposite effects on NCCT expression.* J Am Soc Nephrol, 2009. **20**(6): p. 1314-22.
132. Pacheco-Alvarez, D., et al., *WNK3-SPAK interaction is required for the modulation of NCC and other members of the SLC12 family.* Cell Physiol Biochem, 2012. **29**(1-2): p. 291-302.
133. Wilson, F.H., et al., *Molecular pathogenesis of inherited hypertension with hyperkalemia: the Na-Cl cotransporter is inhibited by wild-type but not mutant WNK4.* Proc Natl Acad Sci U S A, 2003. **100**(2): p. 680-4.
134. Cai, H., et al., *WNK4 kinase regulates surface expression of the human sodium chloride cotransporter in mammalian cells.* Kidney Int, 2006. **69**(12): p. 2162-70.
135. Yang, S.S., et al., *Regulation of apical localization of the thiazide-sensitive NaCl cotransporter by WNK4 in polarized epithelial cells.* Biochem Biophys Res Commun, 2005. **330**(2): p. 410-4.
136. San-Cristobal, P., et al., *WNK3 and WNK4 amino-terminal domain defines their effect on the renal Na+-Cl- cotransporter.* Am J Physiol Renal Physiol, 2008. **295**(4): p. F1199-206.
137. San-Cristobal, P., et al., *Angiotensin II signaling increases activity of the renal Na-Cl cotransporter through a WNK4-SPAK-dependent pathway.* Proc Natl Acad Sci U S A, 2009. **106**(11): p. 4384-9.

138. Castaneda-Bueno, M., et al., *Activation of the renal Na+:Cl- cotransporter by angiotensin II is a WNK4-dependent process.* Proc Natl Acad Sci U S A, 2012. **109**(20): p. 7929-34.
139. van der Lubbe, N., et al., *Aldosterone does not require angiotensin II to activate NCC through a WNK4-SPAK-dependent pathway.* Pflugers Arch, 2012. **463**(6): p. 853-63.
140. Sohara, E., et al., *Acute insulin stimulation induces phosphorylation of the Na-Cl cotransporter in cultured distal mpkDCT cells and mouse kidney.* PLoS One, 2011. **6**(8): p. e24277.
141. Chiga, M., et al., *Dietary salt regulates the phosphorylation of OSR1/SPAK kinases and the sodium chloride cotransporter through aldosterone.* Kidney Int, 2008. **74**(11): p. 1403-9.
142. Mu, S., et al., *Epigenetic modulation of the renal beta-adrenergic-WNK4 pathway in salt-sensitive hypertension.* Nat Med, 2011. **17**(5): p. 573-80.
143. Hoorn, E.J., et al., *The calcineurin inhibitor tacrolimus activates the renal sodium chloride cotransporter to cause hypertension.* Nat Med, 2011. **17**(10): p. 1304-9.
144. Melnikov, S., et al., *Cyclosporine metabolic side effects: association with the WNK4 system.* Eur J Clin Invest, 2011. **41**(10): p. 1113-20.
145. Lang, F., et al., *(Patho)physiological significance of the serum- and glucocorticoid-inducible kinase isoforms.* Physiol Rev, 2006. **86**(4): p. 1151-78.
146. Pearce, D., *SGK1 regulation of epithelial sodium transport.* Cell Physiol Biochem, 2003. **13**(1): p. 13-20.
147. Chen, S.Y., et al., *Epithelial sodium channel regulated by aldosterone-induced protein sgk.* Proc Natl Acad Sci U S A, 1999. **96**(5): p. 2514-9.
148. Fejes-Toth, G., et al., *Epithelial Na+ channel activation and processing in mice lacking SGK1.* Am J Physiol Renal Physiol, 2008. **294**(6): p. F1298-305.
149. Vallon, V., et al., *Expression and phosphorylation of the Na+-Cl- cotransporter NCC in vivo is regulated by dietary salt, potassium, and SGK1.* Am J Physiol Renal Physiol, 2009. **297**(3): p. F704-12.
150. Rozansky, D.J., et al., *Aldosterone mediates activation of the thiazide-sensitive Na-Cl cotransporter through an SGK1 and WNK4 signaling pathway.* J Clin Invest, 2009. **119**(9): p. 2601-12.
151. Gardner, K. and V. Bennett, *Modulation of spectrin-actin assembly by erythrocyte adducin.* Nature, 1987. **328**(6128): p. 359-62.
152. Bianchi, G., et al., *Two point mutations within the adducin genes are involved in blood pressure variation.* Proc Natl Acad Sci U S A, 1994. **91**(9): p. 3999-4003.
153. Cusi, D., et al., *Polymorphisms of alpha-adducin and salt sensitivity in patients with essential hypertension.* Lancet, 1997. **349**(9062): p. 1353-7.
154. Zagato, L., et al., *Genetic mapping of blood pressure quantitative trait loci in Milan hypertensive rats.* Hypertension, 2000. **36**(5): p. 734-9.
155. Dimke, H., et al., *gamma-Adducin stimulates the thiazide-sensitive NaCl cotransporter.* J Am Soc Nephrol, 2011. **22**(3): p. 508-17.
156. Cohen, P.T., *Protein phosphatase 1--targeted in many directions.* J Cell Sci, 2002. **115**(Pt 2): p. 241-56.
157. Fenton, R.A. and M.A. Knepper, *Mouse models and the urinary concentrating mechanism in the new millennium.* Physiol Rev, 2007. **87**(4): p. 1083-112.
158. Mutig, K., et al., *Vasopressin V2 receptor expression along rat, mouse, and human renal epithelia with focus on TAL.* Am J Physiol Renal Physiol, 2007. **293**(4): p. F1166-77.
159. Pedersen, N.B., et al., *Vasopressin induces phosphorylation of the thiazide-sensitive sodium chloride cotransporter in the distal convoluted tubule.* Kidney Int, 2010. **78**(2): p. 160-9.
160. Morel, F., *Sites of hormone action in the mammalian nephron.* Am J Physiol, 1981. **240**(3): p. F159-64.
161. Ceulemans, H. and M. Bollen, *Functional diversity of protein phosphatase-1, a cellular economizer and reset button.* Physiol Rev, 2004. **84**(1): p. 1-39.
162. Li, D., et al., *Protein phosphatase-1 in the kidney: evidence for a role in the regulation of medullary Na(+)-K(+)-ATPase.* Am J Physiol, 1995. **269**(5 Pt 2): p. F673-80.

163. Lin, D.H., et al., *Protein phosphatase 1 modulates the inhibitory effect of With-no-Lysine kinase 4 on ROMK channels.* Am J Physiol Renal Physiol, 2012. **303**(1): p. F110-9.
164. Huang, F.L. and W.H. Glinsmann, *Separation and characterization of two phosphorylase phosphatase inhibitors from rabbit skeletal muscle.* Eur J Biochem, 1976. **70**(2): p. 419-26.
165. Allen, P.B., et al., *Protein phosphatase-1 regulation in the induction of long-term potentiation: heterogeneous molecular mechanisms.* J Neurosci, 2000. **20**(10): p. 3537-43.
166. Nimmo, G.A. and P. Cohen, *The regulation of glycogen metabolism. Phosphorylation of inhibitor-1 from rabbit skeletal muscle, and its interaction with protein phosphatases-III and -II.* Eur J Biochem, 1978. **87**(2): p. 353-65.
167. Nicolaou, P., R.J. Hajjar, and E.G. Kranias, *Role of protein phosphatase-1 inhibitor-1 in cardiac physiology and pathophysiology.* J Mol Cell Cardiol, 2009. **47**(3): p. 365-71.
168. Egloff, M.P., et al., *Structural basis for the recognition of regulatory subunits by the catalytic subunit of protein phosphatase 1.* EMBO J, 1997. **16**(8): p. 1876-87.
169. El-Armouche, A., et al., *Role of calcineurin and protein phosphatase-2A in the regulation of phosphatase inhibitor-1 in cardiac myocytes.* Biochem Biophys Res Commun, 2006. **346**(3): p. 700-6.
170. Foulkes, J.G. and P. Cohen, *The hormonal control of glycogen metabolism. Phosphorylation of protein phosphatase inhibitor-1 in vivo in response to adrenaline.* Eur J Biochem, 1979. **97**(1): p. 251-6.
171. El-Armouche, A., et al., *Evidence for protein phosphatase inhibitor-1 playing an amplifier role in beta-adrenergic signaling in cardiac myocytes.* FASEB J, 2003. **17**(3): p. 437-9.
172. Carr, A.N., et al., *Type 1 phosphatase, a negative regulator of cardiac function.* Mol Cell Biol, 2002. **22**(12): p. 4124-35.
173. El-Armouche, A., et al., *Phosphatase inhibitor-1-deficient mice are protected from catecholamine-induced arrhythmias and myocardial hypertrophy.* Cardiovasc Res, 2008. **80**(3): p. 396-406.
174. Carr, A.N., et al., *Is myosin phosphatase regulated in vivo by inhibitor-1? Evidence from inhibitor-1 knockout mice.* J Physiol, 2001. **534**(Pt. 2): p. 357-66.
175. Avkiran, M., et al., *Protein kinase d in the cardiovascular system: emerging roles in health and disease.* Circ Res, 2008. **102**(2): p. 157-63.
176. Bossuyt, J., et al., *Ca2+/calmodulin-dependent protein kinase IIdelta and protein kinase D overexpression reinforce the histone deacetylase 5 redistribution in heart failure.* Circ Res, 2008. **102**(6): p. 695-702.
177. Johannes, F.J., et al., *PKCu is a novel, atypical member of the protein kinase C family.* J Biol Chem, 1994. **269**(8): p. 6140-8.
178. Valverde, A.M., et al., *Molecular cloning and characterization of protein kinase D: a target for diacylglycerol and phorbol esters with a distinctive catalytic domain.* Proc Natl Acad Sci U S A, 1994. **91**(18): p. 8572-6.
179. Fu, Y. and C.S. Rubin, *Protein kinase D: coupling extracellular stimuli to the regulation of cell physiology.* EMBO Rep, 2011. **12**(8): p. 785-96.
180. McEneaney, V., B.J. Harvey, and W. Thomas, *Aldosterone rapidly activates protein kinase D via a mineralocorticoid receptor/EGFR trans-activation pathway in the M1 kidney CCD cell line.* J Steroid Biochem Mol Biol, 2007. **107**(3-5): p. 180-90.
181. McEneaney, V., B.J. Harvey, and W. Thomas, *Aldosterone regulates rapid trafficking of epithelial sodium channel subunits in renal cortical collecting duct cells via protein kinase D activation.* Mol Endocrinol, 2008. **22**(4): p. 881-92.
182. Fielitz, J., et al., *Requirement of protein kinase D1 for pathological cardiac remodeling.* Proc Natl Acad Sci U S A, 2008. **105**(8): p. 3059-63.
183. Castaneda-Bueno, M., J.P. Arroyo, and G. Gamba, *Independent regulation of Na+ and K+ balance by the kidney.* Med Princ Pract, 2012. **21**(2): p. 101-14.
184. Storz, P. and A. Toker, *Protein kinase D mediates a stress-induced NF-kappaB activation and survival pathway.* EMBO J, 2003. **22**(1): p. 109-20.

185. Qiang, Y.W., et al., *Insulin-like growth factor I induces migration and invasion of human multiple myeloma cells.* Blood, 2004. **103**(1): p. 301-8.
186. Haworth, R.S., et al., *Protein kinase D inhibits plasma membrane Na(+)/H(+) exchanger activity.* Am J Physiol, 1999. **277**(6 Pt 1): p. C1202-9.
187. Vantus, T., et al., *Doxorubicin-induced activation of protein kinase D1 through caspase-mediated proteolytic cleavage: identification of two cleavage sites by microsequencing.* Cell Signal, 2004. **16**(6): p. 703-9.
188. Iglesias, T., R.T. Waldron, and E. Rozengurt, *Identification of in vivo phosphorylation sites required for protein kinase D activation.* J Biol Chem, 1998. **273**(42): p. 27662-7.
189. Matthews, S.A., E. Rozengurt, and D. Cantrell, *Characterization of serine 916 as an in vivo autophosphorylation site for protein kinase D/Protein kinase Cmu.* J Biol Chem, 1999. **274**(37): p. 26543-9.
190. Doppler, H., et al., *A phosphorylation state-specific antibody recognizes Hsp27, a novel substrate of protein kinase D.* J Biol Chem, 2005. **280**(15): p. 15013-9.
191. Rozengurt, E., *Protein kinase D signaling: multiple biological functions in health and disease.* Physiology (Bethesda), 2011. **26**(1): p. 23-33.
192. Harrison, B.C., et al., *Regulation of cardiac stress signaling by protein kinase d1.* Mol Cell Biol, 2006. **26**(10): p. 3875-88.
193. Meyer, A.H., et al., *In vivo labeling of parvalbumin-positive interneurons and analysis of electrical coupling in identified neurons.* J Neurosci, 2002. **22**(16): p. 7055-64.
194. Makhanova, N., et al., *Kidney function in mice lacking aldosterone.* Am J Physiol Renal Physiol, 2006. **290**(1): p. F61-9.
195. Seaton, B. and A. Ali, *Simplified manual high performance clinical chemistry methods for developing countries.* Med Lab Sci, 1984. **41**(4): p. 327-36.
196. Krege, J.H., et al., *A noninvasive computerized tail-cuff system for measuring blood pressure in mice.* Hypertension, 1995. **25**(5): p. 1111-5.
197. Miller, R.L., et al., *Automated method for the isolation of collecting ducts.* Am J Physiol Renal Physiol, 2006. **291**(1): p. F236-45.
198. Johannes, F.J., et al., *Bruton's tyrosine kinase (Btk) associates with protein kinase C mu.* FEBS Lett, 1999. **461**(1-2): p. 68-72.
199. Johannes, F.J., et al., *Protein kinase Cmu downregulation of tumor-necrosis-factor-induced apoptosis correlates with enhanced expression of nuclear-factor-kappaB-dependent protective genes.* Eur J Biochem, 1998. **257**(1): p. 47-54.
200. Ohta, A., et al., *Targeted disruption of the Wnk4 gene decreases phosphorylation of Na-Cl cotransporter, increases Na excretion and lowers blood pressure.* Hum Mol Genet, 2009. **18**(20): p. 3978-86.
201. Kim, Y.H., et al., *Immunocytochemical localization of pendrin in intercalated cell subtypes in rat and mouse kidney.* Am J Physiol Renal Physiol, 2002. **283**(4): p. F744-54.
202. Higuchi, E., et al., *Phosphorylation of protein phosphatase-1 inhibitors, inhibitor-1 and DARPP-32, in renal medulla.* Eur J Pharmacol, 2000. **408**(2): p. 107-16.
203. Yang, S.S., et al., *Generation and analysis of the thiazide-sensitive Na+ -Cl- cotransporter (Ncc/Slc12a3) Ser707X knockin mouse as a model of Gitelman syndrome.* Hum Mutat, 2010. **31**(12): p. 1304-15.
204. Cruz, D.N., *The renal tubular Na-Cl co-transporter (NCCT): a potential genetic link between blood pressure and bone density?* Nephrol Dial Transplant, 2001. **16**(4): p. 691-4.
205. Ellison, D.H. and J. Loffing, *Thiazide effects and adverse effects: insights from molecular genetics.* Hypertension, 2009. **54**(2): p. 196-202.
206. Traykova-Brauch, M., et al., *An efficient and versatile system for acute and chronic modulation of renal tubular function in transgenic mice.* Nat Med, 2008. **14**(9): p. 979-84.
207. Vallet, M., et al., *Pendrin regulation in mouse kidney primarily is chloride-dependent.* J Am Soc Nephrol, 2006. **17**(8): p. 2153-63.

208. Amlal, H., et al., *Deletion of the anion exchanger Slc26a4 (pendrin) decreases apical Cl(-)/HCO3(-) exchanger activity and impairs bicarbonate secretion in kidney collecting duct.* Am J Physiol Cell Physiol, 2010. **299**(1): p. C33-41.
209. Soleimani, M., et al., *Double knockout of pendrin and Na-Cl cotransporter (NCC) causes severe salt wasting, volume depletion, and renal failure.* Proc Natl Acad Sci U S A, 2012. **109**(33): p. 13368-73.
210. Leviel, F., et al., *The Na+-dependent chloride-bicarbonate exchanger SLC4A8 mediates an electroneutral Na+ reabsorption process in the renal cortical collecting ducts of mice.* J Clin Invest, 2010. **120**(5): p. 1627-35.
211. Andrew Terker, C.-L.Y., James A. McCormick, David H. Ellison. , *Acute Adrenergic Stimulation Activates the Renal Sodium Chloride Cotransporter* ASN 2012, 2012.
212. Meier, K.E., et al., *alpha 1- and beta 2-adrenergic receptor expression in the Madin-Darby canine kidney epithelial cell line.* J Cell Biol, 1983. **97**(2): p. 405-15.
213. Gesek, F.A. and K.E. White, *Molecular and functional identification of beta-adrenergic receptors in distal convoluted tubule cells.* Am J Physiol, 1997. **272**(6 Pt 2): p. F712-20.
214. Greven, J. and O. Heidenreich, *A micropuncture study of the effect of isoprenaline on renal tubular fluid and electrolyte transport in the rat.* Naunyn Schmiedebergs Arch Pharmacol, 1975. **287**(2): p. 117-28.
215. Neumann, J., et al., *Evidence for isoproterenol-induced phosphorylation of phosphatase inhibitor-1 in the intact heart.* Circ Res, 1991. **69**(6): p. 1450-7.
216. Klee, C.B., H. Ren, and X. Wang, *Regulation of the calmodulin-stimulated protein phosphatase, calcineurin.* J Biol Chem, 1998. **273**(22): p. 13367-70.
217. Hoorn, E.J., et al., *Pathogenesis of calcineurin inhibitor-induced hypertension.* J Nephrol, 2012. **25**(3): p. 269-75.
218. Liu, J., et al., *Calcineurin is a common target of cyclophilin-cyclosporin A and FKBP-FK506 complexes.* Cell, 1991. **66**(4): p. 807-15.
219. Kim, H.C., et al., *Primary immunosuppression with tacrolimus in kidney transplantation: three-year follow-up in a single center.* Transplant Proc, 2004. **36**(7): p. 2082-3.
220. Jain, A., et al., *What have we learned about primary liver transplantation under tacrolimus immunosuppression? Long-term follow-up of the first 1000 patients.* Ann Surg, 1999. **230**(3): p. 441-8; discussion 448-9.
221. Marver, D., *Evidence of corticosteroid action along the nephron.* Am J Physiol, 1984. **246**(2 Pt 2): p. F111-23.
222. Pearce, D. and T.R. Kleyman, *Salt, sodium channels, and SGK1.* J Clin Invest, 2007. **117**(3): p. 592-5.
223. Flores, S.Y., et al., *Aldosterone-induced serum and glucocorticoid-induced kinase 1 expression is accompanied by Nedd4-2 phosphorylation and increased Na+ transport in cortical collecting duct cells.* J Am Soc Nephrol, 2005. **16**(8): p. 2279-87.
224. Ring, A.M., et al., *An SGK1 site in WNK4 regulates Na+ channel and K+ channel activity and has implications for aldosterone signaling and K+ homeostasis.* Proc Natl Acad Sci U S A, 2007. **104**(10): p. 4025-9.
225. Velazquez, H., et al., *Adrenal steroids stimulate thiazide-sensitive NaCl transport by rat renal distal tubules.* Am J Physiol, 1996. **270**(1 Pt 2): p. F211-9.
226. Kim, G.H., et al., *The thiazide-sensitive Na-Cl cotransporter is an aldosterone-induced protein.* Proc Natl Acad Sci U S A, 1998. **95**(24): p. 14552-7.
227. Tsybouleva, N., et al., *Aldosterone, through novel signaling proteins, is a fundamental molecular bridge between the genetic defect and the cardiac phenotype of hypertrophic cardiomyopathy.* Circulation, 2004. **109**(10): p. 1284-91.
228. McEneaney, V., et al., *Protein kinase D1 modulates aldosterone-induced ENaC activity in a renal cortical collecting duct cell line.* Mol Cell Endocrinol, 2010. **325**(1-2): p. 8-17.
229. Stanton, B.A. and B. Kaissling, *Regulation of renal ion transport and cell growth by sodium.* Am J Physiol, 1989. **257**(1 Pt 2): p. F1-10.

230. Dimke, H., J.G. Hoenderop, and R.J. Bindels, *Molecular basis of epithelial Ca2+ and Mg2+ transport: insights from the TRP channel family.* J Physiol, 2011. **589**(Pt 7): p. 1535-42.
231. Schlingmann, K.P., et al., *Hypomagnesemia with secondary hypocalcemia is caused by mutations in TRPM6, a new member of the TRPM gene family.* Nat Genet, 2002. **31**(2): p. 166-70.
232. Walder, R.Y., et al., *Mutation of TRPM6 causes familial hypomagnesemia with secondary hypocalcemia.* Nat Genet, 2002. **31**(2): p. 171-4.
233. Nijenhuis, T., et al., *Enhanced passive Ca2+ reabsorption and reduced Mg2+ channel abundance explains thiazide-induced hypocalciuria and hypomagnesemia.* J Clin Invest, 2005. **115**(6): p. 1651-8.
234. Wang, Z., et al., *Cloning of a novel kinase (SIK) of the SNF1/AMPK family from high salt diet-treated rat adrenal.* FEBS Lett, 1999. **453**(1-2): p. 135-9.
235. Jaitovich, A. and A.M. Bertorello, *Intracellular sodium sensing: SIK1 network, hormone action and high blood pressure.* Biochim Biophys Acta, 2010. **1802**(12): p. 1140-9.
236. Sjostrom, M., et al., *SIK1 is part of a cell sodium-sensing network that regulates active sodium transport through a calcium-dependent process.* Proc Natl Acad Sci U S A, 2007. **104**(43): p. 16922-7.
237. Berdeaux, R., et al., *SIK1 is a class II HDAC kinase that promotes survival of skeletal myocytes.* Nat Med, 2007. **13**(5): p. 597-603.
238. Mungrue, I.N., et al., *CHAC1/MGC4504 is a novel proapoptotic component of the unfolded protein response, downstream of the ATF4-ATF3-CHOP cascade.* J Immunol, 2009. **182**(1): p. 466-76.
239. Oshima, T., et al., *A 718-kb DNA sequence of the Escherichia coli K-12 genome corresponding to the 12.7-28.0 min region on the linkage map.* DNA Res, 1996. **3**(3): p. 137-55.
240. Zinovieva, R.D., et al., *Structure and chromosomal localization of the human homeobox gene Prox 1.* Genomics, 1996. **35**(3): p. 517-22.
241. Elsir, T., et al., *Transcription factor PROX1: its role in development and cancer.* Cancer Metastasis Rev, 2012. **31**(3-4): p. 793-805.
242. Van Huyen, J.P., et al., *Vasopressin-stimulated chloride transport in transimmortalized mouse cell lines derived from the distal convoluted tubule and cortical and inner medullary collecting ducts.* Nephrol Dial Transplant, 2001. **16**(2): p. 238-45.
243. Gesek, F.A. and P.A. Friedman, *Mechanism of calcium transport stimulated by chlorothiazide in mouse distal convoluted tubule cells.* J Clin Invest, 1992. **90**(2): p. 429-38.
244. Diepens, R.J., et al., *Characterization of a murine renal distal convoluted tubule cell line for the study of transcellular calcium transport.* Am J Physiol Renal Physiol, 2004. **286**(3): p. F483-9.
245. Gesek, F.A. and P.A. Friedman, *Sodium entry mechanisms in distal convoluted tubule cells.* Am J Physiol, 1995. **268**(1 Pt 2): p. F89-98.
246. Dai, L.J., P.A. Friedman, and G.A. Quamme, *Cellular mechanisms of chlorothiazide and cellular potassium depletion on Mg2+ uptake in mouse distal convoluted tubule cells.* Kidney Int, 1997. **51**(4): p. 1008-17.
247. Dai, L.J., et al., *Mechanisms of amiloride stimulation of Mg2+ uptake in immortalized mouse distal convoluted tubule cells.* Am J Physiol, 1997. **272**(2 Pt 2): p. F249-56.
248. Dai, L.J., et al., *Aldosterone potentiates hormone-stimulated Mg2+ uptake in distal convoluted tubule cells.* Am J Physiol, 1998. **274**(2 Pt 2): p. F336-41.
249. Markadieu, N., et al., *A primary culture of distal convoluted tubules expressing functional thiazide-sensitive NaCl transport.* Am J Physiol Renal Physiol, 2012. **303**(6): p. F886-92.

Acknowledgements

First of all I would like to thank Prof. Dr. Johannes Loffing for giving me the possibility to perform my PhD thesis in his lab and to work on such an exciting project. I am grateful for his constant scientific support and constructive and inspiring discussions during the whole time.

I would like to express my gratitude to my committee, Prof. Dr. Carsten Wagner, Prof. Dr. François Verrey and Prof. Dr. Markus Bleich for their contribution to the success of this thesis.

I would like to thank all people who contributed to the thesis and supported and accompanied me during the last 4 years.

I would like to acknowledge the former and current members of the Loffing Lab.
Special thanks to Dr. Nicolas Picard, who introduced me to our friend the "COPAS", as well as "mouse work" and supported me a lot at the beginning of my thesis.
I am grateful to Dominique Loffing and Monique Carrel for their daily help during my whole thesis. Many thanks to Agnieszka Wengi for her great technical support. Furthermore, I would like to thank Claudia, Marian, Yuya, Nicole, Abhijeet, Solveig, Mads and Marianna for the great working atmosphere.

Many thanks to the former and current members of the Sommer lab for the nice working environment on J floor. Special thanks to Iris Miescher, through whom I got in touch with the Loffing Lab, for her endless help and her moral support.

Thank you to the members of the mouse facility.

A warm thanks to Andrea, Nicola, Mareen, Christopher, Gabriela and Niki for their amazing friendship and the many cheerful evenings with good food, beer and wine.

Very special thanks to Dr. Manfred Hallschmid for his endless help, great support and good laughs via Skype.

Very warm thanks to Nikolas for his infinite love and support and for reminding me of the world outside the lab.

Der allergrösste Dank gilt meiner wundervollen Familie die immer an mich geglaubt und unterstützt hat. Papa, Mama, Opa, Oma, Anja, Lisa, Jakob und Paul vielen Dank!

Curriculum Vitae

M Sc. Dipl.-Ing. (FH) Katja Trompf

Date of birth	01/09/1979
Nationality	German
Address	Landenbergstrasse 6 8037 Zürich
Mobile	+41 (0) 77 464 24 50
E-Mail	k.trompf@gmail.com

Education

Since 04/2009	University of Zurich, Switzerland PhD study
02/2008 to 03/2009	University of Zurich, Switzerland Degree: Master of Science in Human Biology
03/2002 to 08/2007	University of Applied Sciences, Hamburg, Germany Degree: Diplom-Ingenieur in Biotechnology (FH)
09/2000 to 07/2001	Specialised Secondary School, Wismar, Germany Specialization in Economy
07/1996 to 08/1999	Training school at the Schwerin Hospital, Germany Degree: Assistant Medical Technician

Research experience

Since 04/2009	University of Zurich, Switzerland Institute of Anatomy (Head: Prof. Dr. Johannes Loffing) PhD thesis: Regulation of kidney distal convoluted tubule (DCT) cell function
07/2008 to 03/2009	University of Zurich, Switzerland Institute of Physiology, (Head: Prof. Dr. Thierry Hennet) Master thesis: Expression and purification of mimiviral glycosyltransferase in *E. coli*
08/2007 to 12/2007	University of Sydney, Australia School of Biological Sciences, (Head: Prof. Dr. Rosalind Hinde) Studies in biochemical interactions between marine Invertebrate animal hosts and their intracellular algae
08/2006 to 07/2007	University of Natural Resources and Applied Life Sciences Vienna, Austria Department of Biotechnology (Head: Prof. Dipl. Ing. Dr. Reingard Grabherr) Diploma Thesis: Evaluation of transfected CHO cell lines via flow cytometry (FACS)

03/2007 to 07/2007	Medical University of Vienna, Austria Max F. Perutz Laboratories, Department of Biochemistry (Head: Prof. Dr. Tim Skern) Enzyme-substrate interaction of leader protease from foot-and-mouth virus

Publications

Mayer C, Nchinda AT, Trompf K, Skern T. Residue L143 of the foot-and-mouth disease virus leader protease is responsible for discrimination between leucine and phenylalanine at P2
(J Virol. 2008 May; 82(9):4656-9)

Grant A, Trompf K, Seung D, Nivison-Smith L, Bowcock H, Kresse H, Holmes S, Radford J, Morrow P. Sub-cellular damage by copper in the cnidarian Zoanthus robustus
(Comp Biochem Physiol C Toxicol Pharmacol. 2010 Sep;152(3):256-262)

Picard N, Trompf K, Yang C, Miller R, Carrel M, Loffing-Cueni D, Ellison D, Loffing J
Reduced phosphorylation of renal NaCl cotransporter by protein phosphatase-1/ inhibitor-1 deficiency causes arterial hypotension
(in revision)

Work experience

03/2008 to 03/2011	University of Zurich, Switzerland Institute of Anatomy (Head: Prof. Dr. Lukas Sommer) Laboratory Organization
09/2004 to 02/2006	University of Applied Sciences Hamburg, Germany Laboratory of Applied Microbiology (Head: Prof. Dr. Paul Scherer) Tutor for Microbiology Trainings
09/1999 to 09/2000	University of Luebeck, Germany Department of Neuroendocrinology (Head: Prof. Dr. Jan Born) Research assistant Experiments on Electroencephalographic and Endocrine Parameters in Humans

Affiliations

Membership	PhD Program: Integrative Molecular Medicine, Center of Integrative Physiology Zurich Swiss Society for Anatomy, Histology, and Embryology